



**Identification and Validation of Cancerous
Targets of Kusunokinin**

Tanotnon Tanawattanasuntorn

**A Thesis Submitted in Partial Fulfillment of the Requirements for the
Degree of Doctor of Philosophy in Biomedical Sciences
Prince of Songkla University
2023**

Copyright of Prince of Songkla University

Thesis Title Identification and validation of cancerous targets of
kusunokinin

Author Mr. Tanotnon Tanawattanasuntorn

Major Program Biomedical Sciences

Major Advisor**Examining Committee:**

.....Chairperson
(Assoc. Prof. Dr. Potchanapond Graidist) (Assoc. Prof. Dr. Paolo Ceppi)

Co-advisor

.....Committee
(Assoc. Prof. Dr. Potchanapond Graidist)

.....
(Assoc. Prof. Dr. Varomyalin Tipmanee)Committee
(Assoc. Prof. Dr. Varomyalin Tipmanee)

.....Committee
(Asst. Prof. Dr. Dennapa Sotthibandhu)

.....Committee
(Asst. Prof. Dr. Poonsit Hiransai)

The Graduate School, Prince of Songkla University, has approved this
thesis as partial fulfillment of the requirements for the Doctor of Philosophy Degree in
Biomedical Sciences

.....
(Asst. Prof. Dr. Thakerng Wongsirichot)
Acting Dean of Graduate School

This is to certify that the work here submitted is the result of the candidate's own investigations. Due acknowledgement has been made of any assistance received.

.....Signature
(Assoc. Prof. Dr. Potchanapond Graidist)
Major Advisor

.....Signature
(Mr. Tanotnon Tanawattanasuntorn)
Candidate

I hereby certify that this work has not been accepted in substance for any degree, and is not being currently submitted in candidature for any degree.

.....Signature

(Mr. Tanotnon Tanawattanasuntorn)

Candidate

ชื่อวิทยานิพนธ์ การระบุและพิสูจน์เป้าหมายที่เกี่ยวข้องกับมะเร็งของสารคูชูโนคินิน

ผู้เขียน นายธนพนธ์ วัฒนสุนทร

สาขาวิชา ชีวเวชศาสตร์

ปีการศึกษา 2566

บทคัดย่อ

สารคูชูโนคินินสามารถยับยั้งการเจริญเติบโตของเซลล์มะเร็งเต้านมโดยการไปยับยั้งโปรตีนเป้าหมายหลายชนิด เช่น CSF1R และ AKT จากการศึกษาก่อนหน้านี้แสดงให้เห็นว่าสารคูชูโนคินินสามารถจับกับโปรตีนเป้าหมายที่เกี่ยวข้องกับการแบ่งตัวและการเคลื่อนย้ายของเซลล์ได้หลายชนิดด้วย ดังนั้นเพื่อให้ได้ข้อมูลของโปรตีนเป้าหมายของสารคูชูโนคินินมากขึ้น การศึกษาในครั้งนี้จึงใช้เทคนิคการจำลองการจับด้วยคอมพิวเตอร์และพิสูจน์โดยการจับทางอ้อมในเซลล์มะเร็งเต้านมและรังไข่ จากการศึกษาด้วยเทคนิคโมเลกุลาร์ดอกกิงพบว่าโปรตีน AKR1B1 และ MEK2 น่าจะเป็นเป้าหมายของสารคูชูโนคินิน โดยโปรตีน AKR1B1 ให้ผลการจับที่ดีที่สุด ซึ่งจากการศึกษาพลวัตเชิงโมเลกุลบ่งชี้ว่าสารคูชูโนคินินมีลักษณะการจับใกล้เคียงกับสารที่เป็นตัวยับยั้งโปรตีน AKR1B1 ทั้งในแง่ของพลังงานอิสระในการเข้าจับ อันตรกิริยา และลักษณะทางวางตัวของโครงสร้างในบริเวณเร่ง จากนั้นจึงทำการพิสูจน์ผลที่ได้นี้เพิ่มเติมในเซลล์มะเร็งเต้านม (Hs578T และ BT549) และเซลล์มะเร็งรังไข่ (SKOV3 และ A2780) ซึ่งพบว่าสารคูชูโนคินินยับยั้งเซลล์มะเร็งเต้านมและรังไข่ได้ดีกว่าสารที่เป็นตัวยับยั้งโปรตีน AKR1B1 (ได้แก่ zopolrestat และ epalrestat) ยิ่งไปกว่านั้นสารคูชูโนคินินยังมีฤทธิ์ในการยับยั้งเอนไซม์ AKR1B1 โดยมีค่า IC_{50} เท่ากับ 9.72 ± 0.18 ไมโครโมลาร์ ซึ่งให้ผลดีกว่าสาร *trans*-(-)-artiin (13.65 ± 0.49 ไมโครโมลาร์) แต่มีฤทธิ์น้อยกว่าสาร epalrestat (0.77 ± 0.01 ไมโครโมลาร์) และ zopolrestat (31.03 ± 1.40 นาโนโมลาร์) นอกจากนี้ยังพบอีกว่าการจับของสารคูชูโนคินินกับโปรตีน AKR1B1 ภายในเซลล์ Hs578T และ SKOV3 สามารถป้องกันการสลายตัวของโปรตีน AKR1B1 จากความร้อนที่อุณหภูมิ 75 และ 60 องศาเซลเซียส ได้ตามลำดับ สิ่งที่น่าสนใจ คือ การยับยั้งโปรตีน AKR1B1 ของสารคูชูโนคินินสามารถป้องกันการเกิดปฏิกิริยาออกซิเดชันของไขมันจากการชักนำของกลูโคสในเซลล์ Hs578T ได้ โดยให้ผลแปรผันตรงกับความเข้มข้นของสารคูชูโนคินินและยังมีฤทธิ์ที่ดีกว่าสาร epalrestat ซึ่งการยับยั้งนี้ส่งผลในการยับยั้งโปรตีนปลายน้ำของโปรตีน AKR1B1 ได้แก่ PKC δ , NF- κ B, AKT, Nrf2, COX2 และ Twist2 ยิ่งไปกว่านั้นยังพบการเปลี่ยนแปลงของระดับโปรตีนของตัวบ่งชี้ในกระบวนการเปลี่ยนแปลงเซลล์เยื่อบุผิวไป

เป็นเซลล์มีเซ็นไคน์ (Epithelial Mesenchymal Transition; EMT) โดยพบการเพิ่มขึ้นของระดับโปรตีน E-cadherin และการลดลงของระดับโปรตีน N-cadherin ในเซลล์ Hs578T จากผลการศึกษานี้สามารถสรุปได้ว่าสารคูชูโนคินินสามารถจับกับโปรตีน AKR1B1 ได้ดี ส่งผลให้เกิดการยับยั้งการเกิดสถานะเครียดของเซลล์ที่เกิดจากอนุมูลอิสระ และยังชักนำให้เกิดการเปลี่ยนแปลงของโปรตีนในกระบวนการ EMT ของเซลล์มะเร็งเต้านมระยะลุกลาม

คำสำคัญ: คูชูโนคินิน, มะเร็งเต้านม, มะเร็งรังไข่, เอเคอาร์วันปีวัน

Thesis Title	Identification and validation of cancerous targets of kusunokinin
Author	Mr. Tanotnon Tanawattanasuntorn
Major Program	Biomedical Sciences
Academic Year	2023

ABSTRACT

Trans-(–)-kusunokinin hampers breast cancer growth by suppressing many target proteins, such as CFS1R and AKT. Previous results showed that it could bind other targets involved in cancer proliferation and migration. To fill in more information on the *trans*-(–)-kusunokinin target protein, this study used computational simulations and validated its target on breast and ovarian cancer cells. The results from molecular docking showed that AKR1B1 and MEK2 were potential targets. AKR1B1 represented the strongest binding affinity. *Trans*-(–)-kusunokinin indicated comparable binding affinity, interaction and orientation in the binding site to AKR1B1 inhibitors. Then, these results were indirect proof on breast (Hs578T and BT549) and ovarian (SKOV3 and A2780) cancer cells. *Trans*-(±)-kusunokinin had the cytotoxic effect on breast and ovarian cancer cells that were markedly stronger than well-known AKR1B1 inhibitors (zopolrestat and epalrestat). Moreover, *trans*-(±)-kusunokinin inhibited AKR1B1 enzyme activity with an IC₅₀ value of 9.72 ± 0.18 μM which was stronger than *trans*-(–)-arctiin (13.65 ± 0.49 μM) but weaker than epalrestat (0.77 ± 0.01 μM) and zopolrestat (31.03 ± 1.40 nM). Moreover, binding between *trans*-(±)-kusunokinin and intracellular AKR1B1 protected the degradation of AKR1B1 at 75 °C and 60 °C on Hs578T and SKOV3 cells, respectively. Notably, the inhibitory effect of *trans*-(±)-kusunokinin on AKR1B1 led to the protection of glucose-induced cellular lipid peroxidation in a dose-dependent manner, which was stronger than epalrestat on Hs578T cells. In addition, *trans*-(±)-kusunokinin suppressed AKR1B1, resulting in the suppression of its signaling molecules, including PKCδ, NF-κB, AKT, Nrf2, COX2, Twist2. *Trans*-(±)-kusunokinin also altered epithelial mesenchymal transition (EMT) markers by increasing E-cadherin levels and decreasing N-cadherin levels on Hs578T cells. In conclusion, *trans*-(–)-kusunokinin exhibited a strong binding affinity with

AKR1B1, thereby mitigating oxidative stress and changing EMT protein levels on aggressive breast cancer.

Keywords: kusunokinin, breast cancer, ovarian cancer, AKR1B1

ACKNOWLEDGEMENT

The boundlessness of the universe corresponds to the boundlessness of knowledge, a realm surpassing the bounds of our imagination. Nevertheless, I take pride in my capacity to unravel certain of the universe's enigmas, notwithstanding their minuscule scale. When I become an integral part of the universe, I expect to feel no regret, for I will have left behind an enduring heritage. Permit me to express gratitude for the culmination of my educational journey, a feat facilitated by my unwavering effort. However, I recognize that my accomplishments would have remained elusive without the presence of a pivotal individual. My heartfelt appreciation extends to my family for their steadfast support and motivation, and to my friends for their invaluable counsel concerning my mental well-being and daily life.

I would like to express my deepest gratitude to my advisor, Assoc. Prof. Dr. Potchanapond Graidist, for her patience, encouragement and dedicated support of my research. Not only the abundant knowledge that I got from her but also how to live socially. I am also grateful to my co-advisor, Assoc. Prof. Dr. Varomyalin Tipmanee, for his encouragement, guidance and consultation.

I would like to be highly grateful to the examination committee: Assoc. Prof. Dr. Paolo Ceppi, Asst. Prof. Dr. Dennapa Sotthibandhu and Asst. Prof. Dr. Poonsit Hiransai for their suggestions to fulfill and complete my thesis.

This research was supported financially by the Thailand Research Fund through the Royal Golden Jubilee (RGJ) Ph.D. Program (PHD/0186/2561), Agricultural Research Development Agency (ARDA) (Public Organization) (CRP6205031700) and Faculty of Medicine (REC 64-066-4-2), Prince of Songkla University, Songkhla, Thailand.

I sincerely thank all staff and students in the Department of Biomedical Sciences and Biomedical Engineering, Faculty of Medicine, Prince of Songkla University, particularly my advisor's team, Dr. Thidarath Rattanaburee, Miss. Nadeeya Mad-adam, Miss Chompunud Chompunud Na Ayudhya, Mr. Muhammad Faisal, Miss Sirinapa Dokduang and Miss Siriporn Taraporn.

Tanotnon Tanawattanasuntorn

CONTENTS

	Page
Contents	x
List of tables	xiv
List of figures	xv
List of abbreviations and symbols	xviii
Chapter	
1. Introduction	
1.1 Background and rationale	1
1.2 Literature reviews	3
1.2.1 Breast and ovarian cancers	3
1.2.2 Breast cancer progression pathway	6
1.2.3 Ovarian cancer progression pathway	8
1.2.4 Targets of breast and ovarian cancer drugs and mechanism of action	9
1.2.4.1 Estrogen receptor: Tamoxifen	9
1.2.4.2 Aromatase: Letrozole	9
1.2.4.3 DNA	10
1.2.4.3.1 Alkylating agents	10
1.2.4.3.2 Platinum-based agents	11
1.2.1.4.3 Antibiotics agents	11
1.2.1.4.4 Antimetabolites	11
1.2.4.4 Topoisomerase: etoposide	13
1.2.4.5 Microtubule	14
1.2.1.5.1 Taxane-diterpenes: paclitaxel and docetaxel	14
1.2.1.5.2 Vinca-alkaloids: vincristine and vinblastine	14
1.2.4.6 HER2: Trastuzumab	15
1.2.4.7 Trop2: Sacituzumab govitecan	15
1.2.4.8 VEGFR: Bevacizumab	15
1.2.4.9 TrkA/B/C receptor: entrectinib	16
1.2.4.10 EGFR: gefitinib	16
1.2.4.11 PARP: Olaparib	16

CONTENTS (Continued)

	Page
1.2.5 General treatment of breast and ovarian cancer	16
1.2.6 Drugs for breast cancer treatment	16
1.2.7 Drugs for ovarian cancer treatment	20
1.2.8 Aldo-keto reductase family 1 member B1 (AKR1B1)	23
1.2.9 Aldose reductase inhibitors (ARIs)	24
1.2.10 Lignans	28
1.2.11 Lignan as an anticancer compound	29
1.2.12 Kusunokinin	33
1.2.13 Signaling pathway related to carcinogenesis	36
1.2.13.1 Cancer cell proliferation	36
1.2.13.2 Cell cycle signaling	39
1.2.13.3 Apoptosis pathway	41
1.2.13.4 Multidrug resistance (MDR)	42
1.2.13.5 Migration	43
1.2.14 Breast and ovarian cancers develop through multiple pathways	43
1.2.14.1 DNA damage pathway	45
1.3 Objectives	47
2. Research methodology	48
Part I. Identification of trans-(–)-kusunokinin target by <i>in silico</i> studies	49
1. Computer system	49
1.1 Hardware	49
1.2 Software	49
1.3 Bioinformatics tools and database	49
2. Computational methods	49
2.1 Protein structure preparation	49
2.2 Ligand preparation	50
2.3 Molecular docking parameters	50
2.4 Molecular docking operation	51
2.5 Molecular dynamics simulation	51

CONTENTS (Continued)

	Page
2.6 Binding free energy evaluation	53
Part II. Validation of <i>trans</i> -(±)-kusunokinin target by <i>in vitro</i> studies	54
1. Methods	54
1.1 Cell culture condition	53
1.2 Compounds for cancer cell treatment	56
1.3 Cytotoxicity by MTT assay	56
1.4 Aldose reductase activity assay	57
1.5 Cellular thermal shift assay (CETSA)	58
1.6 Thiobarbituric acid reactive substances assay (TBARS)	59
1.7 Cells treatment and protein extraction	59
1.8 SDS-PAGE	60
1.9 Protein transfer and Western blotting	60
1.10 Small interfering RNA condition	62
1.11 Statistical analysis	62
2. Materials	63
3. Results	68
Part I. Identification of <i>trans</i> -(–)-kusunokinin target by <i>in silico</i> studies	68
1. <i>Trans</i> -(–)-kusunokinin target screening	68
2. Preliminary predicted binding energy and interaction of <i>trans</i> -(–)-kusunokinin and AKR1B1 inhibitors on active site	73
3. Molecular dynamics trajectory analysis	78
4. Binding mode insight of <i>trans</i> -(–)-kusunokinin, ARIs and AKR1B1 substrate throughout the MD progression	82
Part II. Validation of <i>trans</i> -(±)-kusunokinin target by <i>in vitro</i> studies	84
1. AKR1B1 expression on breast and ovarian cancer cells	84
2. Cell viability of breast and ovarian cancer cells with (±)KU treatment	86
3. Aldose reductase activity	90
4. Cellular thermal shift assay (CETSA)	92

CONTENTS (Continued)

	Page
5. (±)KU inhibited lipid peroxidation in high glucose condition	94
6. (±)KU suppressed AKR1B1 level	95
7. Down-regulation of AKR1B1 by (±)KU led to alteration of signaling molecules of oxidative stress and EMT markers	96
4. Discussion	100
Part I. Identification of <i>trans</i> -(-)-kusunokinin target by <i>in silico</i> studies	100
Part II. Validation of <i>trans</i> -(±)-kusunokinin target by <i>in vitro</i> studies	103
5. Conclusions	110
Part I. Identification of <i>trans</i> -(-)-kusunokinin target by <i>in silico</i> studies	110
Part II. Validation of <i>trans</i> -(±)-kusunokinin target by <i>in vitro</i> studies	111
References	113
Vitae	126

LIST OF TABLES

Table	Page
1. Drugs for breast cancer treatment	17
2. Drugs for ovarian cancer treatment	20
3. Aldose reductase inhibitors (ARIs) with anticancer effects <i>in vitro</i> and <i>in vivo</i> experiments	26
4. Anticancer compounds from lignan	30
5. Breast and ovarian cancer cells used in this study	55
6. Substances for cancer cell treatment	56
7. Steps for adding solution in each condition of aldose reductase activity	58
8. SDS-PAGE gel solution	61
9. Small interfering RNA procedures	64
10. List of antibodies used in this study	65
11. Chemicals and reagents used in this study	66
12. Equipment used in this study	67
13. Binding energy of <i>trans</i> -(-)-kusunokinin and native ligands	69
14. Binding energy between ligands and AKR1B1 from molecular docking	77
15. <i>Trans</i> -(-)-kusunokinin and selective ARIs with the values of MM/GBSA binding energy toward AKR1B1	82

LIST OF FIGURES

Figure	Page
1. Estimated age-standardized incidence and mortality rates in 2020	5
2. Breast cancer	6
3. Ovarian cancer origin and classification	6
4. Breast cancer pathway and molecular mechanism of drugs for breast cancer treatment	7
5. Ovarian cancer pathway and molecular mechanism of drugs for ovarian cancer treatment	8
6. Mechanism of action of tamoxifen and aromatase inhibitors	10
7. Mechanism of action of alkylating agents	11
8. Mechanism of action of platinum-based agents	12
9. Mechanism of action of bleomycin	12
10. Mechanism of action of antimetabolites	12
11. Mechanism of action of topoisomerase inhibitor	13
12. Mechanism of action of taxane-diterpenes and vinca alkaloids	14
13. Mechanism of action of trastuzumab	15
14. Role of AKR1B1 signaling in cancer	24
15. Molecular mechanism of action of ARIs in anticancer activity	25
16. Lignan biosynthesis	29
17. Molecular mechanism of action of lignan compounds in anticancer activity	33
18. <i>Trans</i> -(±)-kusunokinin structure	35
19. Relay signaling of cell proliferation	37
20. Signaling pathways of cell proliferation	39
21. Cell cycle signaling pathways	40
22. Network that signals apoptosis	42
23. Regulation of multidrug resistance and migration pathway	43
24. Breast and ovarian cancers develop through multiple molecular pathways	46
25. Study workflow of this research	48
26. IDD594 overlay orientation of self-redocking	73
27. <i>Trans</i> -(–)-kusunokinin binding site on AKR1B1	74

LIST OF FIGURES (Continued)

Figure	Page
28. Structure of carboxylic ARIs	75
29. Structure of hydantoin ARIs	75
30. Structure of suggested potential ARIs	76
31. Structures of AKR1B1 substrate and substrate analog	76
32. Observed interaction of <i>trans</i> -(-)-kusunokinin and ARIs with AKR1B1	78
33. RMSD of the molecular dynamic trajectory from the simulation of AKR1B1	79
34. RMSF of molecular dynamic trajectory from the simulation of AKR1B1	80
35. Pattern of distance geometry	81
36. Distance pattern of AKR1B1 complexes with and without ligands in molecular dynamic simulations	81
37. Insight binding mode of <i>trans</i> -(-)-kusunokinin, ARIs and AKR1B1 substrate throughout the MD progression	83
38. Expression level of AKR1B1 on the breast and ovarian cancer cells	85
39. IC ₅₀ values of (±)KU, ARIs, and chemotherapeutic drugs against breast and ovarian cancer cells	86
40. Cell viability of BT549 cells	87
41. Cell viability of Hs578T cells	87
42. Cell viability of MCF7 cells	88
43. Cell viability of A2780 cells	88
44. Cell viability of SKOV3 cells	89
45. Cell viability of OVCAR3 cells	89
46. Aldose reductase activity	91
47. CETSA with various of temperatures	93
48. CETSA with various concentration of (±)KU	94
49. Lipid peroxidation on Hs578T in high glucose conditions	97
50. Suppression of AKR1B1 and regulation of signaling molecules by (±)KU	98
51. Effect of (±)KU on signaling molecules through the downregulation of AKR1B1	99
52. Prediction of targets and propose mechanism of action of <i>trans</i> -(-)-kusunokinin	102
53. Propose mechanism of action of <i>trans</i> -(±)-kusunokinin in AKR1B1 pathway	109

LIST OF FIGURES (Continued)

Figure	Page
54. Proposed binding model of <i>trans</i> -(-)-kusunokinin and ARIs to prevent the substrate PGH ₂ access into the catalytic site of AKR1B1	112
55. Proposed <i>trans</i> -(\pm)-kusunokinin mechanism of action in breast cancer cells	112

LIST OF ABBREVIATIONS AND SYMBOLS

(±)KU	=	<i>Trans</i> -(±)-kusunokinin
(-)AR	=	<i>Trans</i> -(-)-arctiin
(-)KU	=	<i>Trans</i> -(-)-kusunokinin
ABC	=	ATP-binding-cassette
AGEs	=	Advanced glycation end products
AKR1B1	=	Aldo-keto reductase family 1 member B1
ARIs	=	Aldose reductase inhibitors
ASMR	=	Age-standardized mortality rate
ASR	=	Age-standardized incidence rate
ATCC	=	American Type Culture Collection
ATM	=	Ataxia telangiectasia–mutated gene
ATR	=	Ataxia-telangiectasia mutated and Rad3-related
Bak	=	Bcl-2 homologous antagonist killer
Bax	=	Bcl-2 associated X proteins
Bcl-2	=	B cell lymphoma 2
Bcl-XL	=	B cell lymphoma-extra large
BRAF	=	B-Raf proto-oncogene serine/threonine-protein kinase
BRCA1/2	=	Breast cancer susceptibility gene
BRCP	=	Breast cancer resistance protein
BSA	=	Bovine serum albumin
c-Myc	=	C-mycproto-oncogene
CDC42	=	Cell division control protein 42 homolog
CDK	=	Cyclin-dependent kinase
CETSA	=	Cellular thermal shift assay
CIS	=	Cisplatin
CO ₂	=	Carbon dioxide
COX2	=	Cyclooxygenase-2
CSF1	=	Colony stimulating factor 1
CSF1R	=	Colony stimulating factor 1 receptor
DI	=	Deionized

LIST OF ABBREVIATIONS AND SYMBOLS (continued)

DMEM	=	Dulbecco's Modified Eagle Medium
DMSO	=	Dimethyl sulfoxide
DNA	=	Deoxyribonucleic acid
DOX	=	Doxorubicin
EDTA	=	Ethylenediaminetetraacetic acid
EGFR	=	Epidermal growth factor receptor
EMT	=	Epithelial–mesenchymal transition
EP	=	Epalrestat
ER	=	Estrogen receptor
ERK	=	Extracellular-signal regulated kinase
et al.	=	Et ali (Latin), and others
Fas	=	FS-7-associated surface antigen
GPCR	=	G protein-couple receptor
GS-DHN	=	Glutathionyl-1,4-dihydroxynonene
GS-HNE	=	Glutathionyl-4-hydroxynonenal
GSH	=	Reduced glutathione
GSSG	=	Oxidized glutathione
h	=	Hour (s)
HBOC	=	Hereditary breast and ovarian cancer
HCl	=	Hydrochloric acid
HER2	=	Human epidermal growth factor receptor 2
HNE	=	4-hydroxy-trans-2-nonenal
HSP90- α	=	Heat shock protein-90alpha
IC ₅₀	=	Half maximal inhibitory concentration
MAPK	=	Mitogen-activated protein kinase
MD	=	Molecular Dynamics
MDA	=	Malondialdehyde
MEK1/2	=	Mitogen-activated protein kinase kinase $\frac{1}{2}$
mg	=	Milligram
min	=	Minute (s)

LIST OF ABBREVIATIONS AND SYMBOLS (continued)

ml	=	Milliliter
MM/GBSA	=	Molecular mechanics/Generalized Born-Surface Area
MMP-12	=	Matrix metalloproteinase-12
MRP	=	Multidrug resistance associated protein
MTT	=	3-(4,5-dimethylthiazol-2-yl)-2,5-diphenyltetrazolium bromide
MW	=	Molecular weight
Na ₂ HPO ₄	=	Disodium phosphate
NaCl	=	Sodium chloride
NADH	=	Nicotinamide adenine dinucleotide (NAD) + Hydrogen (H)
NADPH	=	Dihydro-nicotinamide-adenine-dinucleotide phosphate
NaHCO ₃	=	Sodium hydrogen carbonate
NaOH	=	Sodium hydroxide
NF-κB	=	Nuclear factor kappa-light-chain-enhancer of activated B cells
Nrf2	=	Nuclear factor erythroid 2-related factor 2
°C	=	Degree Celsius
p21	=	Cyclin-dependent kinase inhibitor 1
p53	=	Protein 53
PAGE	=	Polyacrylamide gel electrophoresis
PAK	=	p21-activated kinase
PARP	=	Poly(ADP-ribose) polymerase
PBS	=	Phosphate buffer saline
PD-L	=	Programmed Cell Death Ligand
PDB	=	Protein Data Bank
PGH ₂ /PGF _{2α}	=	Prostaglandin H ₂ /F _{2α}
pH	=	Power of hydrogen
PI3K	=	Phosphoinositide 3-kinase
PKCδ	=	Protein kinase C delta
PLA ₂	=	Phospholipases A ₂
PLC	=	Phospholipase C
PR	=	Progesterone receptor

LIST OF ABBREVIATIONS AND SYMBOLS (continued)

PTEN	=	Phosphatase and tensin homolog
Rac	=	Ras-related C3 botulinum toxin substrate
Raf	=	Rapidly accelerated fibrosarcoma
Ras	=	Rat sarcoma
Rho	=	Ras homologous
RMSD	=	Root mean square deviation
RMSF	=	Root mean square fluctuation
ROCK	=	Rho-associated protein kinase
ROS	=	Reactive oxygen species
RPMI	=	Roswell Park Memorial Institute medium
RXR	=	Retinoid X receptor
SD	=	Standard deviation
SDH	=	Sorbitol dehydrogenase
SDS	=	Sodium dodecyl sulfate
siRNA	=	Small interfering ribonucleic acid
Smad	=	Suppressor of Mothers against Decapentaplegic
Src	=	Proto-oncogene tyrosine-protein kinase sarcoma
STAT3	=	Signal transducer and activator of transcription 3
T ₃	=	Triiodothyronine
TBARS	=	Thiobarbituric acid reactive substances assay
TEMED	=	N,N,N',N'-Tetramethyl ethylenediamine
TNBC	=	Triple negative breast cancer
TRE	=	Thyroid hormone response element
Tris	=	Tris (hydroxymethyl) aminomethane
Tris-HCl	=	Tris (hydroxymethyl) aminomethane hydrochloride
TrkA/B/C	=	Tropomyosin receptor kinase A/B/C
Trop2	=	Tumor-associated calcium signal transducer 2
TR _{α/β}	=	Thyroid hormone receptor alpha/beta
TTBS	=	Tris buffer saline with Tween 20
Twist2	=	Twist family bHLH transcription factor 2

LIST OF ABBREVIATIONS AND SYMBOLS (continued)

VEGFR	=	Vascular endothelial growth factor receptor
VMD	=	Visual Molecular Dynamics
w/v	=	Weight per volume
WASP	=	Wiskott–Aldrich syndrome protein
ZP	=	Zopolrestat
μg	=	Microgram
μl	=	Microliter
μM	=	Micromolar

CHAPTER 1

INTRODUCTION

1.1 Background and rational

Cancer is an aggressive disorder that ranks as a primary cause of mortality and is a significant hindrance to increasing lifespan. The World Health Organization (WHO) approximates that cancer stands as either the primary or secondary foremost contributor to mortality among individuals below 70 years of age in 112 out of 183 countries. Cancer can occur in several parts of the body. The top ten cancer sites by estimated age-standardized world incidence rates, both by sex and across all ages, are breast, prostate, lung, colorectum, cervix uteri, stomach, liver, corpus uteri, ovary and thyroid, respectively. Among them, the most common area that can be found is the breast. Moreover, breast cancer is reported as having the second-highest age-standardized mortality rate. Interestingly, the ovary is the common site of gynecologic cancer (Sung et al., 2021) and is linked to breast cancer through several comparable molecular oncogenesis pathways, especially in the hereditary breast and ovarian cancer (HBOC) syndrome (Kobayashi et al., 2013). Therefore, breast and ovarian cancers piqued our interest and we selected them as models for this study.

Breast and ovarian cancer treatment is based on the subtype and stage of the cancer. In general, the combination of chemotherapeutic drugs is usually recommended after the surgery. For example, paclitaxel and the platinum-based combination is used as the first line chemotherapy for ovarian cancer, doxorubicin and cyclophosphamide combination is the regimen for early-stage breast cancer treatment. Chemotherapy followed by surgery (neoadjuvant) is a strategy for treating patients with advanced stage of breast and ovarian cancers to reduce the tumor volume and make it easier for surgery (Kayl et al., 2006). However, several side effects of chemotherapeutic drugs hinder the quality of life in breast and ovarian cancer patients. In addition, due to the low specificity of eliminating cancer cells of chemotherapeutic drugs, targeted therapy has recently played an important role in cancer treatment. Unfortunately, the high cost of most targeted medications makes them unaffordable in economically developing countries (Prasad et al., 2021). Hence, phytochemical-based drugs are interesting for

developing in clinical use and could be considered for lessening strong side effects and medical expenses.

Target identification and validation is an early process of drug discovery and development. Most chemotherapeutic drugs for breast and ovarian cancer treatments target DNA, such as alkylating agents, platinum-based agents and antibiotics agents. These drugs attach alkyl groups to DNA, resulting in DNA cross-linking, DNA fragmentation and abnormal base pairing leading to DNA synthesis inhibition and cell death at last (Roy et al., 1999). In addition, microtubule is one of the targets of chemotherapeutic drugs that are derived from a natural compound such as paclitaxel binds to β -tubulin to inhibit depolymerization. Whereas vincristine and vinblastine, vinca-alkaloid compounds, act to inhibit microtubule polymerization. Both events suppress microtubule dynamic instability that inhibits mitotic progression leading to cell cycle arrest at the M phase and cell death (Lichota and Gwozdziński, 2018). Moreover, lignans are a fascinating natural compound that has potential anticancer activity. Food and Drug Administration (FDA) approved chemotherapeutic drugs such as etoposide and teniposide which are semisynthetic derivatives from podophyllotoxin act as topoisomerase II inhibitors that inhibit re-ligation of cleaved DNA leading to critical errors in DNA synthesis at the premitotic stage of cell division (Yousefzadi et al., 2010; Pan et al., 2012). However, a multitude of proteins possess the capacity to govern various aspects of cancer cell behavior, including proliferation, cell cycle progression, cell survival, migration, DNA repair, and resistance to multiple drugs. These proteins represent promising candidates for targeted interventions through anticancer drugs. (Alimbetov et al., 2018).

Trans-(-)-kusunokinin, a lignan compound from *Piper nigrum*, revealed the potential anticancer activity through induced cell apoptosis and G2/M phase arrest on breast cancer cells (Sriwiriyan et al., 2017). In the mammary tumor rat model, *trans*-(-)-kusunokinin exhibited the inhibition of tumor growth and migration with no side effects (Tedasen et al., 2020). However, *trans*-(-)-kusunokinin from the extraction of *P. nigrum* provides a low yield percentage and requires complicated extraction techniques (Rattaburee et al., 2019). Therefore, the synthetic racemic *trans*-(\pm)-kusunokinin (equimolar mixture of *trans*-(-)-kusunokinin and *trans*-(+)-kusunokinin) could be encouraged for further study.

Trans-(±)-kusunokinin showed significantly decreased topoisomerase II, STAT3 and cyclin D1 levels leading to inhibits proliferation of breast cancer cells (Rattanaburee et al., 2019). Interestingly, not only on breast cancer cells that *trans*-(±)-kusunokinin showed potential cytotoxicity but also on colon, cholangiocarcinoma and ovarian cancer cells (Rattanaburee et al., 2019 and Mad-adam et al., 2022). Computational analysis of *trans*-(–)-bursehernin, a structure similar to *trans*-(–)-kusunokinin, showed that could bind strong affinity with the colony-stimulating factor 1 receptor (CSF1R), which relates to the proliferation pathway and high expression in cancer tissue (Tedasen et al., 2017). Interestingly, *trans*-(–)-kusunokinin was predicted to bind to several target proteins, such as CSF1R, MMP-12, HSP90- α , CyclinB1 and MEK1. Among them, CSF1R revealed the best binding affinity. However, *in vitro* experimental proof revealed that *trans*-(±)-kusunokinin partially binds and suppresses CSF1R and AKT with a fairly different mechanism from pexidartinib, a CSF1R inhibitor (Rattanaburee et al., 2020). These results could be explained that *trans*-(+)-kusunokinin, another enantiomer form, showed less binding affinity (Chompunud Na Ayudhya et al., 2022) leading to a racemic *trans*-(±)-kusunokinin exhibited the half inhibition effect on CSF1R. It was postulated that *trans*-(±)-kusunokinin may exert anti-cancer properties by targeting multiple proteins. Thus, this investigation aims to ascertain and validate the specific target protein of kusunokinin that plays a pivotal role in the progression of breast and ovarian cancer cells, employing both in *silico* and *in vitro* methodologies. The outcomes of this research endeavor may furnish insights into the mechanistic actions of kusunokinin and potentially contribute to the development of anti-cancer agents in the foreseeable future.

1.2 Literature reviews

1.2.1 Breast and ovarian cancers

Breast cancer is the most common female cancer. Breast cancer was the second leading cause of cancer-related deaths among women in Thailand and worldwide. However, the recent trend in incidence and mortality rates has increased considering the world age-standardized incidence rate (ASR) of 47.8 and the world age-standardized mortality rate (ASMR) of 13.6, which are the first and second ranking in

2020, respectively (Figure 1A). In Thailand, breast cancer has a first-ranking ASR of 37.8 and a third-ranking ASMR of 12.7 (Figure 1B) (Sung et al., 2021).

The origins of breast cancer are ducts and lobules (Figure 2A). The major classification is between in situ and invasive carcinoma, which differs from the proliferation of cancer cells in the epithelial tissue with or without invasion of the basement membrane and surrounding tissue. There are four types of breast cancer that are classified by the receptor status of estrogen receptor (ER), progesterone receptor (PR), and human epidermal growth factor receptor 2 (HER2): luminal A, luminal B, HER2-enriched, and basal-like or triple-negative breast cancer (TNBC). Breast cancer treatment is based on receptor status; patients who have ER+ and PR+ will be treated with hormonal therapy; patients who have HER2 overexpression will be treated with anti-HER2; and patients with triple-negative will be treated with chemotherapy only (Figure 2B) (Goldhirsch et al., 2011).

Recently, ovarian cancer incidence and mortality rates have been ranked in the top 10 of ASR and ASMR in Thailand and worldwide in 2020 (Figure 1) (Sung et al., 2021). Ovarian cancer can be classified into 3 major categories according to the anatomic structures from which the tumors originate: Epithelial ovarian cancer, germ cell tumor, and sex cord-stromal tumor. Epithelial ovarian cancer is the most common, accounting for about 90% of all ovarian cancer and found that chemotherapy regimens are different from those for germ cell and sex cord-stromal tumor groups (Figure 3) (Chen et al., 2003).

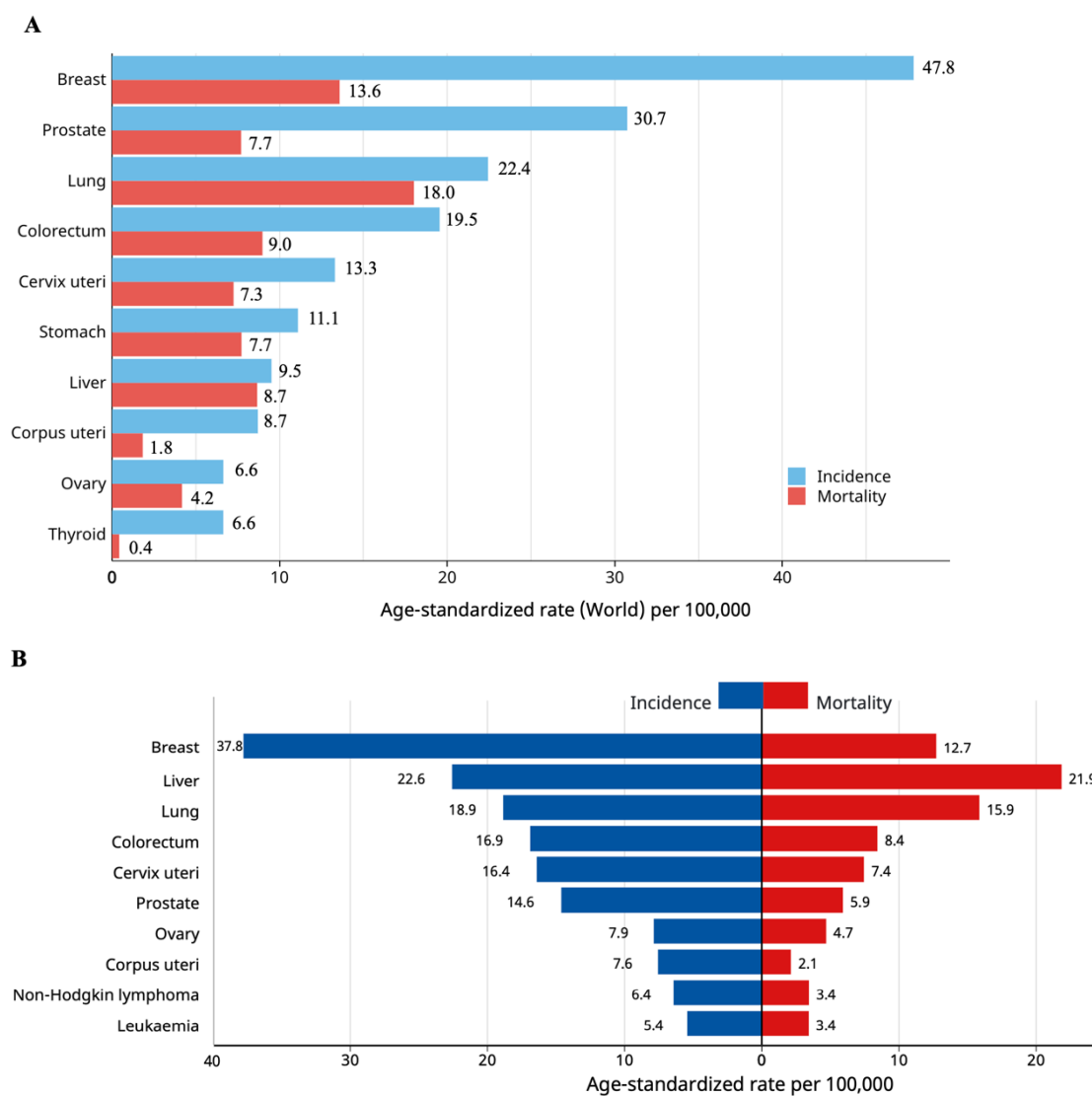


Figure 1. Estimated age-standardized incidence and mortality rates in 2020, both sexes, all ages in (A) Worldwide (B) Thailand (Sung et al., 2021).

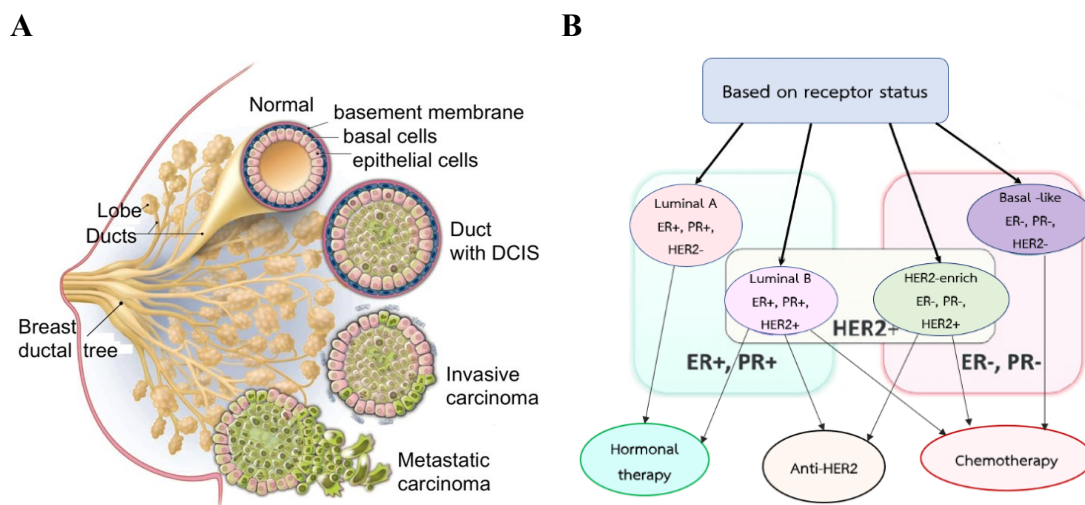


Figure 2. Breast cancer (A) Origin of breast cancer (B) Breast cancer classification based on receptor status (Goldhirsch et al., 2011).

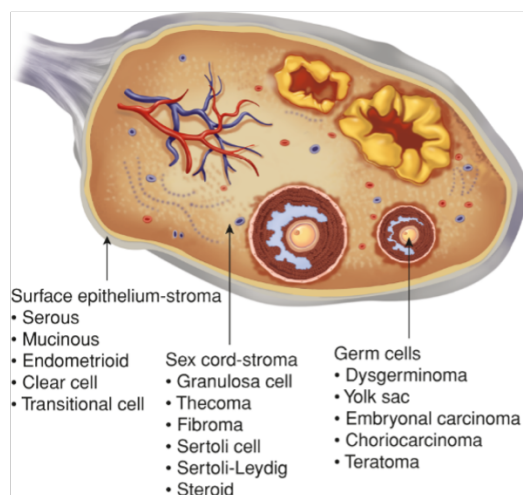


Figure 3. Ovarian cancer origin and classification (Chen et al., 2003).

1.2.2 Breast cancer progression pathway

Breast cancer subtypes exhibit distinct molecular pathways (Figure 4). Hormone receptor-positive subtypes, specifically ER⁺ and HER⁺ breast cancers, are primarily driven by ER or HER receptors, which regulate cellular proliferation and growth. In the case of ER⁺ breast cancer, the common treatment approach involves inhibiting estrogen synthesis. Medications such as tamoxifen and letrozole are employed for the management of ER⁺ cancer (Jordan et al., 1993; Nabholz et al., 2008). HER⁺ breast cancer, on the other hand, is characterized by HER2 activation of the PI3K/AKT and Ras/MAPK/ERK

pathways, leading to signaling cascades that stimulate cell proliferation, survival, and differentiation. As a result, monoclonal antibodies targeting HER2, including trastuzumab and pertuzumab, assume critical roles in the treatment regimen (Albanell et al., 2003). Conversely, triple-negative breast cancer (TNBC), an aggressive subtype lacking ER, HER2, and PR expression, engages various signaling pathways such as EGFR, Trop2, and Wnt/ β -catenin in its regulatory mechanisms. Although chemotherapeutic agents constitute the primary approach for TNBC treatment, therapeutic resistance remains a challenge. Therefore, the consideration of combining the monoclonal antibody sacituzumab govitecan with chemotherapeutic drugs has been proposed to enhance treatment efficacy (Bardia et al., 2019). Additionally, the presence of BRCA1/2 mutations in breast cancer gives rise to hereditary breast and ovarian cancer syndrome (HBOC). These mutations impair DNA repair mechanisms, leading to abnormal repair of damaged DNA. The standard treatment for HBOC involves the use of PARP inhibitors, which capitalize on defective DNA repair processes to induce cell death in affected cells.

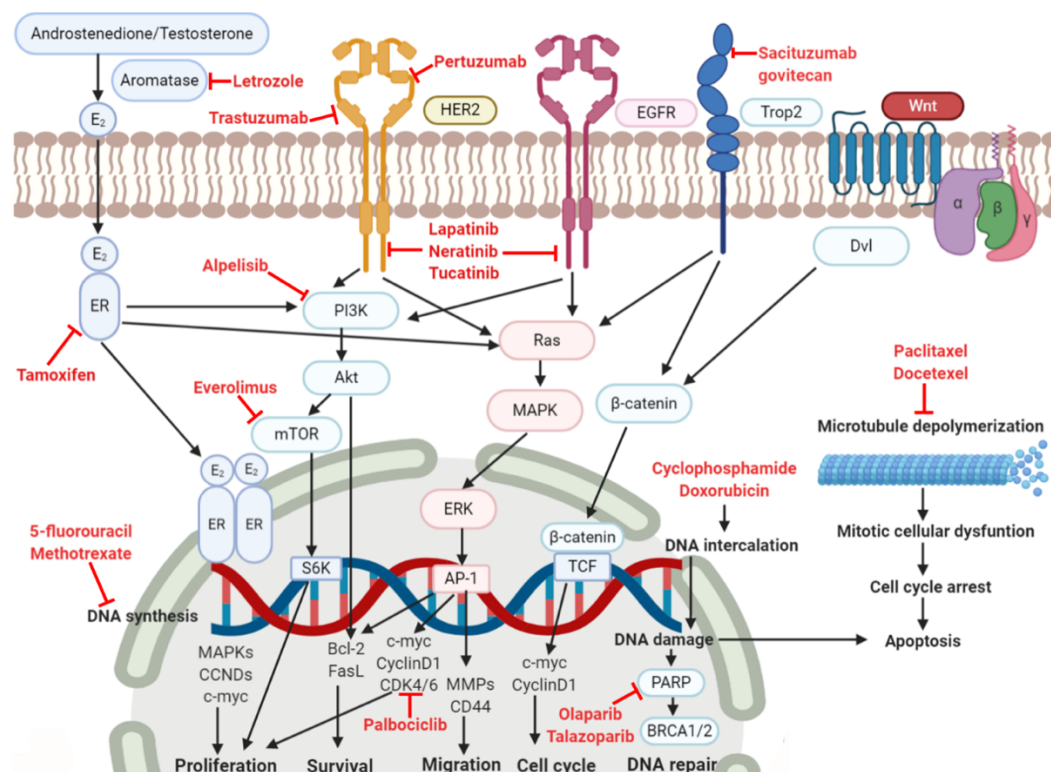


Figure 4. Breast cancer pathway and molecular mechanism of drugs for breast cancer treatment.

1.2.3 Ovarian cancer progression pathway

Ovarian carcinogenesis is generally associated with HER2 overexpression that activates PI3K/AKT and Ras/MAPK/ERK signaling, leading to cell proliferation, survival and invasion. Moreover, the VEGFR pathway plays an important role in angiogenesis. Hence, the inhibition of VEGFR by bevacizumab is the vital approach for primary systemic therapy of fallopian tube/epithelial ovarian cancer. Besides, patients with NRTK gene-fusion-positive tumors that highly activate the Trk receptor are encouraged to receive treatment with entrectinib or larotrectinib. Furthermore, PARP inhibitors are considered in HBOC patients because the BRCA1/2 mutation leads to abnormal repair of the damaged DNA. However, chemotherapy is commonly considered for first- or second-line drugs that usually target DNA and microtubules. These drugs have similar mechanisms of action: they attach an alkyl group to DNA, resulting in DNA cross-linking, DNA fragmentation and abnormal base pairing, leading to DNA synthesis inhibition and cell death at last. While, targeting microtubules, drugs drive mitotic spindle dysfunction, leading to cell cycle arrest and cell apoptosis (Figure 5) (Morgan et al., 2016).

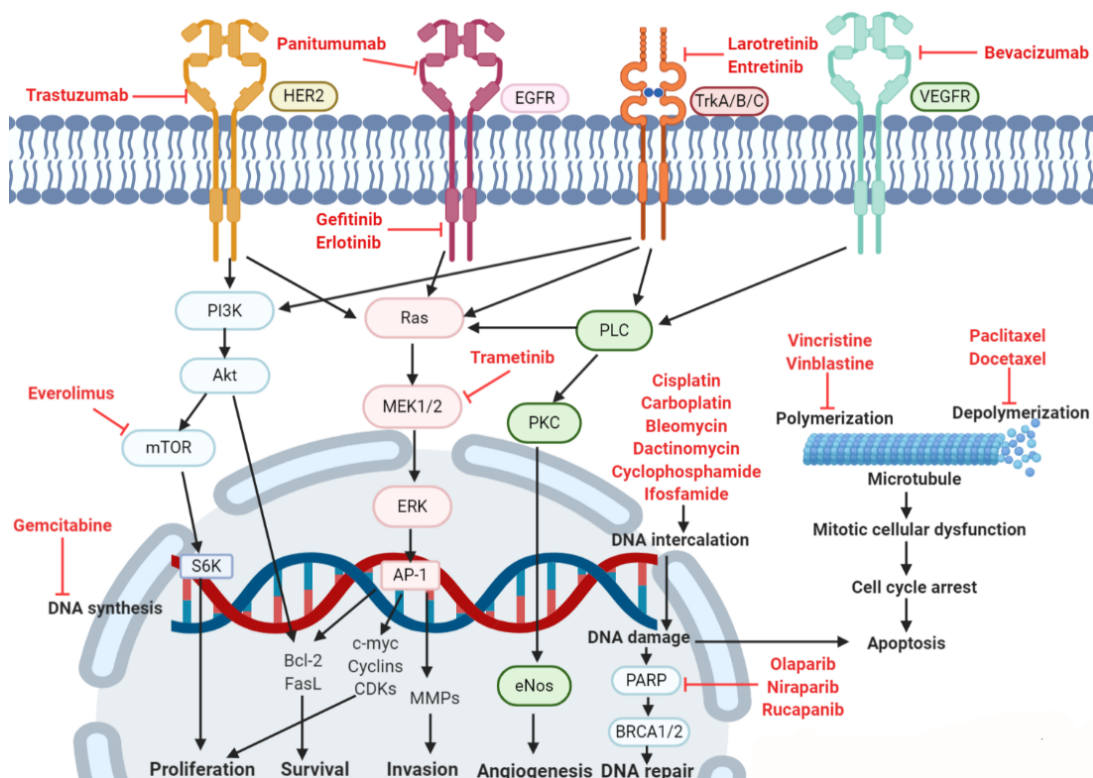


Figure 5. Ovarian cancer pathway and molecular mechanism of drugs for ovarian cancer treatment.

1.2.4 Targets of breast and ovarian cancer drugs and mechanism of action

1.2.4.1 Estrogen receptor: Tamoxifen

Tamoxifen is a nonsteroidal triphenylethylene derivative employed for the treatment of estrogen receptor-positive breast cancers and for the prevention of breast cancer incidence in individuals at high risk (Figure 6). Its mechanism of action revolves around binding to the estrogen receptor, thereby obstructing estrogen's proliferative effects on the mammary epithelium. Tamoxifen's impact includes an elevation in sex hormone binding globulin and a reduction in tumor growth factor and insulin-like growth factor levels. The surge in sex hormone-binding globulin confines the availability of free estradiol, curtailing the presence of substances that stimulate tumor growth. Furthermore, tamoxifen has been observed to induce apoptosis in estrogen receptor-positive cells. This effect is likely linked to the inhibition of protein kinase C, impeding DNA synthesis. An alternative explanation for tamoxifen's apoptotic influence involves a potential approximately three-fold elevation in intracellular and mitochondrial calcium ion concentrations upon administration or tumor growth factor production (Jordan, 1993).

1.2.4.2 Aromatase: Letrozole

Letrozole is an oral non-steroidal type II aromatase inhibitor prescribed for the treatment of hormone receptor-positive early breast cancer in postmenopausal women. It is also indicated for postmenopausal women with early breast cancer who have previously undergone tamoxifen therapy. This medication functions by obstructing the active site of aromatase, resulting in competitive inhibition and preventing the conversion of androgens to estrogen (Figure 6). This action prompts an elevation in luteinizing hormone levels and a reduction in uterine weight. Notably, the primary source of estrogen in postmenopausal women stems from the enzymatic activity of aromatase. The scarcity of estrogen, due to the inhibition of its production, leads to the regression of estrogen-dependent cancers (Nabholtz, 2008).

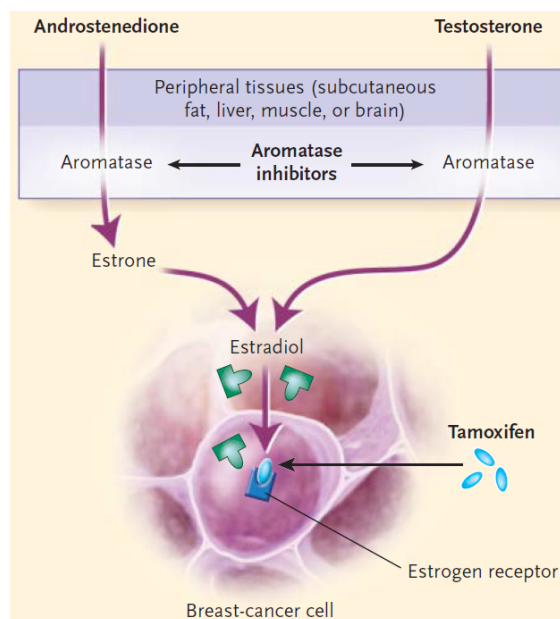


Figure 6. Mechanism of action of tamoxifen and aromatase inhibitors (Nabholtz, 2008).

1.2.4.3 DNA

1.2.4.3.1 Alkylating agents

Alkylating agents are chemotherapeutic drugs that are not specific to any particular phase of the cell cycle. They exert their effects by directly targeting DNA. Examples of these agents include nitrogen mustards such as cyclophosphamide and ifosfamide. Cyclophosphamide, a precursor of alkylating nitrogen mustard with antineoplastic and immunosuppressive properties, requires activation in the liver to form the active aldophosphamide through CYP450 metabolism. This drug has found utility in treating breast cancer, ovarian cancer, lymphoma, and leukemia. Cyclophosphamide operates through three distinct mechanisms. First, alkyl groups are attached to DNA bases, leading to DNA fragmentation when repair enzymes attempt to replace the alkylated bases. This interference hampers DNA synthesis and RNA transcription from the affected DNA. Second, cross-links (bonds between atoms in the DNA) form, causing DNA damage that prevents the separation necessary for synthesis or transcription. The third mechanism involves inducing nucleotide mispairing, culminating in the occurrence of mutations (Figure 7) (Roy et al., 1999).

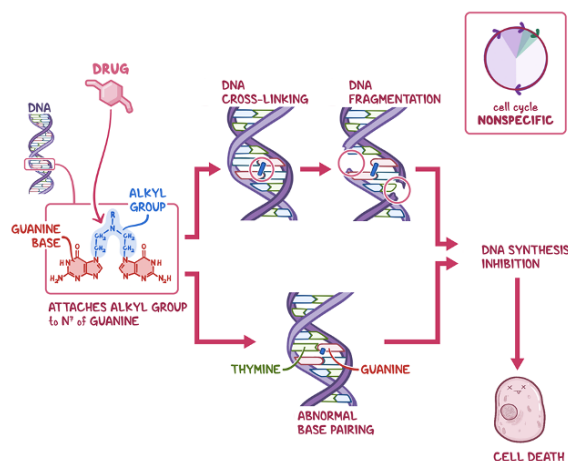


Figure 7. Mechanism of action of alkylating agents (Roy *et al.*, 1999).

1.2.4.3.2 Platinum-based agents

Platinum-based drugs, including cisplatin and carboplatin, are widely employed in the treatment of various cancer types, such as ovarian cancer, lymphomas, and germ cell tumors. They work similar to alkylating agents that attach to DNA leading to DNA cross-linking. Moreover, they can activate extrinsic pathway of apoptosis by increase the expression Fas and PD-L (Figure 8) (Theile, 2017).

1.2.4.3.3 Antibiotics agents

Bleomycin, derived from *Streptomyces verticillus*, is classified as a glycopeptide antibiotic. Its primary function lies in the inhibition of DNA metabolism, making it a valuable component in antineoplastic treatments targeting various cancers, including ovarian cancer, squamous cell carcinoma, and lymphomas. Bleomycin achieves its cytotoxic effects by binding to Fe²⁺, resulting in the generation of free radicals upon exposure to oxygen. These free radicals subsequently insert themselves between DNA strands, thereby inducing both single- and double-stranded breaks in the DNA structure (Figure 9) (Bardal *et al.*, 2011).

1.2.4.3.4 Antimetabolites

Antimetabolites are the cell cycle-specific chemotherapeutic drugs that interrupt the cell cycle in S phase by hinder the metabolism of DNA synthesis for example, 5-fluorouracil, gemcitabine, and methotrexate (Figure 10) (Kim, 2020).

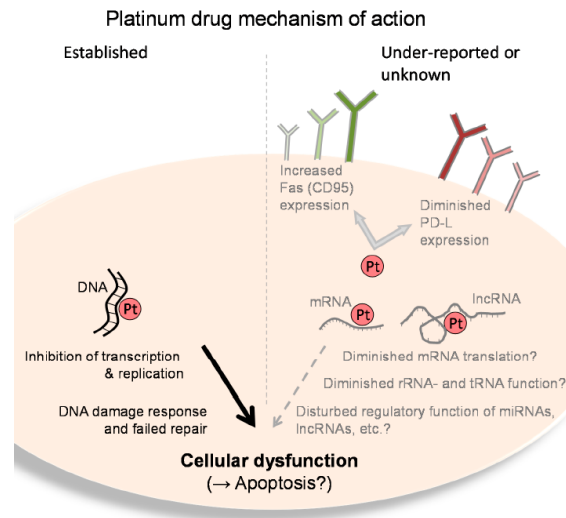


Figure 8. Mechanism of action of platinum-based agents (Theile, 2017).

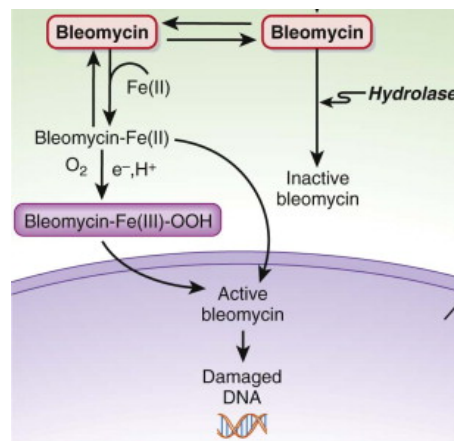


Figure 9. Mechanism of action of bleomycin (Bardal et al., 2011).

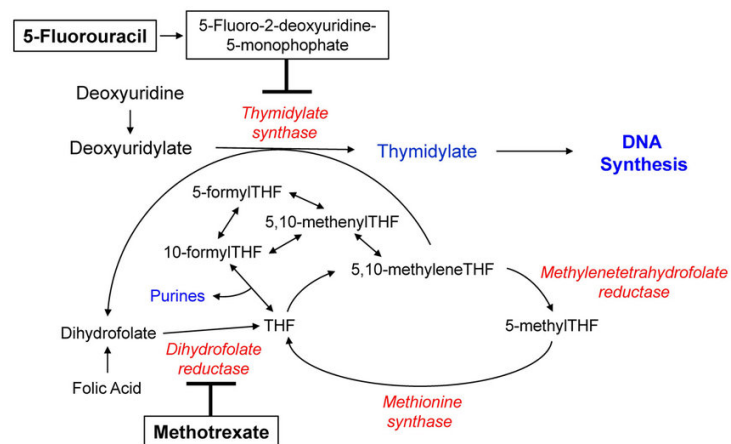


Figure 10. Mechanism of action of antimetabolites (Kim, 2020).

1.2.4.4 Topoisomerase: etoposide

Etoposide, a semi-synthetic derivative derived from podophyllotoxin, possesses significant anticancer properties. Its mechanism of action involves interaction with topoisomerase II and DNA, leading to the inhibition of DNA synthesis. This interaction with topoisomerase II results in the formation of a complex that induces double-stranded DNA breaks and impedes their repair. The accumulation of these DNA breaks prevents the cell from progressing into the mitotic phase of cell division, ultimately leading to cell death (Figure 11). Etoposide primarily exerts its effects during the G2 and S phases of the cell cycle. Clinically, etoposide finds application in the treatment of various cancers. It is used in combination with other chemotherapeutic agents for treating refractory testicular tumors and serves as a first-line treatment for patients with small cell lung cancer. Additionally, etoposide is employed in the management of other malignancies, including ovarian cancer, lymphoma, non-lymphocytic leukemia, and glioblastoma multiforme (Yousefzadi et al., 2010; Jain et al., 2017).

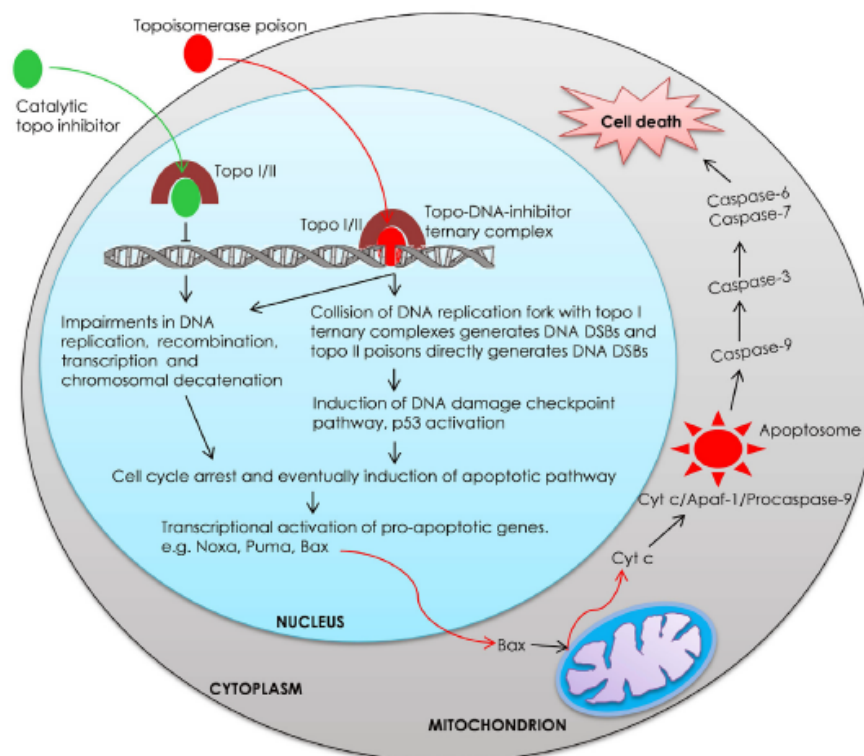


Figure 11. Mechanism of action of topoisomerase inhibitor (Jain et al., 2017).

1.2.4.5 Microtubule

1.2.4.5.1 Taxane-diterpenes: paclitaxel and docetaxel

Paclitaxel is a taxane-diterpene from *Taxus baccata*. (European yew) and *Taxus brevifolia*. (Pacific yew) while docetaxel is semisynthetic derivative of paclitaxel. Both drugs contribute to tubulin dimers forming microtubules and stabilize them by avoiding depolymerization. This stability prevents the microtubule network's dynamic rearrangement, which is necessary for crucial interphase and mitotic cellular processes leading to cell cycle arrest and cell death by apoptosis at last (Figure 12). They are used for combination treatment of advanced or metastatic breast cancer, ovarian cancer and non-small cell lung carcinoma (Lichota and Gwozdziński, 2018).

1.2.4.5.2 Vinca-alkaloids: vincristine and vinblastine

Vincristine and vinblastine are vinca-alkaloids isolated from *Catharanthus spp.* or *Vinca spp.* They inhibit microtubule polymerization by promoting a curved conformation or inhibiting a straightened conformation necessary for proper microtubule formation, leading to mitotic arrest or cell death (Figure 12). Vincristine and vinblastine are indicated for the treatment of ovarian cancer, breast cancer, Hodgkin's disease, Kaposi's sarcoma, and testicular cancer (Lichota and Gwozdziński, 2018).

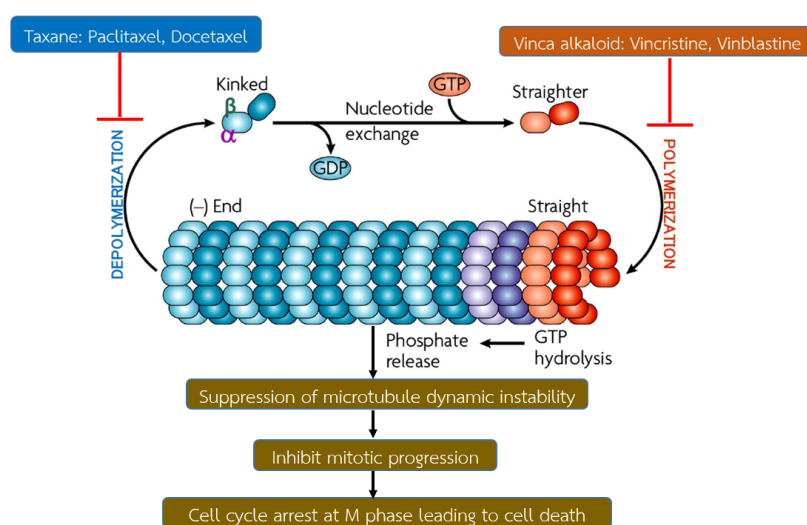


Figure 12. Mechanism of action of taxane-diterpenes and vinca alkaloids (Lichota and Gwozdziński, 2018).

1.2.4.6 HER2: Trastuzumab

Trastuzumab has a strong and specific binding affinity for the extracellular domain of the human epidermal growth factor receptor protein, HER2. It is primarily used to treat HER2-positive breast cancer, which occurs when the HER2 gene is amplified or the HER2 protein is overexpressed in tumor cells. Approximately 20-30% of breast tumors show this genetic alteration, leading to excessive HER2 activation. This heightened activation triggers abnormal cell proliferation through downstream signaling pathways like Ras/Raf/MAPK/ERK and PI3K/Akt. Trastuzumab works by binding to HER2, inhibiting cancer cell growth, proliferation, and survival (Figure 13) (Albanell et al., 2003).

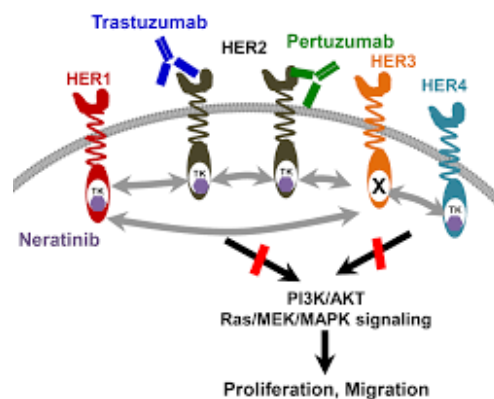


Figure 13. Mechanism of action of trastuzumab (Albanell et al., 2003).

1.2.4.7 Trop2: Sacituzumab govitecan

Tumor-associated calcium signal transducer 2 (Trop2) is a transmembrane glycoprotein that plays an importance role in metastasis in various cancer such as, breast cancer and ovarian cancer. Sacituzumab govitecan, a selective Trop2 inhibitor, is recommend for metastatic triple-negative breast cancer treatment (Bardia et al., 2019).

1.2.4.8 VEGFR: Bevacizumab

Bevacizumab selectively binds to VEGFR that plays an importance role in angiogenesis through PLC/PKC/eNos pathway. The indication of bevacizumab is stage I/II of fallopian tube/epithelial ovarian cancer treatment (Morgan et al., 2016).

1.2.4.9 TrkA/B/C receptor: entrectinib

Entrectinib is a Trk inhibitor that encourage to use in recurrent platinum-resistant epithelial ovarian cancer patient who has a *NRTK* gene-fusion positive. Trk is a tyrosine kinase receptor that plays an importance role in cell proliferation, cell survival, cell invasion through the signaling pathway of PI3K/AKT and Ras/MEK/ERK (Morgan et al., 2016).

1.2.4.10 EGFR: gefitinib

EGFR is a tyrosine kinase receptor that plays an importance role in cancer cell proliferation. Gefitinib is the one of EGFR inhibitors that used as combination treatment with cisplatin in ovarian cancer patient with EGFR overexpression. (Yuan et al., 2014).

1.2.4.11 PARP: olaparib

PARP plays an importance role in DNA repair which regulate BRCA1/2. Olaparib is the one of PARP inhibitor that used in hereditary breast and ovarian cancer syndrome (HBOC), patient with BRCA1/2 mutation (Morgan et al., 2016).

1.2.5 General treatment of breast and ovarian cancer

In general, a surgery is considered for both breast and ovarian cancers treatment. In breast cancer, removing the tumor with preserving breast (Lumpectomy) or entire breast (Mastectomy) will be done depending on the condition of patient. In ovarian cancer, surgical treatment regularly removes both ovaries and fallopian tubes that called bilateral salpingo-oophorectomy including uterus that called hysterectomy (Morgan et al., 2016). In addition, radiation therapy is also recommended in patient who have a larger tumor. Given after surgery is most commonly whereas given before surgery is only considered when a tumor cannot be removed with surgery. However, the spreading of cancer cell into lymph vessel and circulation hinders the achievement of treatment. Hence, systemic treatments of drugs play an important role in cancer treatment (Sangkhatat et al., 2017).

1.2.6 Drugs for breast cancer treatment

Chemotherapeutic, hormonal, and targeted drugs for breast cancer treatment are used depending on the subtype and stage of breast cancer (Table 1).

Table 1. Drugs for breast cancer treatment.

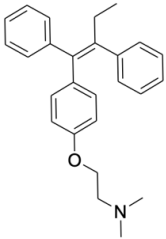
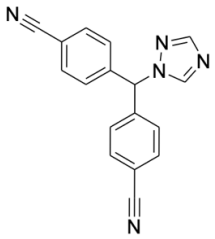
Drugs	Target and mechanism of action	Indication	References
<p data-bbox="185 459 454 496">Hormonal therapy</p> <p data-bbox="241 515 398 547">Tamoxifen</p> 	<p data-bbox="477 515 1144 826">It binds to the estrogen receptor and blocks the proliferative actions of estrogen on mammary epithelium leading to reduce levels of factors that stimulate tumor growth. It also induces apoptosis through the inhibition of protein kinase C leading to DNA synthesis prevention.</p>	<p data-bbox="1167 515 1693 826">Tamoxifen is indeed a commonly used treatment for premenopausal patients with early-stage and metastatic breast cancer who have estrogen receptor-positive (ER+) tumors, including subtypes luminal A and luminal B.</p>	<p data-bbox="1715 515 1951 547">Jordan et al., 1993</p>
<p data-bbox="253 855 387 887">Letrozole</p> 	<p data-bbox="477 855 1144 1054">It blocks the active site of aromatase enzyme and shows competitive inhibition preventing the conversion of androgens to estrogen leading to a reduction in uterine weight.</p>	<p data-bbox="1167 855 1693 1158">Letrozole is a medication commonly used in the treatment of postmenopausal women with hormone receptor-positive early breast cancer. It is also prescribed for postmenopausal women who have previously been treated with tamoxifen.</p>	<p data-bbox="1715 855 1984 887">Nabholtz et al., 2008</p>

Table 1. Drugs for breast cancer treatment (continued).

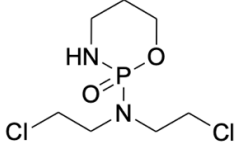
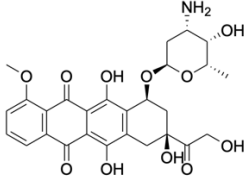
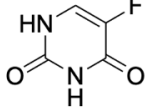
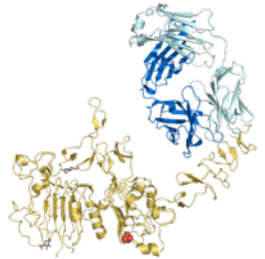
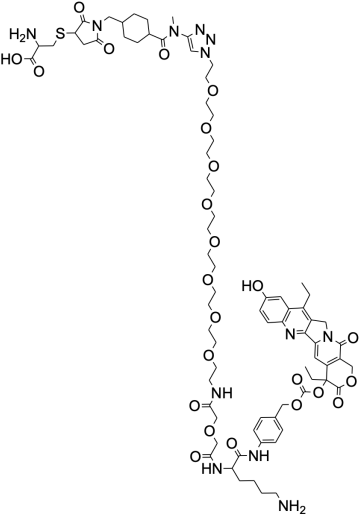
Drugs	Target and mechanism of action	Indication	References
<p>Chemotherapy</p> <p>Cyclophosphamide</p> 	<p>Cyclophosphamide's metabolites attach alkyl groups to DNA bases, leading to several disruptive effects on DNA such as, DNA fragmentation, inhibition of DNA synthesis, RNA transcription inhibition, formation of DNA cross-links, nucleotide mispairing and mutations.</p>	<p>Cyclophosphamide is an adjuvant chemotherapy for early stage and metastatic stage of breast cancer with the combination of other chemotherapeutic drugs.</p>	<p>Roy et al., 1999</p>
<p>Doxorubicin</p> 	<p>Doxorubicin exerts its cytotoxic effects primarily by intercalating into DNA molecules. This intercalation disrupts the normal structure and function of DNA, leading to several cellular consequences, including, DNA damage, inhibition of DNA replication, induction of apoptosis and generation of reactive oxygen species.</p>	<p>Doxorubicin is an adjuvant chemotherapy for early and metastatic stage of breast cancer.</p>	<p>Goldhirsch et al., 2011</p>
<p>5-fluorouracil</p> 	<p>Uracil is replaced by the active metabolite 5-fluoroxymethyluridine monophosphate, which prevents RNA processing and limits cell development. Thymidylate is inhibited by the active metabolite 5-fluoro-2'-deoxyuridine-5'-O-monophosphate.</p>	<p>5-Fluorouracil is indeed used in the treatment of breast cancer, particularly as part of adjuvant chemotherapy regimens for both early-stage and metastatic breast cancer.</p>	<p>Goldhirsch et al., 2011</p>

Table 1. Drugs for breast cancer treatment (continued).

Drugs	Target and mechanism of action	Indication	References
<p data-bbox="280 464 465 491">Trastuzumab</p> 	<p data-bbox="584 464 1196 719">Trastuzumab selectively binds with high affinity to the extracellular domain of the HER2 and suppresses cancer cells growth, proliferation, and survival through HER2 downstream signaling such as Ras/Raf/MAPK/ERK and PI3K/Akt signaling.</p>	<p data-bbox="1227 464 1688 719">Trastuzumab is used as a treatment of HER2 positive breast cancer, where there is a proven amplification of the HER2 oncogene or overexpression of the HER2 protein in tumors.</p>	<p data-bbox="1720 464 1973 491">Albanell et al., 2003</p>
<p data-bbox="219 810 533 837">Sacituzumab govitecan</p> 	<p data-bbox="584 810 1196 1278">Its mechanism of action involves the targeted delivery of a potent chemotherapy drug to cancer cells overexpressing TROP2, thereby inhibiting cancer cell growth and promoting cell death. This targeted approach represents an important advancement in cancer treatment, especially for patients with metastatic triple-negative breast cancer and metastatic urothelial cancer.</p>	<p data-bbox="1227 810 1688 1007">Sacituzumab govitecan is approved for the treatment of metastatic triple-negative breast cancer and metastatic urothelial cancer.</p>	<p data-bbox="1720 810 1951 837">Bardia et al., 2019</p>

1.2.7 Drugs for ovarian cancer treatment

Chemotherapy is a common recommendation for the first/second-line drugs of ovarian cancer treatment. These drugs usually work similar mechanism of action by targeting DNA and microtubule. A few of usage of targeted therapy as show in Table 2.

Table 2. Drugs for ovarian cancer treatment.

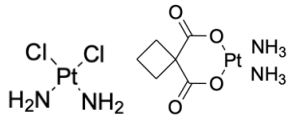
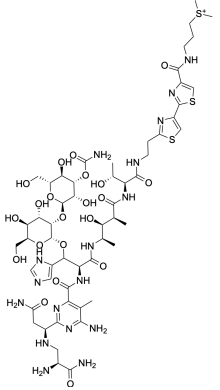
Drugs	Target and mechanism of action	Indication	References
<p>Chemotherapy</p> <p>Cisplatin/Carboplatin</p> 	<p>Cisplatin and carboplatin work similar to alkylating agents that attach to DNA leading to DNA cross-linking. Moreover, they can activate extrinsic pathway of apoptosis by increase the expression Fas and PD-L.</p>	<p>Cisplatin and carboplatin are commonly used in the treatment of various cancers, including ovarian cancer and lung cancer.</p>	<p>Theile et al., 2017</p>
<p>Bleomycin</p> 	<p>Bleomycin forms a complex with Fe^{2+}, and when exposed to oxygen, this complex triggers the generation of free radicals. Subsequently, these free radicals insert themselves between the strands of DNA, resulting in the creation of both single-stranded and double-stranded breaks within the DNA molecule.</p>	<p>Bleomycin is a first-line/adjuvant chemotherapy in malignant ovarian germ cell tumors and malignant sex cord-stromal tumors.</p>	<p>Brown et al., 2005</p>

Table 2. Drugs for ovarian cancer treatment (continued).

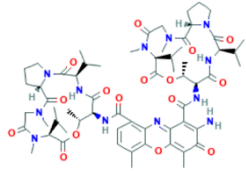
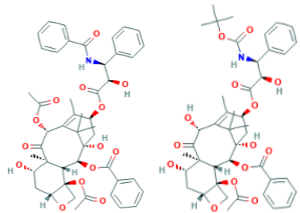
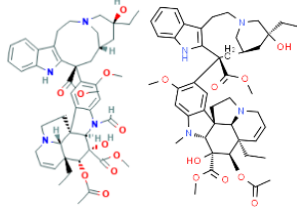
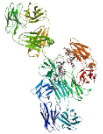
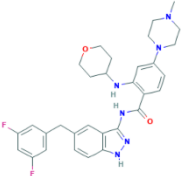
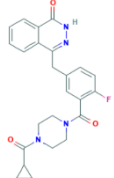
Drugs	Target and mechanism of action	Indication	References
<p data-bbox="248 427 448 456">Dactinomycin</p> 	<p data-bbox="533 427 1218 679">Dactinomycin causes guanine-cytosine intercalation leading to prevention of RNA polymerase from transcription of DNA. Additionally, it results in DNA breakage, presumably as a result of an interaction with topoisomerase II or a free radical intermediate.</p>	<p data-bbox="1249 427 1711 624">Dactinomycin is a first line/adjuvant chemotherapy in malignant ovarian germ cell tumors and malignant sex cord-stromal tumors.</p>	<p data-bbox="1742 427 1951 456">Hadi et al., 2020</p>
<p data-bbox="203 710 492 738">Paclitaxel/ Docetaxel</p> 	<p data-bbox="533 710 1218 1015">Paclitaxel and docetaxel target microtubules by promoting the assembly of microtubules from tubulin dimers and stabilizing microtubules by preventing depolymerization. Resulting in mitotic cellular functions leading to cell cycle arrest and cell death by apoptosis.</p>	<p data-bbox="1249 710 1711 959">Paclitaxel is the first/second-line adjuvant/neoadjuvant in epithelial ovarian cancer. While docetaxel is an adjuvant chemotherapy for early stage of breast cancer.</p>	<p data-bbox="1742 710 1989 738">Lichota et al., 2018</p>
<p data-bbox="188 1045 501 1074">Vincristine/Vinblastine</p> 	<p data-bbox="533 1045 1218 1294">Vincristine and vinblastine target microtubules and inhibit microtubule polymerization by promoting a curved conformation or inhibiting a straightened conformation necessary for proper microtubule formation, leading to mitotic arrest or cell death.</p>	<p data-bbox="1249 1045 1711 1350">Vincristine and vinblastine are used for the treatment of malignant ovarian germ cell tumors and malignant sex cord stromal tumors. However, a combination with other chemotherapeutic drugs is required.</p>	<p data-bbox="1742 1045 1989 1074">Lichota et al., 2018</p>

Table 2. Drugs for ovarian cancer treatment (continued).

Drugs	Target and mechanism of action	Indication	References
Targeted therapy			
Bevacizumab 	Selectively binds to VEGFR that plays an importance role in angiogenesis	Stage II-IV epithelial ovarian cancer	Morgan et al., 2016
Entrectinib 	Inhibit TrkA/B/C receptor	NRTK gene-fusion positive tumors in recurrent platinum-resistant epithelial ovarian cancer	Morgan et al., 2016
Olaparib 	Inhibitor of the nuclear enzyme poly(ADP-ribose) polymerase (PARP)	Hereditary breast and ovarian cancer syndrome (HBOC) patient with BRCA1/2 mutation	Morgan et al., 2016

1.2.8 Aldo-keto reductase family 1 member B1 (AKR1B1)

Aldo-keto reductase family 1 member B1 (AKR1B1) is a NADPH-dependent enzyme that catalyzes various substrates, including retinal (Crosas et al., 2003), glucose, glyceraldehyde (Hamada et al., 1991), and prostaglandin H₂ (Nagata et al., 2011). AKR1B1 is a metabolic enzyme that upregulates gene expression by the signaling from Triiodothyronine (T₃) binding with thyroid hormone receptor alpha (TR_α) or thyroid hormone receptor beta (TR_β) and heterodimerizes with retinoid X receptor (RXR) located on thyroid hormone response elements (Chi et al., 2013).

AKR1B1 plays an important role in cell proliferation and the aggressiveness of various human cancers. Ramana and colleagues reveal that the inhibition of AKR1B1 hinders epidermal growth factor (EGF) and fibroblast growth factor (FGF)-induced colon cancer cell proliferation by inhibiting G1/S phase transition through the PI3K/AKT pathway. Inhibition of AKR1B1 also prevented DNA binding activity of E2F-1, the phosphorylation of cyclin-dependent kinase 2 and retinoblastoma protein (pRb), and the expression of G1/S transition regulatory proteins such as cyclin D1, cyclin E and c-myc (Figure 14A) (Ramana et al., 2010). Moreover, AKR1B1 is highly expressed in triple negative breast cancer and is associated with aggressive metastasis. AKR1B1 expression is induced by the transcription of Twist2. It converts PGH₂ to PGF_{2α} that relays NF-κB activation leading to up-regulation of Twist2 expression in consequence of the positive feedback loop that activates the epithelial–mesenchymal transition process (Wu et al., 2017) (Figure 14B).

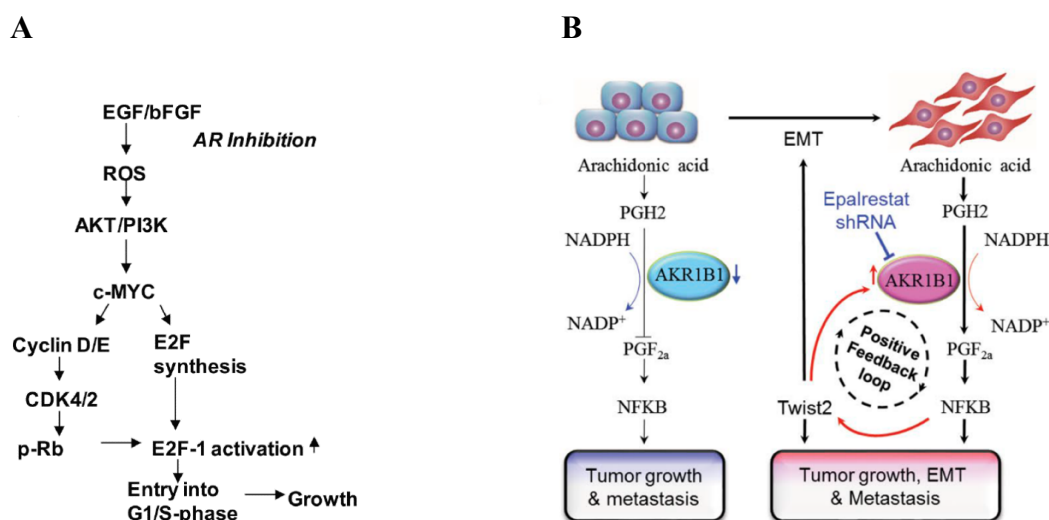


Figure 14. Role of AKR1B1 signaling in cancer **(A)** AKR1B1 regulation in colon cancer cell proliferation **(B)** The regulation of EMT by AKR1B1 through a positive feedback loop leading to tumorigenicity and metastasis on triple negative breast cancer (Ramana et al., 2010; Wu et al., 2017).

1.2.9 Aldose reductase inhibitors (ARIs)

According to the extreme attempt to develop an effective drug for targeting AKR1B1, only some aldose reductase inhibitors (ARIs) can hit clinical trials. Generally, ARIs can be classified into two groups based on their structure. Carboxylic acid-containing ARIs, the largest group of ARIs, exhibit activity through carboxylate anion head groups that are suitable for insertion into the anion binding pocket of ARIs and aromatic moiety, which stabilizes orientation in the hydrophilic domain (Chatzopoulou et al., 2012). As a result of their severe hepatotoxic side effects, several carboxylic acid-containing ARIs, including alrestatin, tolrestat, zenarestat, and zopolrestat, were discontinued. Hydantoin containing ARIs, another ARI that has a hydantoin ring combined with a chroman ring to form the rigid structure, such as sorbinil, fidalrestat, minalrestat, and ranirestat. However, hypersensitivity reactions are usually found in these drugs (Sarges et al., 1988; Lipinski et al., 1992). Among of them, only epalrestat is marketed and used to treat diabetic neuropathy in Asian countries (Hotta et al., 2008) and used for metastatic triple-negative breast cancer in a clinical trial (Khaled et al., 2019). However, as a result of the withdrawal in other

countries, its low effectiveness and adverse effects continue to be an issue. Hence, the exploration of new ARIs with high efficacy and less toxic is still important. Recently, only a few ARIs that the researcher investigates their anticancer activity as show in Table 3 and Figure 15.

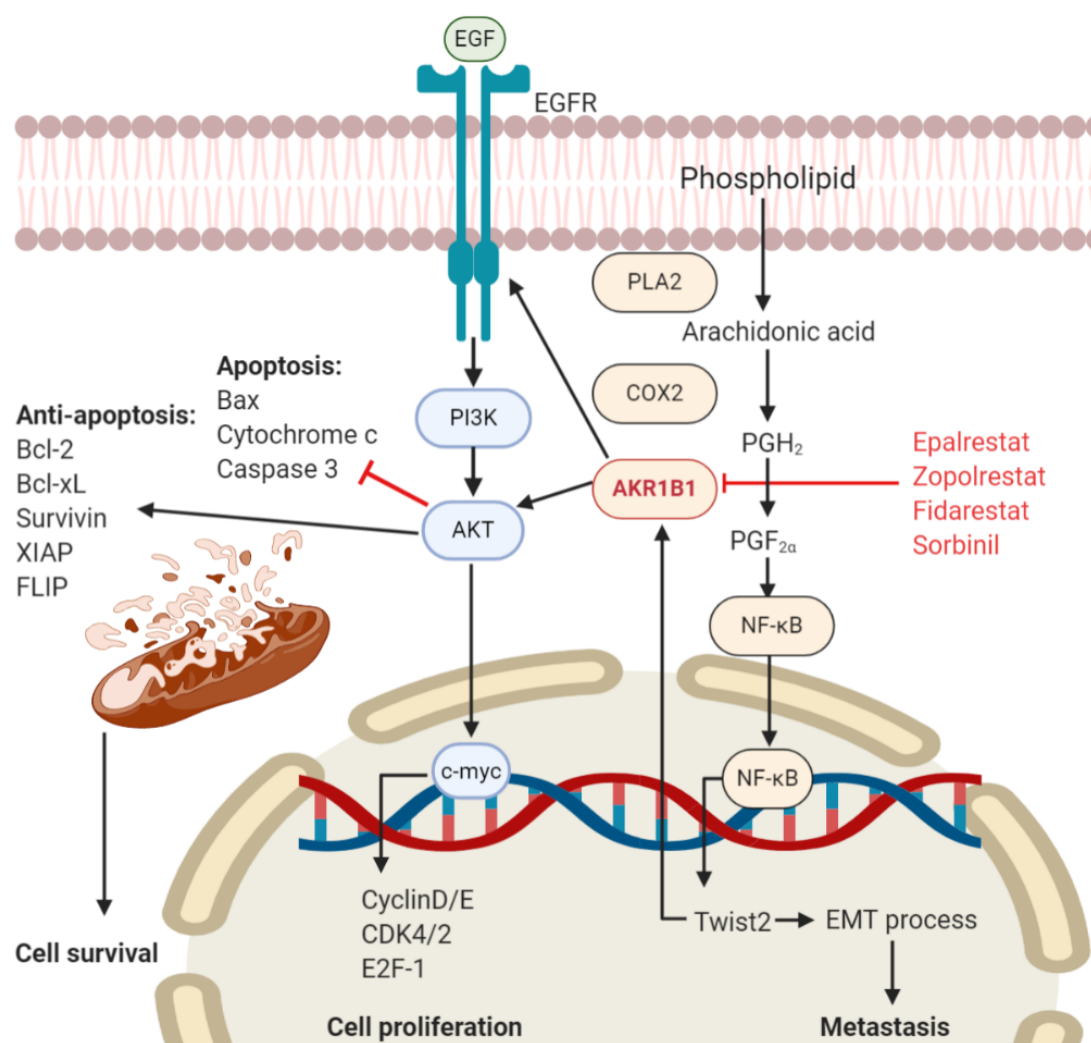


Figure 15. Molecular mechanism of action of ARIs in anticancer activity.

Table 3. Aldose reductase inhibitors (ARIs) with anticancer effects *in vitro* and *in vivo* experiments.

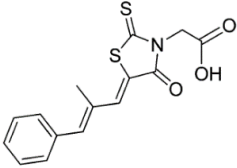
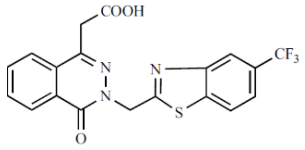
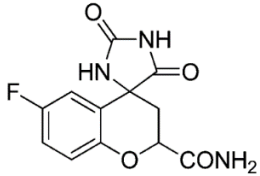
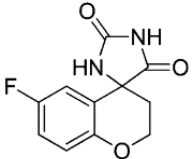
Drugs	Description	Adverse effects	References
<p data-bbox="264 483 409 515">Epalrestat</p> 	<ul style="list-style-type: none"> - Triple-negative breast cancer treatment (phase II clinical trial) - Suppressed invasion and migration on MDA-MB231 and SUM159 - Tumor size reduction and suppression of lung tumor spread - Targeted co-delivery with doxorubicin increased apoptosis and cell cycle arrest in the G2/M phase on MDA-MB-231 and 4T1 	<p>Hepatic dysfunction, Elevation of aspartate transaminase and alanine transaminase</p>	<p>Wu et al., 2010, Ramirez et al., 2008 Banala et al., 2019</p>
<p data-bbox="253 868 421 900">Zopolrestat</p> 	<p>- Prevented EGF and bFGF-induced DNA binding activity of E2F-1 and phosphorylation of retinoblastoma protein on colon cancer cell</p>	<p>Liver and renal toxicity</p>	<p>Ramana et al., 2010 Maccari et al., 2015</p>

Table 3. Aldose reductase inhibitors (ARIs) with anticancer effects *in vitro* and *in vivo* experiments (continued).

Drugs	Description	Adverse effects	References
<p>Fidarestat</p> 	<ul style="list-style-type: none"> - Decreased the expression of anti-apoptotic proteins including, Bcl-xL, Bcl-2, survivin, XIAP and FLIP - Increased the expression of pro-apoptotic proteins leading to release of cytochrome c and activation of caspases-3 - Activated the forkhead transcription factor FOXO3a to control AKT/PI3K signaling 	Hypersensitivity reaction	Shoeb et al., 2013
<p>Sorbinil</p> 	<ul style="list-style-type: none"> - Prevented retinoblastoma protein phosphorylation and EGF and bFGF-induced DNA binding activity of E2F-1 on colon cancer cells 	Hypersensitivity reaction	Ramana et al., 2010 Maccari et al., 2015

1.2.10 Lignans

Lignans, the natural plant products which are biosynthesized through shikimate pathway that provides aromatic compounds, especially l-phenylalanine which is the precursor to form lignans by multi-process of shikimate pathway. Briefly, phosphoenolpyruvate (PEP) from the glycolytic pathway and D-erythrose 4-phosphate from the pentose phosphate cycle are incorporated to biosynthesize shikimic acid. Then, it turns to chorismic acid which is an important initiator molecule in aromatic amino acids L-phenylalanine and L-tyrosine (Figure 16A). They are precursors of 4-hydroxycinnamyl alcohol, coniferyl alcohol and sinapyl alcohol that act as C₆C₃ unit (phenylpropanoid core) building blocks to form lignins and lignans. Lignans are characterized by dimeric C₆C₃ units linked at carbons 8 and 8' position whereas lignins are polymeric (Figure 16B) (Simpson et al., 2017)

Several lignan reported as anticancer property such as flaxseed lignans that effect by multiple targets of hallmarks of cancer (De Silva et al., 2019). In addition, FDA approved lignans as chemotherapeutic drug namely etoposide and teniposide, semisynthetic derivative from podophyllotoxin, act as topoisomerase II inhibitor leading to occur critical errors in DNA synthesis at the premitotic stage of cell division (Yousefzadi et al., 2010; Pan et al., 2012).

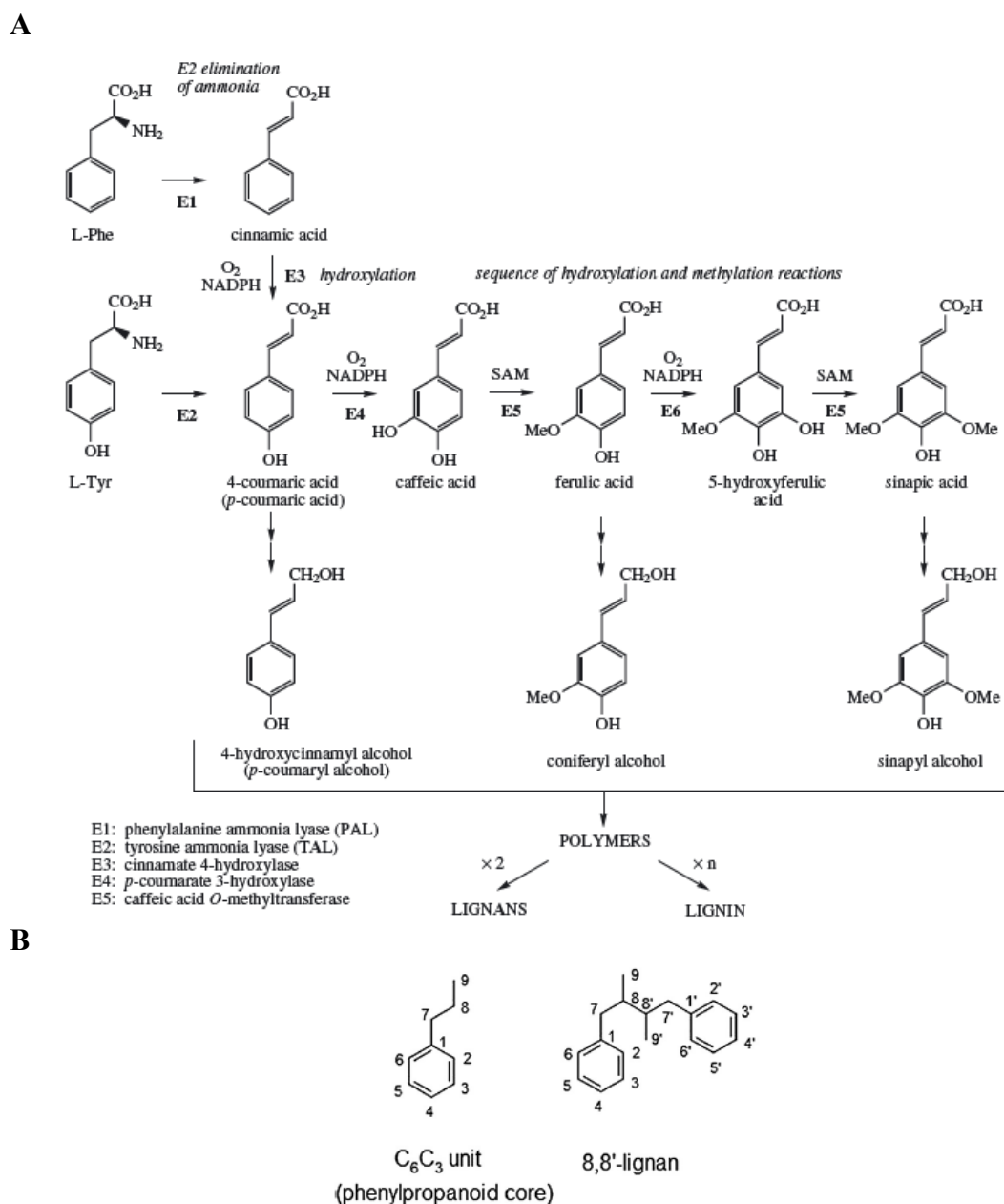


Figure 16. Lignan biosynthesis. Lignans are biosynthesized from L-phenylalanine and L-tyrosine (**A**) and the core structure of lignans (**B**) (Simpson et al., 2017).

1.2.11 Lignan as an anticancer compound

Etoposide and other semi-synthetic derivatives of podophyllotoxin are lignan-based medications that are well-known cases of anticancer for clinical-used and approved by FDA. In addition, several natural lignan compounds have been reported the potential hinder breast and ovarian cancer as show in Table 4 and Figure 17.

Table 4. Anticancer compounds from lignan.

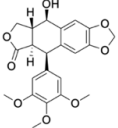
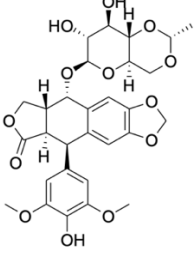
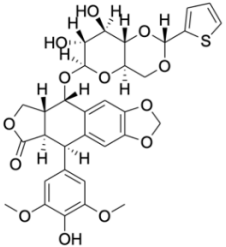
Lignans	Sources	Anticancer effects	References
<p>Podophyllotoxin</p> 	<p><i>Podophyllum peltatum</i></p>	<p>It has a potent antiproliferation on various cancer cell lines by binds to α, β-tubulin that effect on loss of microtubule and the formation of abnormal mitotic spindles leading to G2/M arrest. However, it rarely used in cancer therapy due to highly toxicity.</p>	<p>You et al., 2005</p>
<p>Etoposide</p> 	<p>Semisynthetic derivative of podophyllotoxin</p>	<p>Etoposide operates by forming a complex with topoisomerase II and DNA, effectively halting DNA synthesis. This complex, through its interaction with topoisomerase II, induces double-stranded DNA breaks, impeding their repair mechanisms. The accumulation of DNA damage prevents cells from progressing into the mitotic phase of cell division, ultimately leading to cell death. Etoposide is utilized in the treatment of ovarian cancer.</p>	<p>You et al., 2005</p>
<p>Teniposide</p> 	<p>Semisynthetic derivative of podophyllotoxin</p>	<p>Teniposide is a phase-specific cytotoxic drug that disrupts cell division during the late S or early G2 phase of the cell cycle. It achieves this by inducing breaks in both single- and double-stranded DNA and forming protein-DNA crosslinks. The primary mechanism of action appears to be the inhibition of topoisomerase II activity.</p>	<p>You et al., 2005</p>

Table 4. Anticancer compounds from lignan (continued).

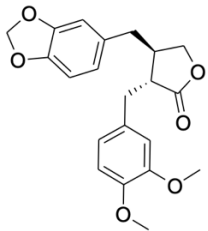
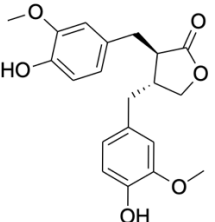
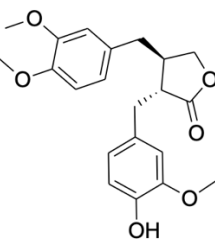
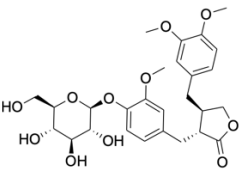
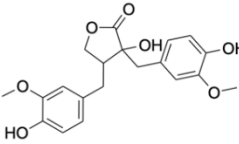
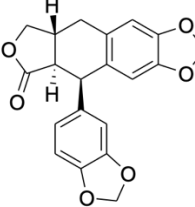
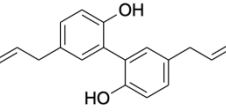
Lignans	Sources	Anticancer effects	References
<p>Bursehernin</p> 	<i>Bursera spp.</i>	Bursehernin shows a cytotoxic effect on breast, colorectal and cholangiocarcinoma cells. It significantly induces cell cycle arrest at the G2/M phase and inhibits proliferation by significantly decreasing topoisomerase II, cyclin D1 and STAT3. In addition, it induces apoptosis through enhanced multi-caspase activity.	Rattanaburee et al., 2019
<p>Matairesinol</p> 	<i>Wikstroemia sikokiana</i> , <i>Wikstroemia indica</i> , <i>Piper philippinum</i>	Matairesinol has cytotoxicity against breast cancer and inhibits Akt signaling. It sensitizes cancer cells to TRAIL-induced apoptosis. Moreover, it has inhibitory effect on aldose reductase.	Peuhu et al., 2010
<p>Arctigenin</p> 	<i>Wikstroemia indica</i> , <i>Fructus arctii</i> .	Arctigenin has cytotoxicity against breast cancer (MCF-7) with IC ₅₀ values of 9.6 μM and strongly inhibits Akt activation. Moreover, it has inhibitory effect on aldose reductase.	Xu et al., 2010

Table 4. Anticancer compounds from lignan (continued).

Lignans	Sources	Anticancer effects	References
<p>Arctiin</p> 	<p><i>Fructus arctii.</i></p>	<p>Arctiin exhibits anti-angiogenesis by inhibition of STAT3 phosphorylation. Moreover, it has inhibitory effect on aldose reductase.</p>	<p>Xu et al., 2010</p>
<p>Wikstromol</p> 	<p><i>Wikstroemia sikokiana,</i> <i>Wikstroemia indica</i></p>	<p>Wikstromol inhibits several components of the RTK/PI3K/Akt pathway in LNCaP prostate cancer cells and enhances TRAIL-induced apoptosis.</p>	<p>Peuhu et al., 2013</p>
<p>Polygamain</p> 	<p><i>Haplophyllum tuberculatum,</i> <i>Amyris madrensis</i></p>	<p>It exhibits antiproliferation activities on various cancer cell lines such as MDA-MB-453, MDA-MB-231, SKOV-3 and SKOV-3-MDR-1-6/6 with IC₅₀ values of 26.3, 78.2, 51.3 and 102.1 nM, respectively. Furthermore, it binds to α,β-tubulin that effect on loss of microtubule and the formation of abnormal mitotic spindles leading to G2/M arrest.</p>	<p>Hartley et al., 2012</p>
<p>Magnolol</p> 	<p><i>Magnolia officinalis</i></p>	<p>Magnolol inhibits HER2 expression on SKOV-3 and downregulate PI3K/Akt signaling.</p>	<p>Chuang et al., 2011</p>

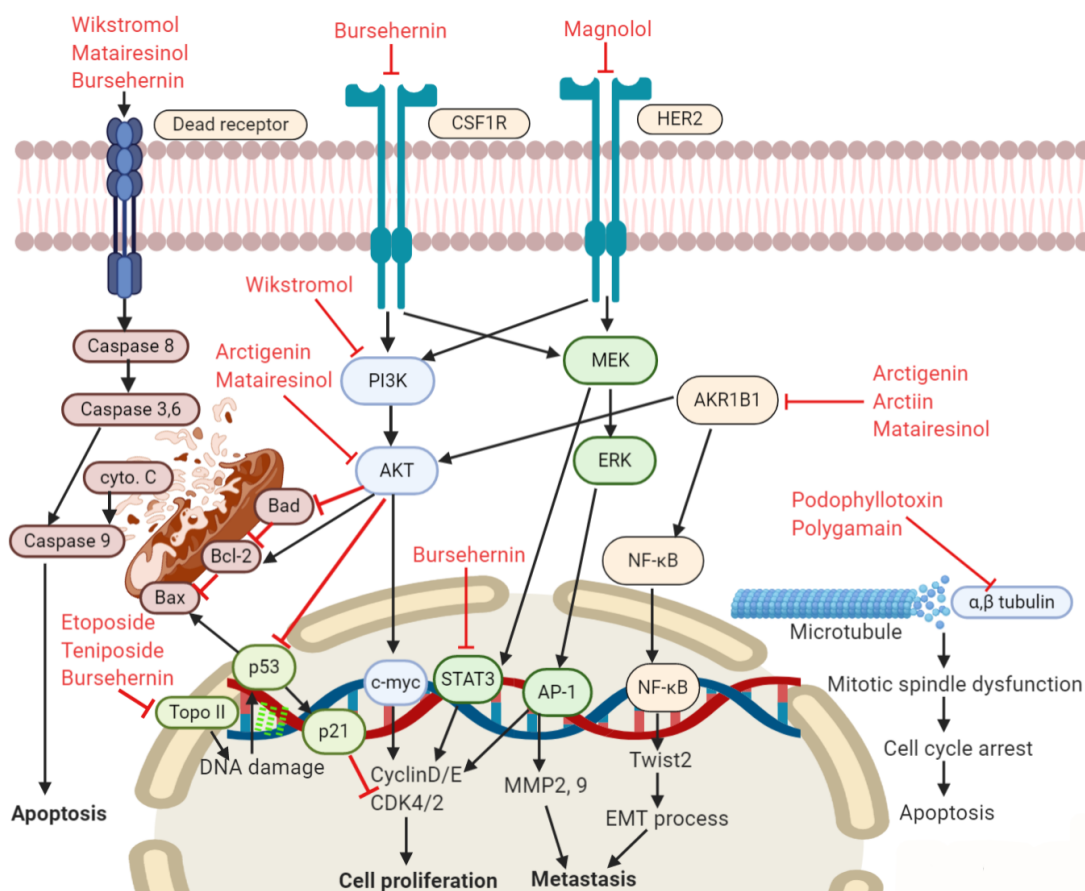


Figure 17. Molecular mechanism of action of lignan compounds in anticancer activity.

1.2.12 Kusunokinin

Kusunokinin is one of the dibenzylbutyrolactone lignans. The International Union of Pure and Applied Chemistry (IUPAC) nomenclature of kusunokinin is (3R,4R)-3-(1,3-benzodioxol-5-ylmethyl)-4-[(3,4-dimethoxyphenyl)methyl]oxolan-2-one. The molecular formula of kusunokinin is $C_{21}H_{22}O_6$ and its molecular weight is 370.4 g/mol (Figure 18). This compound has no hydrogen bond donor but has 6 hydrogen bond acceptors. Kusunokinin was first isolated from *Cinnamomum camphora* along with two novel lignan compounds, cinnamonol and kusunokinol (Takaoka et al., 1977). Kusunokinin was also isolated from various plants such as *Zanthoxylum setulosum* (Mora et al., 2011), *Haplophyllum spp.* (Gözler et al., 1996), *Virola spp.* (Kato et al., 1990), and *Wikstroemia spp.* (Kato et al., 2014).

Kusunokinin plays a crucial role in protecting plants from insects. Messiano and colleagues isolated kusunokinin from *Aristolochia malmeanahas* which revealed insecticidal activity on *Anticasia gemmatalis* at an LD₅₀ value of 230.1 µg/µL (Messiano et al., 2008). The results from these studies were concordant with the Bicalho studies that isolated it from *Virola sebifera* and showed insecticidal activity on *Anticasia gemmatalis* at LD₅₀ value of 230.1 µg/µL and on *Atta sexdens rubropilosa* at 90% mortality after 25 days and fungicidal activity on *Leucoagaricus gongylophorus*. (a symbiotic fungus on ants) at 100% mycelial growth inhibition (Bicalho et al., 2012). Several reports identified kusunokinin as an active antiparasite. Sartorelli and colleagues isolated kusunokinin from *Aristolochia cymbifera* which revealed antitrypanosomal activity at IC₅₀ 51.51 and 17.02 µM on *Trypanosoma cruzi*. trypomastigotes and amastigotes stages, respectively, with an absence of hemolytic activity (Sartorelli et al., 2010) similar result to Morais and colleagues that isolated from *Piper cernuum* showed activity against trypomastigotes at an IC₅₀ value of 31.8 µM (Moraisa et al., 2019). In addition, it was selectively docked to *Leishmania mexicana* pyruvate kinase with a binding energy value of -130.5 kJ/mol (Ogungbe et al., 2019). Moreover, Mohamed and colleagues investigated the potential antibacterial targeting of penicillin binding protein and penicillin-binding protein2a of methicillin-resistant *Staphylococcus aureus* (MRSA) strain SO-1977. They revealed that the docking binding free energy of kusunokinin with PBP2a is -12.74 kcal/mol (Mohamed et al., 2019).

Karahisar and co-workers studied the neurobiological potential of *Haplophyllum sahinii* and *Haplophyllum vulcanicum* extracts containing kusunokinin and several of its derivatives that showed inhibitory activity on acetylcholinesterase, butyrylcholinesterase and tyrosinase, which are associated with Alzheimer's disease and Parkinson's disease (Karahisar et al., 2019). In addition, Kusunokinin, which has been isolated from *Piper philippinum*, showed anti-platelet aggregation at 83.7%, 79.8%, 79.9% and 80.8% inhibitory effects that were induced by thrombin, arachidonic acid, collagen and platelet-activating factor, respectively (Chen et al., 2007).

Interestingly, a growing number of recent studies indicate kusunokinin as an anticancer compound. *Trans*-(-)-kusunokinin from *Piper nigrum* showed a cytotoxic

effect on breast cancer cell lines (MCF-7, MDA-MB-468 and MDA-MB-231) and colorectal cancer cells (SW-620) with IC₅₀ values of 1.18, 1.62, 91.79 and 2.60 µg/ml, respectively. These suggest that *trans*-(–)-kusunokinin induced cell cycle arrest at the G2/M phase by decreasing topoisomerase II level and increasing p53 and p21 levels, including induced apoptosis by the decreasing bcl-2 level and the increasing bax, cytochrome c and caspase-8, -7 and -3 activities (Sriwiriyan et al., 2017). These results were similar to the study of the synthetic racemic kusunokinin that showed the cytotoxic effect on breast cancer cell lines (MCF-7, MDA-MB-468 and MDA-MB-231), colorectal cancer cells (HT-29) and cholangiocarcinoma cell lines (KKU-M213, KKU-K100 and KKU-M055) with IC₅₀ values of 4.30, 5.90, 7.57, 5.51, 5.93, 7.16 and 12.19 µM, respectively. The results concluded that it modulates cell cycle and proliferation by decreasing topoisomerase II, STAT3 and cyclin D1, while p21 was significantly increased. Furthermore, it induced apoptosis by enhancing multi-caspase activity (Rattanaburee et al., 2019). In addition, the studies in mouse models revealed the inhibition of tumor growth and migration with no adverse effect (Tedasen et al., 2020). Interestingly, computational stimulation revealed that *trans*-(–)-kusunokinin was predicted to bind several target proteins, such as CSF1R, MMP-12, HSP90-α, cyclinB1 and MEK1. Among them, CSF1R revealed the best binding affinity. *Trans*-(–)-kusunokinin binds the juxtamembrane region and forms π-π stacking at the binding site of CSF1R (Rattanaburee et al., 2020). Moreover, it also binds to the ATP binding domain of HER2 but revealed low binding affinity and a different mode of action from the HER2 inhibitor (neratinib) (Rattanaburee et al., 2021).

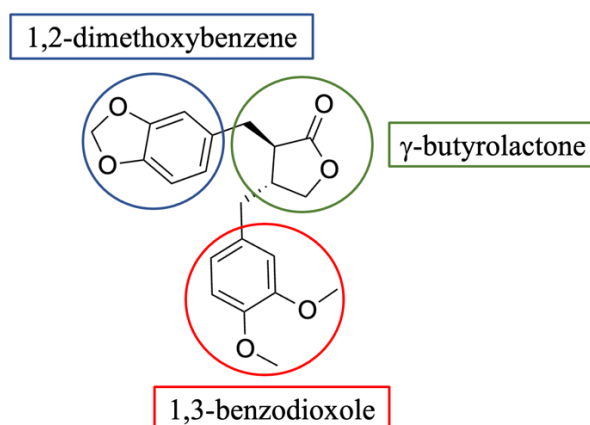


Figure 18. *Trans*-(±)-kusunokinin structure.

1.2.13 Signaling pathway related to carcinogenesis

1.2.13.1 Cancer cell proliferation

Self-sufficiency in growth signals is one of the molecular hallmarks of cancer that leads to uncontrollable proliferation. Normal cells from different tissues are in various stages of cell progression by modulation of growth-promoting signals to homeostasis of cell amount and function. Cell proliferation requires cell communication that interacts between growth factors, receptors on the cell membrane and intracellular signaling pathways. In overview, total activation of cell proliferation depends on classes and amount of growth factors and receptors. Growth factors may be hormones from the endocrine system, activated proliferation protein from contact cells or extracellular matrix (paracrine) and adhesion molecules. Cancer cells have a potential strategy for cell proliferation mechanism by creating growth factors for autoactivation (autocrine) leading to independent from environment signaling, for example, platelet-derived growth factor (PDGF), colony-stimulating factor (CSF) and tumor growth factor beta (TGF- β) from cancer cell that activated itself and adjacent cells. Furthermore, cancer cells may communicate with stromal cells, fibroblasts, or white blood cells in inflammatory processing that enhances growth factor release (Kharraishvili et al., 2014).

Another strategy that cancer cells use to activate proliferation is increasing the copy number of receptors on the cell membrane surface. Breast cancer patients found that 15-30% with amplification of HER2/neu gene leads to high expression of HER2 receptor that can be detected by immunohistochemistry on breast tissue. Another instance pertains to gastroesophageal adenocarcinoma, where a notable observation is the elevated expression of epidermal growth factor receptor (EGFR), a prominent member of the tyrosine kinase receptor family. Increasing of copy number leads to abundantly signal activation of proliferation into cells, even though the amount of growth factor is not alterative. Amount receptor alteration from high expression is not only one reason but also abnormal pathology on the receptor that may have abundant signaling such as EGFR mutation found in lung cancer leading to the intracellular domain of the receptor is self-sufficiency in growth signals from environment (Sharma et al., 2007).

Signaling activation of cell proliferation from the receptor into the nucleus is done through an intracellular signaling pathway. Signaling from tyrosine kinase receptors will be relayed into MAPkinase through Ras/Raf proteins. Abnormal pathology on intracellular signaling pathways may lead to signaling autoactivation such as K-RAS mutation that is found in pancreatic and colorectal cancer leading to continually signal RAS into downstream molecules (Figure 19). Both of MAPkinase pathway and PI3K pathway signal activation into an expression of the gene in the nucleus that gets free from modulation of all growth factor (acrine) (Sangkhatat et al, 2017).

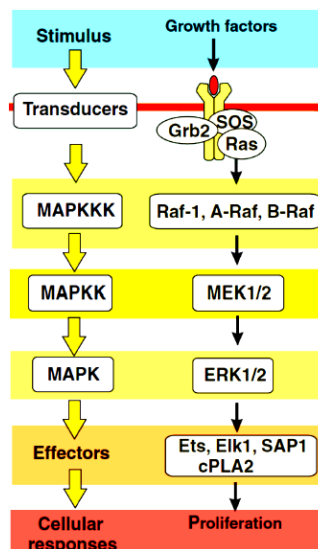


Figure 19. Relay signaling of cell proliferation. Linear transfer of information through a phospho relay system based on a sequential series of phosphorylation events (Berridge, 2014).

Receptors that play an important role in cancer cell proliferation are enzyme-linked receptors and G protein-coupled receptors (GPCRs). The enzyme-linked receptor is a single-pass transmembrane receptor. The extracellular domain is the binding site of ligands or growth factors, leading to signal activation from the intracellular domain to the intracellular signaling pathway. The binding interaction of ligands causes dimerization of receptors and enzymatic activity on the intracellular side, which leads to phosphorylation on the downstream molecules that act to retrieve the γ -phosphate group from ATP to tyrosine by tyrosine kinases such as FGFR, TrkB, TrkC and PDGFR. Tyrosine kinase receptors operate as a relay for the MAPK

(mitogen-activated protein kinase) signaling pathway, which is essential for cell growth. Extracellular-signal regulated kinases 1/2 (ERK1/2) are phosphorylated as a result of tyrosine kinase-linked receptor activation, and they subsequently go into the nucleus. Cyclic adenosine monophosphate (cAMP) response element binding protein is a transcription factor that ERK1/2 primarily targets in the nucleus (CREB). ERK1/2 also stimulates a variety of other transcription factors (Heit et al., 2006).

Another group is serine/threonine kinases such as TGF- β R, ACVR and BMPR. Transforming growth factor (TGF)-mediated suppression of cell proliferation is carried out through the Smad signaling pathway. The Smad transcription factors are activated by stimulation of the TGF- receptor and subsequently go into the nucleus. Inhibitor of cyclin-dependent kinase (CDK) (p15) expression, which reduces cell proliferation, is one of the Smads' roles (Figure 20) (Heit et al., 2006).

G protein-coupled receptors (GPCRs) are transmembrane receptors with seven membrane-spanning segments. They fulfill a pivotal role as receptors that are triggered by neurotransmitters, hormones, and growth factors, subsequently engaging with diverse signaling pathways. The intracellular (cytoplasmic) domain of GPCRs is coupled to the G protein, which is a 3-subunit protein (heterotrimeric protein) consisting of $G\alpha$, $G\beta$ and $G\gamma$. The $G\alpha$ subunit can be classified by its role in action. In general, GPCRs that regulate proliferation are coupled to $G\alpha_q$. When the growth factor binds to the extracellular domain of GPCRs, it causes conformational changes in the receptor and activates heterotrimeric G proteins, leading them to detach from the receptor and separate into GTP-bound and $G\beta/\gamma$ dimers. The subsequence has two main pathways. One is the activation of c-Jun N-terminal kinase (JNK) and p38 pathway through Rac and RhoA which are guanine nucleotide-exchange factor (GEF). JNK and p38 pathway activation leads to the activation of a number of transcription factors that relate to cell proliferation and apoptosis. Another one is the activation of phospholipase C β (PLC β), which is an enzyme on the cell membrane that catalyzes phosphatidylinositol 4,5-bisphosphate [IP(4,5)P $_2$] to inositol 1,4,5-trisphosphate (IP $_3$) and diacylglycerol (DAG). DAG will activate protein kinase C (PKC), which regulates numerous cellular responses, including cell proliferation and apoptosis, through the Ras/Raf/MEK/ERK, JNK and NF- κ B pathways. IP $_3$ will operate the gate Ca $^{2+}$ ion channel and release Ca $^{2+}$ to the cytoplasm, stimulating cell proliferation in various pathways such as targeting

transcription factors nuclear factor of activated T cells (NFAT) and NF- κ B. The Janus kinase (JAK) is a non-receptor tyrosine kinase protein that works with cytokine receptors such as interleukin-2. When it is activated, the signal transducer and activator of transcription (STAT) will be recruited and form dimerization. After that, STAT dimers will be translocated into the nucleus and act as activators of gene transcription (Figure 20) (Heit et al., 2006).

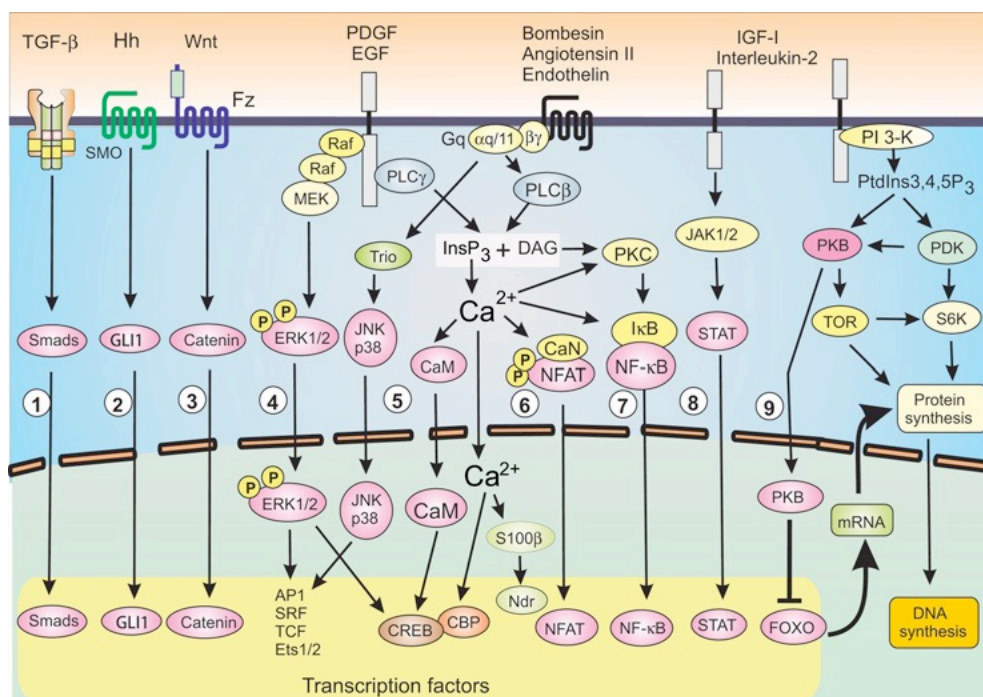


Figure 20. Signaling pathways of cell proliferation. Numerous signaling pathways are activated by growth factors to promote cell division. Several signaling pathways work together to modulate the effects of growth factors (Berridge, 2014).

1.2.13.2 Cell cycle signaling pathway

Cell cycle signaling regulates and controls the cell for cell division. The main protein that regulates cell cycle progression is cyclins, which alters expression during each phase. Based on the premise that cyclins lack intrinsic enzymatic activity, their functional effects are mediated through interaction with cyclin-dependent kinases (CDKs) to establish complexes known as cyclin/CDK complexes (Cobrinik, 2005).

CDKs are serine/threonine kinase proteins that specifically bind with each cyclin and regulate each phase of cell division. The G1 phase is regulated by cyclin D/CDK4,6

complex which is activated by several mitogens or growth factors through signaling that regulates cyclin D expression. Phosphorylation of retinoblastoma protein (pRB), orchestrated by the cyclin D/CDK4,6 complex, induces its dissociation from E2F, a transcription factor that binds to promoters, thereby activating gene expression crucial to cell cycle regulation. This encompasses genes encoding cyclin E, cyclin A, and enzymes engaged in nucleotide processes, such as thymidylate synthase and ribonucleotide reductase. Therefore, this step can be called ‘restriction point’ then following by activation of cyclin E/CDK2 which operates G1 to S phase including cyclin A/CDK2 which regulate DNA synthesis in S phase. However, the activation of cyclin E/CDK2 and cyclin A/CDK2 can be inhibited by p21^{Cip1} and p27^{Kip1} whereas cyclin D/CDK4,6 is inhibited by p15^{INK4B}. For G2/M phase is regulated by cyclin B/CDK1 which is activated by the cyclin-dependent kinase -activating kinase (CAK) that containing cyclin H/CDK7 complex (Figure 21) (Pei and Xiong, 2005).

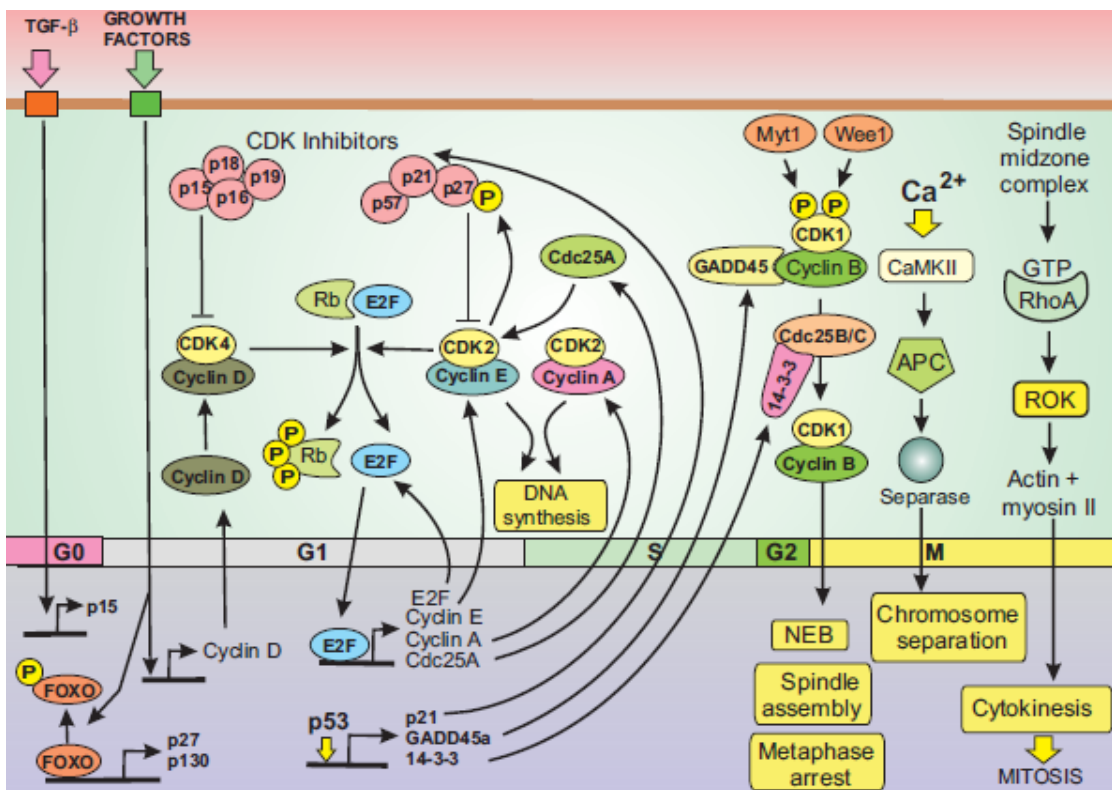


Figure 21. Cell cycle signaling pathways (Berridge, 2014).

1.2.13.3 Apoptosis pathway

The apoptosis signaling pathway regulates the cell's decision of whether it survives or dies. Program cell death through the apoptosis process begins with the activation of death receptors such as the Fas receptor, tumor necrosis factor receptor (TNF-R) and TRAIL-R, which are mediated by extracellular activation such as hypoxia and survival factor deficiency. This process is called the extrinsic pathway or death receptor pathway. Whereas intracellular abnormalities such as DNA damage are activated by intracellular molecules such as p53. This process is called the intrinsic pathway or mitochondrial pathway and the two of these processes are linked together into an integrated network of caspase cascades. For the extrinsic pathway, cytokines such as the Fas ligand (FasL) and tumor necrosis factor α (TNF α) activate death receptors and relay signaling to caspase 8 or caspase 10, which activate caspases 3, 6 and 7. Whereas the intrinsic pathway, caspase, cooperates with the Bcl-2 superfamily, which can be classified into three groups. (1) pro-survival proteins which have 4 conserved domains (BH1-BH4) such as Bcl-2, Bcl-xl, Mcl-1 and BFL1, (2) Bax/Bak-like proteins that have conserved domains like pro-survival proteins but act as pro-apoptosis, and (3) BH3 only, which is pro-apoptotic proteins that have only BH3 conserved domains, such as Bim, Puma, Noxa, Bik, Bad and Bid (Mayer and Oberbauer, 2003).

The initiator caspases (caspases 8, and 10 from the extrinsic pathway and caspase 9 from the intrinsic pathway) activate the executioner caspases (caspases 3, 6 and 7) that respond to drive the apoptosis process (Figure 22). The intrinsic pathway is associated with the interaction of the endoplasmic reticulum (ER) and mitochondria, which regulate calcium ions (Ca²⁺) which play an important role in modulating Bcl-2 superfamily function and leading to the initiation of apoptosis. ER stress constitutes a signaling pathway that triggers an influx of Ca²⁺ into the cytoplasm, subsequently serving as an output signal for the activation of caspase 12. This activation feeds into the caspase cascade. However, the mitochondria, which release a variety of apoptotic factors including cytochrome c and a second mitochondrial-derived activator of caspase (SMAC), which feed into the caspase cascade, as well as apoptosis-inducing factor (AIF) and endonuclease G (EndoG), which feed into the caspase-independent pathway, provide the majority of the output signals from the intrinsic pathway (Figure 22) (Orrenius et al., 2013).

The Bcl-2 superfamily consists of proapoptotic and antiapoptotic factors that play an important role in regulating the intrinsic pathway (Figure 22). Moreover, there are various cell signaling pathways that can regulate the expression of proapoptotic and antiapoptotic genes. Some signaling pathways regulate apoptosis by changing the Bcl-2 superfamily's activity, e.g., AKT phosphorylation of Bim. Genotoxic stress is one of the processes that activate the transcription factor p53, which plays an important role as a tumor suppressor by increasing the expression of apoptotic factors such as puma and noxa (Figure 22) (Distelhorst and Shore, 2004).

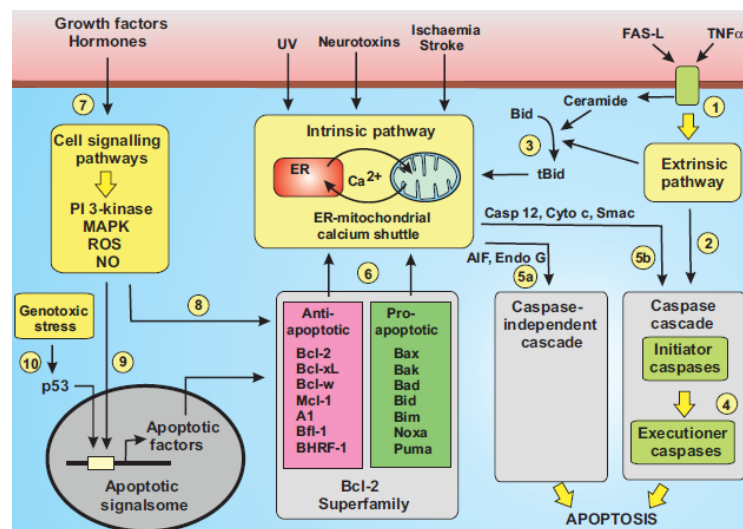


Figure 22. Network that signals apoptosis. Several interrelated pathways regulate the beginning of apoptosis (Berridge, 2014).

1.2.13.4 Multidrug resistance (MDR)

The most common mechanism of MDR is increased efflux pumps in the cell membrane that pump anticancer drugs out of cells. The ATP-binding cassette (ABC) transporter superfamily could be considered for targeting in MDR since they play the main mechanism of several anticancer efflux pumps such as ABCB1 (P-glycoprotein), ABCC (MRP) and ABCG2 (BCRP). Overexpression of the ABC transporter results from the activation of various growth factors that relay to activate JAK/STAT and AKT/mTOR signaling, leading to increased expression of the ABC transporter. Finally, increased exportation of chemotherapeutic drugs out of the cancer cells (Figure 23) (Arumugam et al., 2019).

1.2.13.5 Migration

Migratory progression of cancer cells is required several processes to occur this mechanism such as epithelial–mesenchymal transition (EMT) process that associated with loss of the epithelial cell-cell adhesion molecule (E-cadherin) and increased mesenchymal cell–cell adhesion proteins such as N-cadherin, P-cadherin and vimentin. Furthermore, reorganization of the actin cytoskeleton process plays an importance role of migration by regulates actin dynamics, lamellipodia and filopodia. There are several proteins that can activate regulation of actin such as Rho protein family (Rho, Rac, CDC42), PAK, ROCK and WASP (Figure 23) (Arumugam et al., 2019).

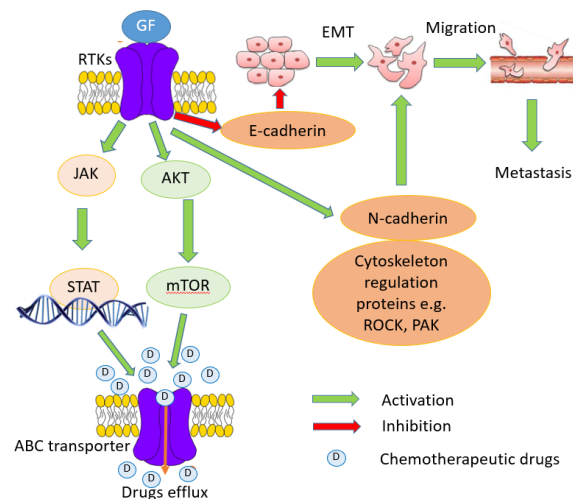


Figure 23. Regulation of multidrug resistance and migration pathway (Modified pathway from Arumugam et al., 2019).

1.2.14 Breast and ovarian cancers develop through multiple molecular pathways

Hereditary breast and ovarian cancer syndrome (HBOC syndrome) is a hereditary propensity to develop breast, ovarian, and other cancers. It is assumed that this propensity is passed down by certain gene abnormalities. The likelihood of BRCA germline mutations is predicted by clinical factors such as the kind of tumor, age of incidence, and family history. The youngest breast cancer patient's age, the number of ovarian cancer instances in the family, and the pathological diagnosis are all factors that certain physicians often consider. *BRCA1* or *BRCA2* gene mutations

are to account for up to 80% of HBOC cases. There are several *BRCA1* and *BRCA2* mutations spread out throughout the whole set of coding exons (Dohrn et al., 2012).

DNA repair mechanisms are present in normal cells to preserve and restore the genomic integrity. Cancer and mutation are caused by structural alterations such as DNA strand breaks, DNA-protein crosslinks, DNA inter/intra-strand crosslinks, and DNA base damage. Prominent components in the detection and regulation of the DNA damage response, exemplified by *BRCA1* and *BRCA2*, possess the capability to identify and rectify single-strand breaks (SSBs) or double-strand breaks (DSBs) by initiating DNA repair mechanisms and activating checkpoints for cell division. The DNA damage spots attract the *BRCA1* and *BRCA2* genes. *BRCA1* serves as a pivotal element in DNA damage repair, effectively engaging homologous recombination (HR), nucleotide excision repair (NER), and potentially non-homologous end joining (NHEJ) pathways. Its interaction network extends to several partner proteins. Through the Fanconi anemia-breast cancer susceptibility gene (FA-BRCA) pathway, *BRCA1*, when prompted by *cdk1*, establishes a direct interaction with *MutL*. On the other hand, *BRCA2*, also recognized as *FANCD1*, holds a significant role in DNA repair, particularly in homologous recombination (HR). This is achieved by its direct modulation of *RAD51*, a central gene within the HR pathway, and its interaction with *PALB2*, a gene vital to HR repair and checkpoint functions. An intriguing observation lies in the intricate control exerted by the FA-BRCA, MMR (mismatch repair), BER (base excision repair), and NER pathways over the nuclear activities of BRCA proteins. (Dohrn et al., 2012).

The intricate mechanisms governing the interaction and aggregation of additional DNA repair proteins associated with BRCA, however, remain predominantly unexplored. Consequently, hereditary mutations within other susceptibility genes such as those involved in Fanconi anemia (FA), mismatch repair (MMR), and general DNA repair processes, might constitute the underlying basis for hereditary breast and ovarian cancer (HBOC) instances. These predisposing genes include mutations in the *ATM*, *ATR*, *CDH1*, *CHK2*, *MSH1*, *MSH2*, *MLH1*, *FANCD1*, *FANCD2*, *FANCI*, *FANCP*, *STK11*, *TP53*, *PTEN* and *PMS2* genes, and they may also be connected with the BRCA core complex. These genes also encode for the regulators of BRCA gene products. Families with various disorders, including Fanconi anemia, Cowden syndrome (*PTEN* mutations), Li-Fraumeni syndrome (*TP53* mutations), xeroderma pigmentosum, and ataxia-telangiectasia, display

additional cancer forms beyond the HBOC cancer spectrum (Figure 24) (Kobayashi *et al.*, 2013).

1.2.14.1 DNA damage pathway

Base excision repair (BER), a pivotal mechanism for rectifying DNA single-strand breaks (SSBs), is under the governance of the enzyme poly(ADP-ribose) polymerase (PARP), which additionally contributes to cellular recovery post DNA damage. Focusing on malignancies characterized by compromised homologous recombination (HR)-mediated DNA repair, the inhibition of PARP prompts synthetic lethality and cell demise (Tinker and Gelmon, 2012). Cancers marked by deficient BRCA1, BRCA2, or TP53 functionality demonstrate heightened susceptibility to PARP inhibition. Several protein clusters, including those involved in DNA repair checkpoints (ATR, ATM, CHK1, and CHK2), BRCA-associated proteins, CDK cluster, NER cluster, FA cluster, and TP53 cluster, play roles in homologous recombination and contribute to the sensitivity to PARP inhibition. Consequently, PARP inhibitors present a plausible therapeutic avenue for tumors with dysregulated BRCA and hold promise across diverse cancer types, including breast and ovarian malignancies. These heritable mutations and epigenetic changes can potentially serve as indicators of BRCA-related conditions and biomarkers for susceptibility to PARP inhibition (Lederman *et al.*, 2012).

The effectiveness and safety of olaparib, a strong oral PARP inhibitor, in patients with germline BRCA mutations and recurrent ovarian cancer were recently compared in a phase II clinical trial research (Kaye *et al.* 2012). Regrettably, discernible variations in progression-free survival (PFS) were not evident between the cohorts administered olaparib and pegylated liposomal doxorubicin. An alternative clinical inquiry demonstrated that employing olaparib as maintenance therapy prolonged PFS, albeit without a corresponding extension in overall survival for individuals afflicted with progressed, platinum-sensitive high-grade serous ovarian cancer (Lederman *et al.*, 2012).

The NER pathway oversees removing large DNA damages. NER serves as a defensive mechanism against many forms of DNA damage and is essential for preserving genomic integrity. Replication protein A1 (RPA1), a protein that binds to single-stranded DNA, is involved in the employment of the two structure-specific DNA

endonucleases xeroderma pigmentosum complementation group F with excision repair cross complementation group 1 (XPF-ERCC1 complex), which forms the 5' incision in NER, and XPG (xeroderma pigmentosum, also known as ERCC5). Cutting the broken DNA strand and repairing the DNA through the NER pathway both need the XPF-ERCC1 complex. As a part of the MRE11-RAD50-NBS1 complex, NBN (nibrin, also known as NBS1) played a role in DNA-DSB repair and DNA damage-induced checkpoint activation. It is believed that NBN mutations increase the likelihood of developing breast cancer. Additionally, the repair of DNA-SSB and oxidative damage is accomplished by X-ray repair complementing deficient repair in Chinese hamster cells 1 (XRCC1). In the BER pathway, the XRCC1 protein interacts with DNA ligase III, polymerase, and PARP1 (Figure 24). Chemoradiation may be conferred by reduced XRCC1 expression, which increases patient survival (Veazi *et al.*, 2011).

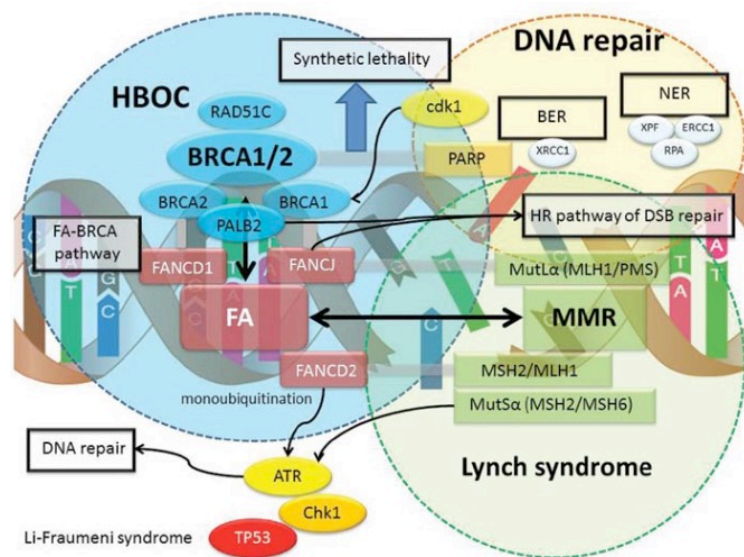


Figure 24. Breast and ovarian cancers develop through multiple molecular pathways. Molecular processes including interaction with the FA, MMR, and other DNA repair genes in HBOC disease include DNA repair mechanism in BRCA pathways or networks of several proteins that the breast and ovarian cancer sensitivity genes and their functional networks of several proteins in promoting DNA repair. BRCA1 and BRCA2 keep cellular processes related to genomic integrity in check. Genome instability results from mutations that impact the processes that identify, stabilize, and repair DNA damage (Kobayashi *et al.*, 2013).

1.3 Objectives

Part I. Identification of *trans*-(-)-kusunokinin target by *in silico* studies

1. To screen the possible target proteins of *trans*-(-)-kusunokinin in proliferation, cell cycle, apoptosis, multidrug resistance and migration pathway on breast and ovarian cancers using molecular docking and molecular dynamics.

Part II. Validation of *trans*-(±)-kusunokinin target by *in vitro* studies

1. To determine the cytotoxicity effect of *trans*-(±)-kusunokinin on breast and ovarian cancer cells.

2. To determine the inhibition effect of *trans*-(±)-kusunokinin toward enzyme activity.

3. To prove the cellular target engagement of *trans*-(±)-kusunokinin through affinity-based approach using cellular thermal shift assay (CETSA).

4. To determine the anti-lipid peroxidation activity of *trans*-(±)-kusunokinin using thiobarbituric acid reactive substances assay (TBARS).

5. To determine the mechanism of action of *trans*-(±)-kusunokinin against the target and its downstream molecules using small interfering RNA (siRNA) and Western blot analysis.

CHAPTER 2

RESEARCH METHODOLOGY

This research project was divided into two distinct phases. The initial phase involved the identification of the target of *trans*-(-)-kusunokinin through computational analysis. Subsequently, the outcomes derived from the *in silico* investigation were subjected to directed validation in a cell culture model, and further substantiated through *in vitro* experimentation, thereby providing empirical evidence. (Figure 25).

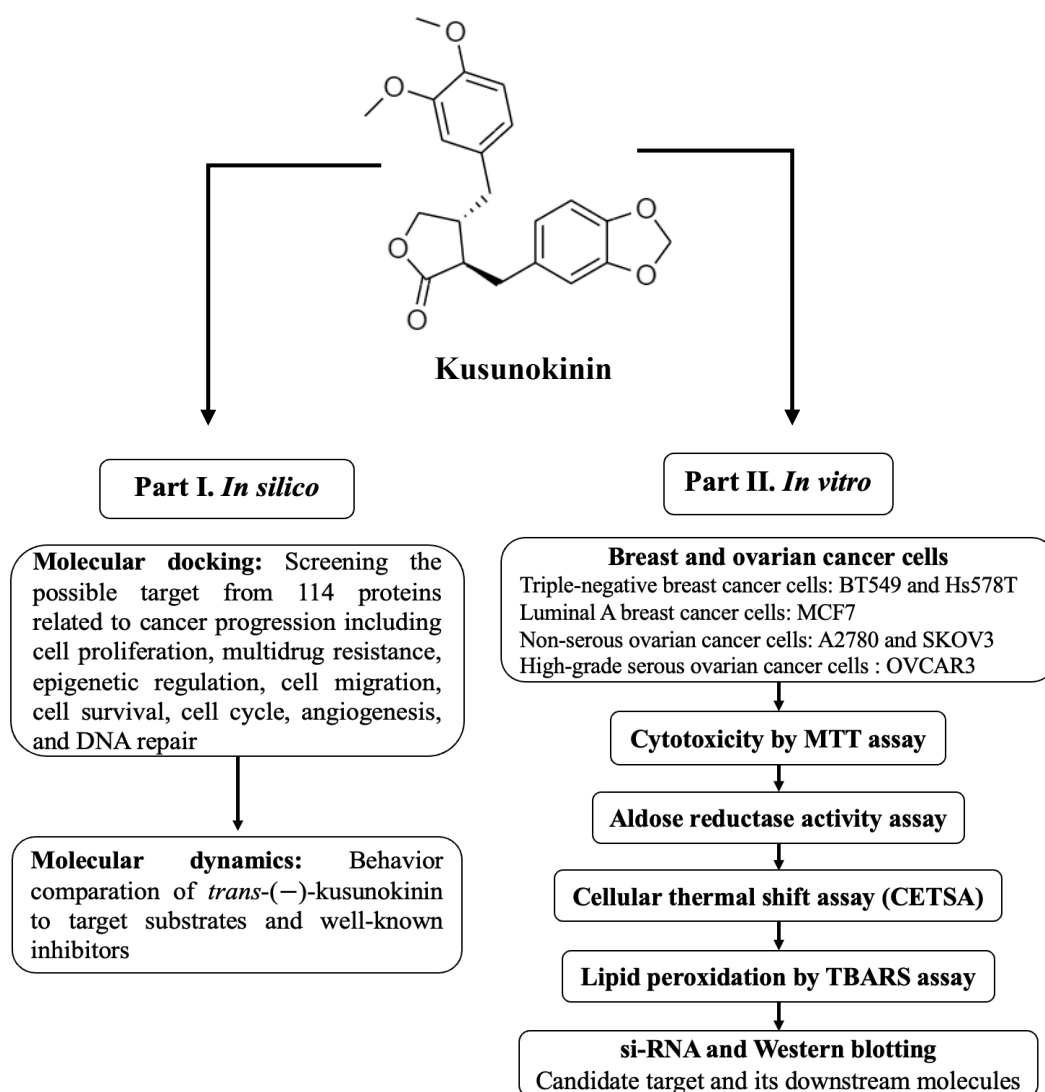


Figure 25. Study workflow of this research.

Part I. Identification of *trans*-(-)-kusunokinin target by *in silico* studies

1. Computer system

1.1 Hardware

- Personal computer, DellTM OptiPlexTM 7010, Rock Cluster on CentOS[®] 7, Integrated Intel[®] HD Graphics 4000, Intel[®] CoreTM i7 (3rd Gen) 3770/3.4 GHz, DDR3 SDRAM – non-ECC 8 GB/1600 MHz of RAM located at Department of Biomedical Science and Biomedical Engineering, Faculty of Medicine, Prince of Songkla University, Hat-Yai, Songkhla, Thailand.

1.2 Software

- AutoDockTools version 1.5.6 (ADT)
- Visual Molecular Dynamics version 1.9.3 (VMD)
- BIOVIA Discovery Studio 2019 Client
- AMBER16 package
- Gaussian16 package
- xmgr program

1.3 Bioinformatics tools and database

- Protein Data Bank (PDB): <https://www.rcsb.org/>
- PubChem: <https://www.pubchem.ncbi.nlm.nih.gov/>
- Online SMILES Translator: <https://cactus.nci.nih.gov/translate/>
- PROPKA: http://nbc-222.ucsd.edu/pdb2pqr_2.0.0/

2. Computational methods

2.1 Protein structure preparation

The three-dimensional structure of 114 proteins that related to breast and ovarian cancer pathogenesis were retrieved from Protein Data Bank as a PDB format file. The water molecules in the crystallographic file were eliminated and polar

hydrogen atoms were put in the crystallographic file using AutoDockTools program version 1.5.6 (ADT) (Morris et al., 2009). The highest occupancy of each atom was considered as a selected atom in the crystallographic file. Then, all PDB format files were generated into PDBQT format files.

2.2 Ligand preparation

The *trans*-(-)-kusunokinin structure file was obtained from the PubChem database (Pubchem CID 384876). The structure was then converted into PDB file using Online SMILES Translator and Structure File Generator (<https://cactus.nci.nih.gov/translate/>). Using the Visual Molecular Dynamics (VMD) software (Humphrey et al., 1996), the native ligands that are readily available on Protein Data Bank were directly isolated from the crystallographic structure as a PDB file. Hydrogen atoms were added in all ligands. The partial charge was computed by Gasteiger charges for the whole molecule and assigned the atom type using automatically formats of ADT. Finally, the structure was translated in the PDBQT file format.

2.3 Molecular docking parameters

Molecular docking studies were accomplished using the abovementioned protein and ligand structures as PDBQT file format to perform by Autodock4 program. In the calculation process, the ligand was configured as a flexible molecule, but the protein structure was set as a rigid molecule. The docking site for the ligand on the target protein was assigned by establishing a grid box with the number of points in the x-y-z dimension of 120-120-120 Å³ and located the grid spacing in the middle of the protein structure. The genetic algorithm (GA) parameters for 50 GA runs with a population size of 200 were used to operate the molecular docking search parameters. Other parameters were set to the ADT package's default settings and the output docking files were done by Lamarckian Genetic algorithm 4.2. The best conformation was considered on the basis of the lowest binding energy. The interactions of the ligand-protein complex including hydrogen bonds and π - π interaction were analyzed using Discovery Studio 2019 Client (Biovia, 2016) and VMD.

2.4 Molecular docking operation

To make sure that the docking procedure was accurate and precise of a reasonable potential binding model, the docking process and parameters were validated by the self-redocking. The reproducibility of Autodock program was described on a basis of the similarity of native reference ligand and docked-ligand in orientation and position. The all-atom root mean square deviation (RMSD) between docked and native reference ligand with value of less than 2 Å was considered as a successful procedure.

AutoDock4 program scores the binding free energy between ligand and protein by semi-empirical AMBER force field that evaluates binding in two steps summation. The first step is calculated by a pair-wise atomic energetic transition (V) of each intramolecular ligand (L) and protein (P) in unbound to bound state:

$$\Delta G = (V_{L\text{-bound}} - V_{L\text{-unbound}}) + (V_{P\text{-bound}} - V_{P\text{-unbound}})$$

The second step is calculated by the intermolecular (LP) energetic transition from separated to ligand-protein complex state and include the entropy lost while binding (ΔS):

$$\Delta G = (V_{LP\text{-separated}} - V_{LP\text{-complex}} + \Delta S)$$

The pair-wise atomic terms are evaluated from the summation of dispersion/repulsion, hydrogen bonding, electrostatics, and desolvation (Huey et al., 2007).

2.5 Molecular dynamics simulation

As the *trans*-(-)-kusunokinin target screening from molecular docking study, AKR1B1 was predicted as a potential *trans*-(-)-kusunokinin target with the lowest binding energy. Thus, AKR1B1 was continued to perform molecular dynamics simulation. AKR1B1 crystallographic structure with the highest resolution was retrieved from PDB (PDB code: 1US0, resolution: 0.66 Å). AKR1B1 crystallographic structure was dehydrated and desolvated but retained the dihydro-nicotinamide-adenine-dinucleotide phosphate (NADPH), an AKR1B1 cofactor. In a case of docked pose for the ligand (*trans*-(-)-kusunokinin, AKR1B1 inhibitors or substrates), all

polar hydrogen from docking conformation structure was eliminated. The leap module included in the AMBER16 package was then used to add the hydrogen atom. At pH 7, the sidechains of all ionizable amino acids were set according to a protonation state in which lysine and arginine sidechains had +1e charges while glutamate and aspartate sidechains had -1e charges. Histidine's imidazole ring was neutral. The AKR1B1 structure lacked any disulfides. Using the Gaussian16 package³⁸, parameters for *trans*-(-)-kusunokinin, AKR1B1 inhibitors, and a substrate (PGH₂) were determined based on calculations of the restrained electrostatic atomic potential (RESP). The prior report's NADPH parameters were used (Ryde U, 1995).

AKR1B1-ligand complexes were retrieved from the molecular docking conformation that provide the best docking score and used as the initial molecular dynamics process. The transferable intermolecular potential with three points (TIP3P) was then used to solve the structure of AKR1B1 or AKR1B1 with docked ligand at a distance of 14 from the surface. This produced around 12000 water molecules. The system was subsequently neutralized with the sodium ions, and 18 NaCl pairs were added, equivalent to 0.1 M NaCl solution.

In the equilibration stage (canonical ensemble, NVT), Langevin Dynamics at 310 K (37° C) was used to equilibrate the AKR1B1 solution. A location of AKR1B1, NADPH, and the ligand were each subjected to the harmonic constraint potential, with force constants of 200, 100, 50, 20, and 10 kcal/mol⁻², respectively. With a time step of 1 fs, each NVT ensemble with the specified force constant lasted for 200 ps. Later, using the Berendsen technique, the system was converted to isobaric-isothermal (NPT) at 310 K and 1.013 Bar (1 atm). With a time step of 2 fs, an MD simulation was ran for 150 ns.

Finally, MD trajectory with 2500 equidistant snapshots was obtained. The first 90 ns simulation omitted and the last 60 ns MD conformation (1000 snapshots) was taken for a configurational average, free binding energy calculation and conformational analysis using cpptraj module. VMD package were used to analyze the parameters of root mean square deviation (RMSD) and structure visualization. Root mean square fluctuation (RMSF) and a pattern of distance geometry were analyzed via cpptraj. MM/GBSA was computed in a unit of kcal/mol.

2.6 Binding free energy evaluation

Molecular mechanics/Generalized Born-Surface Area (MM/GBSA) was used to compute an average binding free energy $\langle(G)\rangle$ (Kollman et al., 2000 and Hou et al 2011). The $\langle(G)\rangle$ was taken from an average molecular mechanical energy $\langle(E_{MM})\rangle$, an average solvation free energy $\langle(G_{GBSA})\rangle$ from a GB model, and a polar free energy with a surface area term (SA). A solute entropy (TS_{MM}) was estimated from quasi-harmonic analysis of molecular dynamics simulation (Jayaram et al., 1998):

$$\langle(G)\rangle = \langle(E_{MM})\rangle + \langle(G_{GBSA})\rangle - TS_{MM}.$$

The average energy was defined as $\langle(E_{MM})\rangle$ and obtained AMBER functional formula (Kollman, 1993):

$$\langle(E_{MM})\rangle = \langle(E_{bond})\rangle + \langle(E_{angle})\rangle + \langle(E_{torsion})\rangle + \langle(E_{vdw})\rangle + \langle(E_{elec})\rangle.$$

Each functional energetic form was written as followed:

$$E_{bond} = \sum_{bond} K(r - r_{eq})^2$$

$$E_{angle} = \sum_{angle} K_{\theta}(\theta - \theta_{eq})^2$$

$$E_{torsion} = \sum_{torsion} \frac{V_n}{2} (1 + \cos(n\phi - \gamma))$$

$$E_{vdw} = \sum_{i<j} \left(\frac{A_{ij}}{R_{ij}^{12}} - \frac{B_{ij}}{R_{ij}^6} \right)$$

$$E_{elec} = \sum_{i<j} \frac{q_i q_j}{\epsilon R_{ij}}.$$

The average binding free energy (ΔG) in kilocalorie per mol (kcal/mol) was calculated from the following equation:

$$\Delta G = \langle(G_{complex})\rangle - \langle(G_{receptor})\rangle - \langle(G_{ligand})\rangle$$

$G_{complex}$, $G_{receptor}$, and G_{ligand} denote free energies from the complex structure, receptor structure, and drug/compound structure, respectively.

Part II. Validation of *trans*-(±)-kusunokinin target by *in vitro* studies

1. Methods

1.1 Cell culture condition

All human breast (MCF7, Hs578T, BT549) and ovarian cancer cells (OVCAR3, A2780, SKOV3) in this study were purchased and grown in proper media as Table 5. All of cell lines were incubated in 5% CO₂ atmosphere, at 37°C and 96% relative humidity.

Table 5. Breast and ovarian cancer cells used in this study.

Cancer cells	Subtype	Medium and supplementation	Migration aggressiveness*	Companies
MCF7	Luminal A breast cancer	RPMI-1640 with 10% FBS, 1% L-glutamine, and 1% penicillin- streptomycin	Low potential	ATCC (Manassas, VA, USA)
Hs578T	Triple negative breast cancer	DMEM with 10% FBS, 1% L-glutamine, and 1% penicillin- streptomycin	Aggressive	ATCC (Manassas, VA, USA)
BT549	Triple negative breast cancer	RPMI-1640 with 10% FBS, 1% L-glutamine, and 1% penicillin- streptomycin	Aggressive	ATCC (Manassas, VA, USA)
OVCAR3	High-grade serous ovarian cancer	RPMI-1640 with 20% FBS, 1% L-glutamine, and 1% penicillin- streptomycin	Low potential	ATCC (Manassas, VA, USA)
A2780	Non-serous ovarian cancer	RPMI-1640 with 10% FBS, 1% L-glutamine, and 1% penicillin- streptomycin	Aggressive	ECACC (Salisbury, Wiltshire, UK)
SKOV3	Non-serous ovarian cancer	RPMI-1640 with 10% FBS, 1% L-glutamine, and 1% penicillin- streptomycin	Aggressive	ATCC (Manassas, VA, USA)

Note: *Yang et al., 2017; Potts et al., 2019

1.2 Compounds for cancer cell treatment

The compounds utilized for the treatment of cancer cells in this study are outlined in Table 6. All of the compounds were initially prepared as stock solutions by dissolving them in DMSO, with the exception of doxorubicin and cisplatin, which were dissolved in DI water.

Table 6. Substances for cancer cell treatment.

Substances	Companies	CAS number
<i>Trans</i> -(±)-kusunokinin ((±)KU)	It was synthesized as a previous report (Rattanaburee et al., 2019)	-
<i>Trans</i> -(-)-arctiin ((-)AR)	MedChemExpress (NJ, USA)	20362-31-6
Zopolrestat (ZP)	Sigma-Aldrich (Saint Louis, MO, USA)	110703-94-1
Epalrestat (EP)	Sigma-Aldrich (Saint Louis, MO, USA)	82159-09-9
Doxorubicin (DOX)	Sigma-Aldrich (Saint Louis, MO, USA)	25316-40-9
Cisplatin (CIS)	Sigma-Aldrich (Saint Louis, MO, USA)	15663-27-1

1.3 Cytotoxicity by MTT assay

Trans-(±)-kusunokinin and other compounds, as shown in Table 5 tested the cytotoxicity in breast and ovarian cancer cells using the 3-(4,5-dimethylthiazol-2-yl)-2,5-diphenyltetrazolium bromide (MTT) assay as previously described (Sriwiriyan et al., 2014). All the cancer cell lines were seeded in a 96-well plate at appropriate density (3.0×10^4 , 2.5×10^4 , 2.0×10^4 , 1.0×10^4 , 2.0×10^4 , 3.7×10^4 cells/well for BT549, Hs578T, MCF7, A2780, SKOV3, and OVCAR3 cells, respectively, with a volume of 100 μ l/well). After 24 h of incubation, cells were treated with various concentrations of *trans*-(±)-kusunokinin, *trans*-(-)-arctiin, zopolrestat, epalrestat, doxorubicin, and cisplatin for 72 h. After that, cells were washed with phosphate buffer solution (PBS), then added 100 μ l/well of MTT solution and incubated at 37°C for 30 min. Next, cells were added 100 μ l/well of DMSO to dissolve the formazan crystals. The cells were incubated at room temperature for 30 min, with measures taken to prevent exposure to light. Subsequently, cell viability was assessed by measuring the absorbance at wavelengths of 570 nm and 650 nm. The half maximal

inhibitory concentration (IC₅₀) value was then computed using a Varioskan™ LUX Multimode Microplate Reader (ThermoFisher Scientific, Waltham, MA, USA).

1.4 Aldose reductase activity assay

The evaluation of aldose reductase activity towards *trans*-(±)-kusunokinin and other compounds including *trans*-(-)-arctiin (a lignan reported as an ARI), zopolrestat (a potential ARI), epalrestat (used as a positive control), and DMSO (solvent control) was conducted utilizing the Aldose Reductase Inhibitor Screening Kit (BioVision, CA, USA). The procedure was executed in accordance with the guidelines provided by the manufacturer. The procedure involved the preparation of the aldose reductase (AR) enzyme solution, containing 10 µM DTT, by diluting it at a ratio of 1:90 with AR buffer, and maintaining it on ice. Additionally, NADPH was prepared by diluting it at a ratio of 1:18 with AR buffer. The AR substrate reaction, involving glucose, was prepared by diluting it at a ratio of 1:10 with AR buffer. The tested compounds were subjected to varying concentrations, as outlined below:

1. *Trans*-(±)-kusunokinin: 5, 10, 20, 40, 80 µM
2. *Trans*-(-)-arctiin: 5, 10, 20, 40, 80 µM
3. Epalrestat: 0.312, 0.625, 1.250, 2.500, 5.000 µM
4. Zopolrestat: 15, 30, 60, 120, 240 nM

The solution formulated according to this protocol was introduced into a 96-well plate, as per the specifications provided in Table 7. Subsequent to the addition of the AR substrate reaction, the plate was promptly subjected to the measurement of the reduction in absorbance at OD 340 nm in kinetic mode. This monitoring spanned a duration of 100 minutes at a temperature of 37°C, accomplished using the Varioskan™ LUX Multimode Microplate Reader (Thermo Fisher Scientific, MA, USA). To ensure accuracy, all the readings were adjusted by subtracting the values obtained from the background control (lacking the enzyme). Subsequently, the percentage of relative activity was computed using the ensuing formula:

$$\% \text{ Relative activity} = \frac{|\text{Slope of [Tested compound]}|}{|\text{Slope of [Enzyme control]}|}$$

Table 7. Steps for adding solution in each condition of aldose reductase activity.

Solutions	Conditions				
	Tested compound	Inhibitor control	Enzyme control	Background control	Solvent control
AR enzyme	90 μ l	90 μ l	90 μ l	-	90 μ l
NADPH	60 μ l	60 μ l	60 μ l	60 μ l	60 μ l
Tested compound	10 μ l				
100 μ M Epalrestat		10 μ l			
AR buffer			10 μ l	100 μ l	
DMSO					10 μ l
Mix thoroughly and incubate at 37°C for 20 min. (protect from light)					
AR substrate	40 μ l	40 μ l	40 μ l	40 μ l	40 μ l
Total volume	200 μ l	200 μ l	200 μ l	200 μ l	200 μ l

1.5 Cellular thermal shift assay (CETSA)

For the implementation of CETSA, cell lines characterized by high AKR1B1 expression were selected. Hs578T and SKOV3 cells were chosen as representative models exhibiting elevated AKR1B1 expression. The procedure was conducted in accordance with previously established methodologies (Jafari et al., 2014). To commence, Hs578T and SKOV3 cells were cultured and subsequently collected in 50 ml conical tubes, with a cell density of 2×10^6 cells/ml, equating to 15 ml for each condition. For each condition, cells were exposed to *trans*-(\pm)-kusunokinin at concentrations of 20 μ M, 10 μ M, and 5 μ M, achieved by adding 30 μ l, 15 μ l, and 7.5 μ l, respectively, to the cells. The control condition consisted of adding 30 μ l of DMSO. Following this, the cells were incubated in a CO₂ incubator at 37°C for 1 h. After the incubation period, cells were harvested and centrifuged at 300x g for 3 min. The cell suspension was removed, and the cells were resuspended with 15 ml of PBS. This washing process was repeated twice. Subsequently, the cells were collected in 1 ml of PBS supplemented with 1x protease inhibitor cocktail (Sigma-Aldrich, Saint Louis, MO, USA) and mixed thoroughly. The resulting cell suspension was divided

into 0.2 ml PCR tubes at a volume of 100 μ l per tube. The samples were subjected to heating at 60°C or 75°C for 3 min, followed by cooling at 25°C for 3 min within a C1000 thermal cycler (Bio-rad, CA, USA). The heated cells were rapidly frozen in liquid nitrogen and stored at -80°C overnight. Following this, cell lysis was carried out through two freeze-thaw cycles involving liquid nitrogen, and the lysate was subsequently subjected to centrifugation at 20,000x g for 20 min at 4°C. The resulting supernatants were analyzed for AKR1B1 protein levels through Western blot analysis.

1.6 Thiobarbituric acid reactive substances assay (TBARS)

Hs578T cells were seeded on 6-well plates at a density of 5×10^5 cells/well for 24 h before being treated with various concentration of *trans*-(\pm)-kusunokinin or epalrestat for 24 h. After that, cells were induced to undergo lipid peroxidation by 100 mM glucose for 1 h. Cells were harvested and resuspended at 1×10^7 cells/ml in PBS and sonicated with 50% amplitude, pulse on/off for 2 sec, time for 1 min, 2 cycles. The quantitation of malondialdehyde (MDA), a marker of oxidative stress, was measured using OxiSelect™ TBARS Assay kit (Cell Biolabs, San Diego, CA, USA) following the manufacturer's protocol. The sonicated cells were diluted 1:1 with an SDS lysis solution. Then, the sonicated cells were incubated at room temperature for 5 min and were added to 125 μ l of thiobarbituric acid (TBA) solution (concentration of 5.2 mg/ml and adjusted to pH 3.5 by NaOH). After that, the samples were heated at 95°C for 1 h. The samples were immediately chilled on ice for 5 min. Then, the samples were centrifuged at 3,000x g for 15 min. The supernatants with a volume of 150 μ l were transferred to a 96-well plate. The samples were measured the absorbance at 532 nm together with the MDA standard (final concentration range of 0 - 62 μ M) which was prepared as per the same procedure.

1.7 Cells treatment and protein extraction

Hs578T cells were seeded on 24-well plates at a density of 7×10^4 cells/well for 24 h. After that, Hs578T cells were treated with *trans*-(\pm)-kusunokinin (1.40 and 2.79 μ M) or epalrestat (24.02 and 48.04 μ M) for 48 h. Cells were harvested by trypsinization and kept at -80°C. Cell pellets were lysed using RIPA buffer. Then, cells were vortexed and chilled on ice for 10 min. After that, homogenized cells were centrifuged at 14,000x g for 10 min at 4

°C. The supernatants were measured the protein quantification by Bradford assay. Protein samples were adjusted to a desired concentration by 4X SDS sample loading dye (0.2 M Tris-HCl pH 6.8, 277 mM SDS, 0.4 M DTT, 4.3 M glycerol, 8% (w/v) β -mercaptoethanol, and 6 mM bromophenol blue) and boiled for 5 min. After that, protein samples were chilled on ice for 10 min and kept at -20°C (Merck KGaA, 2020).

1.8 SDS-PAGE

The glass plates were meticulously cleaned using ethanol and then arranged on a casting stand. Subsequently, the resolving gel solution (as detailed in Table 8) was poured into the glass plates. It was important to take care in adding a layer of distilled water atop the gel to prevent dehydration, and the gel was allowed to solidify over a span of 90 min. Following this, the distilled water was removed, and the space between the glass plates was dried using filter paper. The stacking gel solution (also outlined in Table 8) was then poured, and a comb was cautiously inserted to prevent the formation of air bubbles. This configuration was allowed to solidify over a period of 30 min. The electrophoresis running unit was subsequently assembled. The comb was removed, and the well was washed using 1x running buffer, diluted from 5x running buffer consisting of 15.1 g tris-base, 94 g glycine, 25 ml of 20% SDS, and 1,000 ml of distilled water. The chamber was filled with 1x running buffer. For the electrophoresis process, protein samples were loaded at a quantity of 15 μ g. The voltage was initially set to 80 V for 30 minutes. Subsequently, the voltage was adjusted to 120 V and the process was continued for 1 hour, or until the protein had migrated to the end of the gel (Merck KGaA, 2020).

1.9 Protein transfer and Western blotting

The gel was removed from its cassette and any stacking gel and wells were trimmed away. Subsequently, the gel, nitrocellulose membrane, filter paper, and fiber pad were assembled within the cassette holder. The avoidance of air bubbles between these layers was ensured by rolling. This cassette holder was then positioned within the transfer tank. Transfer buffer, composed of 7.9 g glycine, 5.8 g tris-base, 200 ml methanol, and 600 ml distilled water, was introduced into the tank. The electrophoresis unit was assembled and the voltage was initially set to 35 volts, maintained at 4°C overnight, and then adjusted to

100 volts for 30 min. Following the transfer, the membrane was taken out and subjected to staining with Ponceau S solution (0.3% w/v) in 5% acetic acid (v/v), using agitation for 5 min. The membrane was subsequently rinsed with distilled water, after which the protein band of interest was excised. The membranes were subjected to blocking with either 5% non-fat milk powder or 5% BSA in 1x TTBS buffer (prepared by diluting 5x TTBS buffer, consisting of 5.8 g Tris-base, 5 ml Tween 20, 45 g NaCl, 31.75 g Tris-HCl, with distilled water until reaching a total volume of 1,000 ml) for 1 h on a rotator. Following the blocking step, the membranes underwent three washes with 1% non-fat milk powder in 1x TTBS buffer. Each wash involved rotation for 5 min. The membranes were then subjected to incubation with primary antibodies, suitably diluted in 1% milk or 1% BSA in TTBS buffer. The dilution ratios and rotation times for primary antibodies are as specified in Table 10. Following primary antibody incubation, the membranes were washed thrice with 1% milk in 1x TTBS buffer, again rotating for 5 min each time. Subsequently, the membranes were exposed to secondary antibodies for 1 h (details provided in Table 10), followed by three washes with 1% milk in 1x TTBS buffer, with each wash involving rotation for 5 min. The detection of bound antibodies was executed using a chemiluminescence assay kit (Thermo Scientific, Rockford, IL, USA) and the results were visualized through a CCD camera (Merck KGaA, 2020). The intensity of the protein bands was assessed using Image J software (NIH, Bethesda, MD, USA).

Table 8. SDS-PAGE gel solution.

Solutions	Stacking gel	Resolving gel
	(4%)	(12%)
Deionized water	3.28 ml	1.45 ml
40% Acrylamide (N, N-methylenebisacrylamide, 19:1)	2.31 ml	250 μ l
1.0 M Tris-HCl (pH 6.8)	1.95 ml	-
1.5 M Tris-HCl (pH 8.8)	-	250 μ l
10% Sodium dodecyl sulfate (SDS)	76.92 μ l	20 μ l
10% Ammonium persulfate (APS)*	76.92 μ l	20 μ l
N, N, N', N'-tetramethylethylenediamine (TEMED)*	3.08 μ l	2 μ l

Note: *APS and TEMED must be added in the last and pour immediately after preparation.

1.10 Small interfering RNA condition

Hs578T cells were seeded into 24-well plates, with a cell density of 7×10^4 cells per well and allowed to adhere for a 24 h period. For transfection, the DharmaFECT 4 transfection reagent (Dharmacon, CO, USA) and siRNA-AKR1B1 duplexes were employed. The siRNA-AKR1B1 sequences (Ambion, CA, USA) used were as follows:

1. Cat No: 4390824; targeted exons: 8,9; 5'-UCAGUUCAAGUCAAGACCT-3'
2. Cat No: 492420; targeted exon: 5; 5'-UUAACUGCAGGCUUAUACUTC-3'

The DharmaFECT 4 transfection reagent and siRNA duplexes were diluted at ratios of 1.5:25 and 2.5:25, respectively, using Opti-MEM medium (Gibco, NE, USA). The diluted transfection reagent and siRNA were mixed and allowed to incubate at room temperature for 5 min. Subsequently, the cell media were replaced with 450 μ l per well of Opti-MEM medium. The mixture solution, comprising the transfection reagent and siRNA, was then added to each well at a volume of 50 μ l (resulting in a final siRNA concentration of 100 nM). The cells were further incubated for 24 h. A negative control was introduced using siGENOME control (Horizon Discovery, Waterbeach, Cambridge, UK), which targets firefly luciferase mRNA. Following the transfection period, the cells were treated with 2.79 μ M trans-(\pm)-kusunokinin or 48.04 μ M epalrestat for a duration of 48 hours, in line with specifications in Table 9. Subsequently, the cells were harvested through trypsinization, and the protein levels of AKR1B1 and its downstream elements were assessed using Western blotting.

1.11 Statistical analysis

All data were presented as the mean \pm standard deviation (SD) and were derived from three independent experiments. The statistical significance between the two data sets was assessed using the Student's *t*-test. For comparisons involving multiple groups, a one-way analysis of variance (ANOVA) was performed, followed by Tukey's multiple comparisons test. These analyses were conducted using Prism GraphPad 8.0.1 software (San Diego, CA, USA). A *p*-value less than 0.05 was deemed indicative of statistically significant differences.

2. Materials

2.1 Chemicals, reagents, antibodies and equipment

All the chemicals, reagents, and antibodies employed in this research were procured from the respective companies listed in Table 10 and 11. The equipment utilized for this research was available at the Department of Biomedical Sciences and Biomedical Engineering, Faculty of Medicine, Prince of Songkla University, as detailed in Table 12.

Table 9. Small interfering RNA procedures.

Solution	Conditions				
	Transfection reagent control	siRNA control	siRNA-AKR1B1	siRNA-AKR1B1 + <i>trans</i> -(±)-kusunokinin	siRNA-AKR1B1 + epalrestat
Solution I					
DharmaFECT 4 transfection reagent	1.50 µl	1.50 µl	1.50 µl	1.50 µl	1.50 µl
Opti-MEM medium	23.50 µl	23.50 µl	23.50 µl	23.50 µl	23.50 µl
Solution II					
RNAse free water	2.50 µl				
siGENOME non-targeting control		2.50 µl			
siRNA-AKR1B1 duplexes I			1.25 µl	1.25 µl	1.25 µl
siRNA-AKR1B1 duplexes II			1.25 µl	1.25 µl	1.25 µl
Opti-MEM medium	22.50 µl	22.50 µl	22.50 µl	22.50 µl	22.50 µl
Mixed the solution I and solution II and incubated at room temperature for 5 min before treat the cells for 24 h.					
DMSO	2.00 µl	2.00 µl	2.00 µl		
0.7 mM <i>trans</i> -(±)-kusunokinin				2.00 µl	
12 mM epalrestat					2.00 µl
Replaced the medium and treated the cells for 48 h before harvesting the cells by trypsinization.					

Table 10. List of antibodies used in this study.

Antibodies	MW (kDa)	Companies	Catalogue number	Source	Blocking	1 st Ab dilution	Incubation time	2 nd Ab dilution	Detection kit
Anti-N-cadherin	140	Cell signaling	14215	Mouse	5% Milk	1:1,000	Overnight	1:2,500	Femto
Anti-E-cadherin	120	BD-Bioscience	610181	Mouse	5% Milk	1:5,000	3 h	1:5,000	Femto
Anti-NF- κ B	65	Cell signaling	8242	Rabbit	5% Milk	1:500	3 h	1:2,500	Pico
Anti- β -actin	42	Sigma-aldrich	A5441	Mouse	5% Milk	1:5,000	1 h	1:5,000	Pico
Anti-AKR1B1	36	Sigma-aldrich	AV48180	Rabbit	5% Milk	1:1,000	Overnight	1:2,500	Dura
Anti-Twist2	18	Sigma-aldrich	WH117581M1	Mouse	5% BSA	1:1,000	Overnight	1:2,500	Femto
Anti-COX2	74	Cell signaling	4842	Rabbit	5% Milk	1:500	3 h	1:2,500	Femto
Anti-AKT	60	Cell signaling	9272	Rabbit	5% BSA	1:1,000	3 h	1:2,500	Dura
Anti-PKC δ	78	Cell signaling	2058	Rabbit	5% Milk	1:1,000	3 h	1:2,500	Femto
Anti-STAT3	79,86	Cell signaling	4904S	Rabbit	5% Milk	1:2,000	3 h	1:2,500	Femto
Anti-Nrf2	61	Santa cruz	sc-365949	Mouse	5% Milk	1:1,000	Overnight	1:2,500	Femto
Anti-rabbit IgG	-	Cell signaling	7074S	Goat	-	-	-	-	-
Anti-mouse IgG	-	Cell signaling	7076S	Goat	-	-	-	-	-

Note: MW; molecular weight, 1st Ab; primary antibody, 2nd Ab; secondary antibody.

Table 11. Chemicals and reagents used in this study.

Chemicals and reagents	Cat. No	Companies
Acrylamide/Bis solution (40%, 29:1)	161-0148	Bio-Rad
Aldose Reductase Inhibitor Screening Kit	K174-100	BioVision
Ammonium Persulfate (APS)	161-0700	Bio-Rad
Chromatography paper 3 mm	1001-090	Whatman
Dulbecco's Modified Eagle Medium	31600-034	Gibco
Fetal bovine serum (FBS)	16000036	Gibco
L-glutamine 200 mM	LS25030081	Gibco
Methanol	UN1230	Labscan
MTT reagent	M6494	GibThai
Nitrocellulose membrane (0.45 µm)	162-0115	Bio-Rad
OxiSelect™ TBARS Assay kit	STA-330	Cell Biolabs
Penicillin-streptomycin	15140122	Gibco
Pierce® RIPA Buffer	89900	ThermoFisher
Polyoxyethylene 20 (Tween 20)	9480	Calbiochem
Potassium Chloride (KCl)	0395	Amresco
Potassium Phosphate (KH ₂ PO ₄)	P-0662	Sigma-Aldrich
Precision Plus Protein™ Kaleidoscope™	161-0375	Bio-Rad
Protein assay dye reagent concentrate	500-0006	Bio-Rad
Purified BSA 100X 10 mg/ml	B9001S	Biolabs
RPMI Medium 1640	31800022	Gibco
Sodium Bicarbonate (NaHCO ₃)	0865	Amresco
Sodium Chloride (NaCl)	0241	Amresco
Sodium Dodecyl Sulfate (SDS)	0227	Amresco
SuperSignal™ West Dura Extended Duration	34075	ThermoFisher
SuperSignal™ West Femto Maximum Sensitivity	34095	ThermoFisher
SuperSignal™ West Pico PLUS Chemiluminescent	34079	ThermoFisher
Tris Hydrochloride (Tris-HCL)	M108	Amresco
Tris-base	0826	Amresco
Trypsin-EDTA (0.25%)	25200056	Gibco

Table 12. Equipment used in this study.

Equipment	Companies
C1000 Thermal Cycler	Bio-rad
CO ₂ incubator	Sheldon
Eppendorf centrifuge 5417C	Eppendorf
Esco class II cabinet	Sorenson Bioscience
Fusion FX CCD	Fisher Biotec
Gilson pipetman 0.2-2 µl, 2-20 µl, 20-200 µl and 1000 µl	Gilson
Mettler Toledo pH meter	Metter
Mini rocker MR-1	Bio san
Multifit pipette tips 0.1-10 µl, 1-200 µl and 100-1000 µl	Sorenson Bioscience
Olympus CK2 inverse microscope	Olympus
Olympus microscope digital camera (DPT2 IX71)	Olympus
Safeseal microcentrifuge tubes 11510	Sorenson Bioscience
Sigma Z-16PK centrifuge	Sartorius
Spectra Max M5 microplate reader	Molecular Devices
Universal 30RF centrifuge	Universal
Vortex-2 Genie	Scientific Industries
Water bath shaker ZHWY-110X30	ZHICHENG

CHAPTER 3

RESULTS

Part I. Identification of *trans*-(-)-kusunokinin target by *in silico* studies

1. *Trans*-(-)-kusunokinin target screening

Trans-(-)-kusunokinin target screening was performed using molecular docking by consideration of binding energy between *trans*-(-)-kusunokinin toward 114 possible target proteins from 8 mechanisms, including cell proliferation, multidrug resistance, epigenetic regulation, cell migration, cell survival, cell cycle progression, angiogenesis, and DNA repair. All candidate target proteins were selected based on following criteria

1. Binding free energy (ΔG) of *trans*-(-)-kusunokinin is lower than -10.00 kcal/mol.
2. Binding free energy of *trans*-(-)-kusunokinin can be comparable to native ligand with a discrepancy of 1 kcal/mol.
3. *Trans*-(-)-kusunokinin binding site located in the protein at the same site of native ligand.

The selected candidate protein must match all the mentioned criteria. The binding energy from the docking studies of *trans*-(-)-kusunokinin and native ligand of the exploration protein were shown in Table 13. The results exhibited that hits-target from the filtration with no violation of all criteria were AKR1B1 and MEK2.

Trans-(-)-kusunokinin showed the best binding potential with AKR1B1 and provided the outstanding docking score of -11.11 kcal/mol lower than AKR1B1 native ligand (IDD594) with ΔG of -10.73 kcal/mol. While MEK2, signaling protein mediated-cancer cell proliferation was predicted as the possible *trans*-(-)-kusunokinin target with the binding energy -10.14 kcal/mol and showed lower than native ligand (5EA) with ΔG of -9.56 kcal/mol. However, AKR1B1 was our interest to further investigation in consequence of the lowest binding energy and several supporting report that lignan-base structure revealed the AKR1B1 inhibition such as arctigenin and arctiin.

Table 13. Binding energy of *trans*-(-)-kusunokinin and native ligands.

Protein	PDB code	Relative binding energy (kcal/mol)	
		<i>Trans</i> -(-)-kusunokinin	Native ligand
Cell migration			
AKR1B1	1US0	-11.11	-9.83
WASP	1T84	-8.75	-9.77
ROCK2	4WOT	-8.68	-11.23
PAK6	4KS7	-8.54	-9.80
CDC42	1DOA	-8.36	-7.67
RAC3	2C2H	-8.32	-5.96
ROCK1	6E9W	-8.12	-9.91
PAK1	2HY8	-7.72	-10.76
Cell proliferation			
MEK2	1S9I	-10.14	-9.56
TrkC	3V5Q	-9.67	-13.51
TrkB	4AT3	-9.60	-9.94
FGFR3	4K33	-9.49	-8.60
RSK2	1T7V	-9.46	-8.72
TR α	3ILZ	-9.41	-11.48
EphA3	3DZQ	-9.42	-12.9
SGK1	2R5T	-9.32	-21.57
SHIP-1	6IBD	-9.32	-10.85
PPARD	5XM X^*	-9.32	-10.84
TR β	1N46	-9.31	-11.48
EP3	6M9T	-9.22	-8.08
BMPR2	3G2F	-9.19	-8.29
ACVR2B	2QLU	-9.18	-8.82
EP4	5YHL	-9.18	-11.86
BMPR1B	3MDY	-9.14	-9.97
PDGFRA	5GRN	-9.10	-12.28
MSK2	O75676 *	-9.04	-5.38

Note: * SWISS-MODEL structure was modelled homologically based on the respective PDB.

Table 13. Binding energy of *trans*-(-)-kusunokinin and native ligands (continued).

Protein	PDB code	Relative binding energy (kcal/mol)	
		<i>Trans</i> -(-)-kusunokinin	Native ligand
ADORA2A	6GT3	-9.01	-7.47
MK3	3FHR	-8.94	-10.01
PLA2	1POE	-8.92	-8.40
SGK3	Q96BR1*	-8.90	-9.59
JNK2	3NPC	-8.77	-14.72
ALK	5FTO	-8.75	-11.65
DDR2	6FER	-8.74	-10.35
INSR	3EKK	-8.72	-10.18
LAT1	6IRS	-8.72	-7.81
DDR1	3Z0S	-8.70	-10.79
JNK1	2GMX	-8.70	-7.25
MSK1	3KN5	-8.68	-7.85
RON	3PLS	-8.67	-8.15
YES1	P07947*	-8.67	-9.86
RSK1	2Z7Q	-8.67	-15.87
p70S6K- β	Q9UBS0*	-8.60	-9.26
MEK6	3FMF	-8.59	-10.98
MER	3BPR	-8.52	-7.62
BLVRA	2H63	-8.52	-6.39
PPARA	1KKQ	-8.50	-10.09
ALK1	3MY0	-8.49	-9.65
AKT2	2JDO	-8.39	-9.54
p70 S6K- α	3A62	-8.33	-10.45
PLCB	2ZKM	-8.27	-9.38
LYN	3A4O	-8.25	-8.34
c-RAF	3OMV	-8.24	-9.41
TAK1	3P0U	-8.24	-7.38
BMPR1A	2H62	-8.22	-9.40

Note: *SWISS-MODEL structure was modelled homologically based on the respective PDB.

Table 13. Binding energy of *trans*-(-)-kusunokinin and native ligands (continued).

Protein	PDB code	Relative binding energy (kcal/mol)	
		<i>Trans</i> -(-)-kusunokinin	Native ligand
MEK3	P46734*	-8.21	-18.06
RHEB	6BT0	-8.19	-9.04
EphA7	3DKO	-8.16	-10.47
CTSL2	1FH0	-8.16	-9.66
PLCG	4FBN	-8.15	-7.82
B-Raf	5CSW	-8.13	-10.96
FGFR2	1OEC	-8.07	-10.10
FGFR4	6JPJ	-8.05	-7.52
SHP2	5EHR	-8.03	-10.74
MELK	4D2P	-7.88	-10.58
MTOR	1FAP	-7.87	-20.22
ACVR1B	P36896*	-7.79	-8.91
EphB1	5MJA	-7.78	-9.16
EphB3	5L6O	-7.78	-7.62
AXL	5U6B	-7.75	-9.82
BTK	6O8I	-7.68	-8.99
FAK2	3FZR	-7.67	-7.93
MEK7	5Z1E	-7.61	-7.47
MEK4	3ALO	-7.44	-18.63
IRS-1	1QQG	-7.42	-7.21
WIP1	O15297*	-7.39	-6.64
SHIP-2	4A9C	-7.21	-12.79
GRB7	4WWQ*	-6.89	-8.11
FNTA	1SA4	-6.85	-8.61
CXCR4	3OE9	-6.68	-7.74
SP1	1SP2	-6.45	-5.90
YAP	3KYS	-6.45	-8.86
HSC70	3FZH	-6.36	-6.87

Note: *SWISS-MODEL structure was modelled homologically based on the respective PDB.

Table 13. Binding energy of *trans*-(-)-kusunokinin and native ligands (continued).

Protein	PDB code	Relative binding energy (kcal/mol)	
		<i>Trans</i> -(-)-kusunokinin	Native ligand
p75NTR	2N80	-6.21	-5.98
MYC	6G6K	-5.57	-4.90
Multidrug resistance			
ABCC1/MRP1	2CBZ	-8.66	-8.71
ABCB1/P-gp	6FN1	-6.63	-8.75
ABCC3/MRP3	O15438*	-6.11	-6.16
ABCC2/MRP2	Q92887*	-5.98	-6.82
ABCG2/BCRP	6ETI	-5.45	-5.71
Epigenetic regulation			
BRDT	4KCX	-8.92	-8.92
BRD4	2YEL	-8.75	-10.56
BRD3	3S91	-8.60	-10.42
BRD2	2YEK	-8.57	-9.98
HDAC1	5ICN	-7.87	-4.58
Cell survival			
MCL1	6O6F	-9.11	-12.54
I κ B-alpha	1IKN	-8.65	-11.94
SERCA1	2BY4	-7.83	-1.11
BFL-1	4ZEQ	-7.72	-8.43
BCLW	4CIM	-7.66	-9.59
BAG1	3FZK	-6.13	-4.98
IKKB	4KIK	-6.04	-9.67
IKKA	5EBZ	-5.91	-7.87
Cell cycle			
Aurora B	4AF3	-8.71	-10.01
CDK7	1UA2	-8.52	-11.15
CDK4	2W96	-8.22	-9.02
CCNE1	1CKP	-8.07	-7.90
MPS1	2ZMD	-7.93	-6.75

Table 13. Binding energy of *trans*-(-)-kusunokinin and native ligands (continued).

Protein	PDB code	Relative binding energy (kcal/mol)	
		<i>Trans</i> -(-)-kusunokinin	Native ligand
Angiogenesis			
VEGFR1	3HNG	-8.92	-11.68
TIE2	3L8P	-8.42	-13.04
PHD2	2HBT	-7.76	-11.19
HIF1A	4H6J	-5.92	-6.89
DNA repair			
PARP2	4TVJ	-8.85	-13.07
PARP1	5XSR	-8.71	-9.23
ERCC1	2A1I	-8.53	-8.00

2. Preliminary predicted binding energy and interaction of *trans*-(-)-kusunokinin and AKR1B1 inhibitors on active site

The accuracy and precision of Autodock program were validated by self-redocking. The result showed that IDD594 redocking ligand exhibited almost the same orientation overlay the native ligand from the crystallography structure with RMSD value of 0.37 Å which lower than the cutoff value of 2.0 Å (Figure 26). Moreover, other inhibitors showed a similar binding of AKR1B1 structure. These results suggested reproducibility that process was valid and reliable.

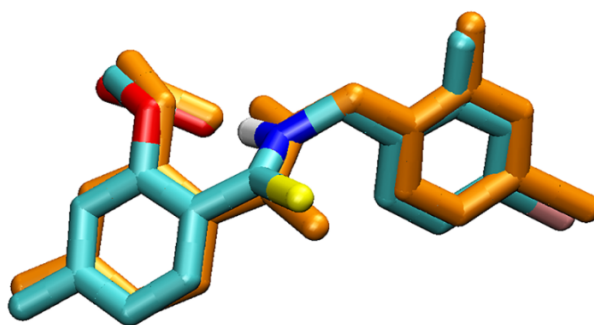


Figure 26. IDD594 overlay orientation of self-redocking. Cyan structure was exhibited as a native ligand; orange structure was exhibited as a redocking orientation. Conformational sampling of self-redocking were executed from 50 genetic algorithm runs with a population size of 200 and were analyzed using VMD package.

The molecular docking study showed that *trans*-(-)-kusunokinin suitably inserted in the AKR1B1 active site that surrounded of hydrophobic and aromatic amino acid (Figure 16). *Trans*-(-)-kusunokinin active site exhibited 3 apparent binding pockets including a large pocket with hydrophobic nature (Trp79, Trp111, Phe115, Phe122, Trp219, Cys298, Leu300, Cys303, and Tyr309), a small pocket with hydrophobic nature (Trp20, Val47 and Tyr48), and an anion binding pocket (Tyr48, His110, and Trp111). The result showed that 2 aromatic rings of *trans*-(-)-kusunokinin were buried in the small and large hydrophobic pockets. A carboxylic group of the compound formed hydrogen bond with the anion binding pocket while γ -butyrolactone ring of *trans*-(-)-kusunokinin was buried in the anion binding pocket (Figure 27).

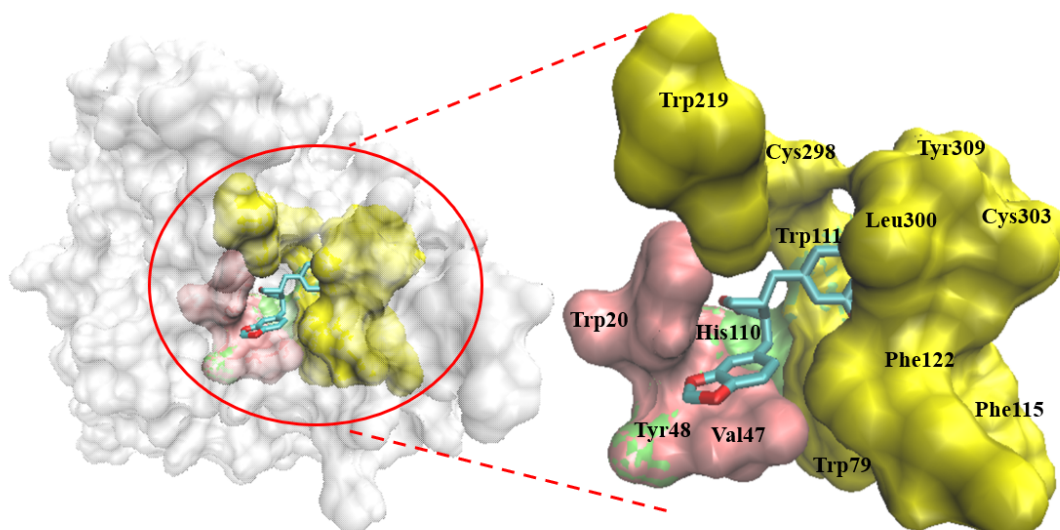


Figure 27. *Trans*-(-)-kusunokinin binding site on AKR1B1. It consists of anion binding pocket (green residues), small hydrophobic pocket (pink residues), and large hydrophobic specific pocket (yellow residues). Conformational sampling was executed from 50 genetic algorithm runs with a population size of 200 and were analyzed using VMD package.

Molecular docking of *trans*-(-)-kusunokinin against AKR1B1 along with other available AKR1B1 substrates or inhibitors was performed. In our study, the selected AKR1B1 inhibitors (ARIs) were classified into 3 categories. The first one is carboxylic ARI which contains carboxylic group and be experimentally approved the binding with AKR1B1 that be available on Protein Data Bank (Figure 28). The result showed that carboxylic ARIs provided the potential binding free energy toward AKR1B1 with the

range of -8.92 to -11.54 kcal/mol, and more than half of them revealed less than -10.00 kcal/mol (Table 6). Interestingly, *trans*-(-)-kusunokinin showed the binding energy of -11.11 kcal/mol which lower than most of carboxylic ARIs except zenarestat and zoplorestat.

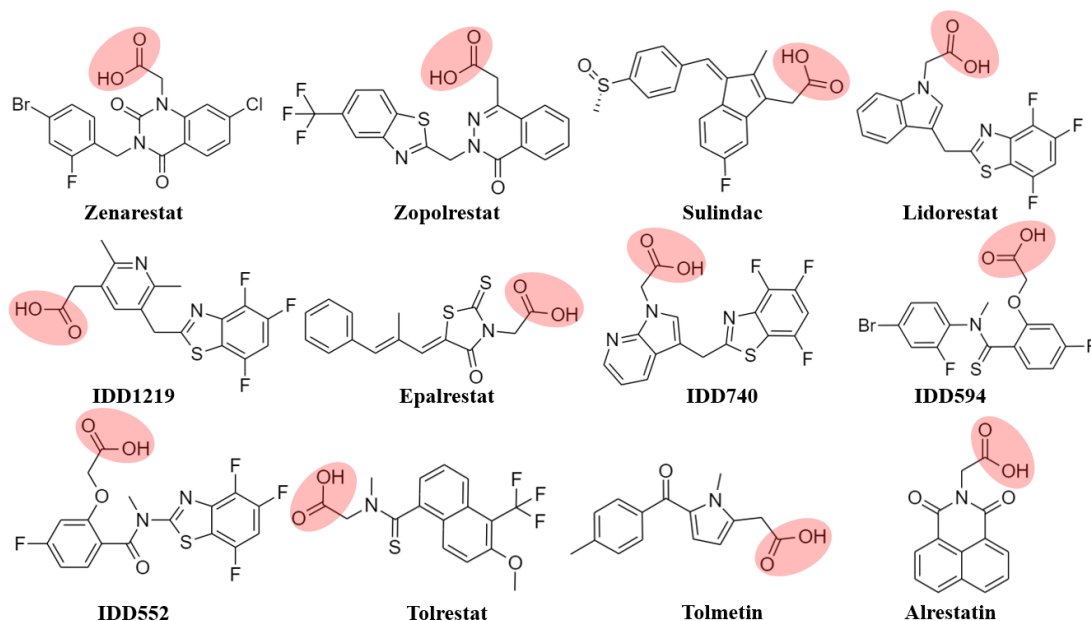


Figure 28. Structure of carboxylic ARIs. A carboxylic group was highlighted in red.

Secondly, hydantoin ARIs, contain hydantoin ring in the structure and be experimentally approved the binding with AKR1B1 that be available on Protein Data Bank (Figure 29). The result showed that minalrestat and ranirestat revealed the potential binding toward AKR1B1 with binding free energy less than -10.00 kcal/mol. While fidarestat and sorbinil revealed poor binding free energy (Table 12). Interestingly, *trans*-(-)-kusunokinin provided the binding free energy lower than all of hydantoin ARIs group.

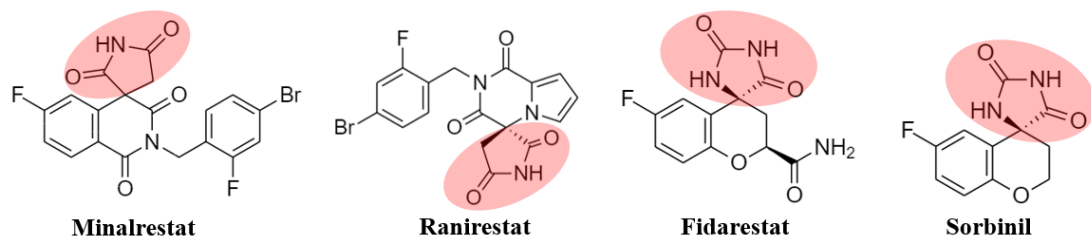


Figure 29. Structure of hydantoin ARIs. A hydantoin ring was highlighted in red.

The last group, suggested potential ARIs were selected from synthetic or natural compounds which have been reported as the potential AKR1R1 inhibitor for example; arctigenin and its glucoside arctiin are lignan compound which have similar structural feature to *trans*-(-)-kusunokinin (Figure 30). The results showed *trans*-(-)-kusunokinin provided the binding free energy better than all of suggested potential ARIs group (Table 14).

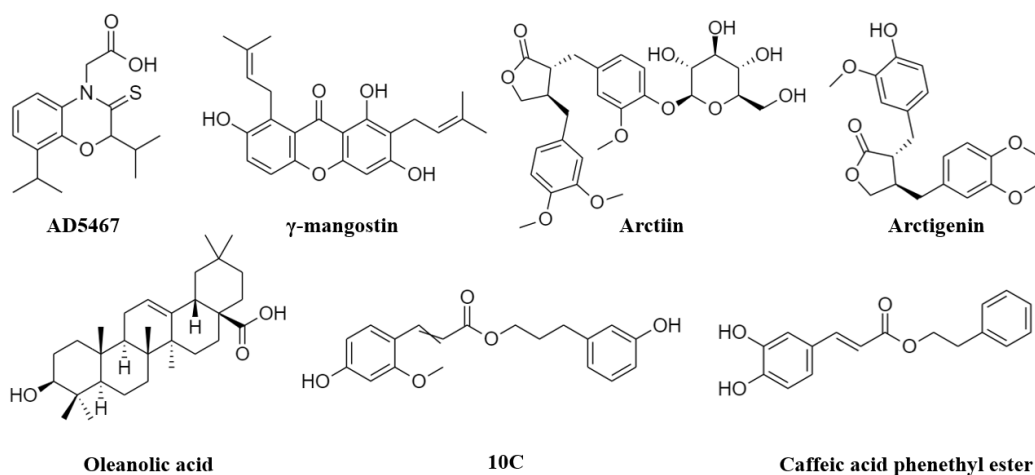


Figure 30. Structure of suggested potential ARIs.

Moreover, we further studies of molecular docking of AKR1B1 substrates and substrate analogs to compare the competitiveness of *trans*-(-)-kusunokinin to inhibit against AKR1B1 (Figure 31). The result revealed that *trans*-(-)-kusunokinin showed the potential binding free energy better than all of AKR1B1 substrates and substrate analogs. Interestingly, *trans*-(-)-kusunokinin binding site revealed the similar site to AKR1B1 substrate. The results predicted that *trans*-(-)-kusunokinin could inhibit AKR1B1 with the potential competitiveness.

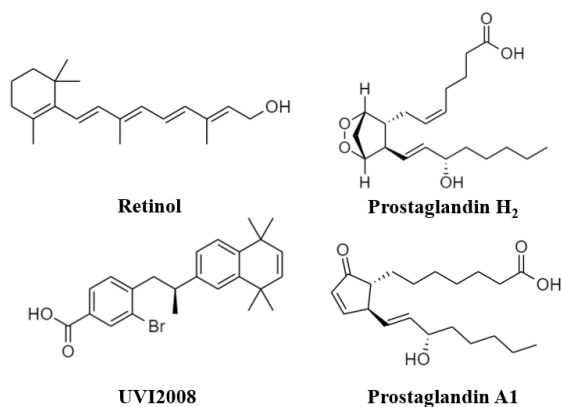


Figure 31. Structures of AKR1B1 substrate and substrate analog.

Table 14. Binding energy between ligands and AKR1B1 from molecular docking.

Ligands	PubChem CID	ΔG (kcal/mol)
<i>Trans</i> -(-)-kusunokinin	384876	-11.11
Carboxylic ARIs		
Zenarestat	5724	-11.54
Zopolrestat	1613	-11.21
Sulindac	11245227	-11.19
Lidorestat	157839	-10.92
IDD1219	10150300	-10.86
Epalrestat	1549120	-10.57
IDD740	10150441	-10.52
IDD594	4369325	-9.83
IDD552	448658	-9.53
Tolrestat	53359	-9.38
Tolmetin	5509	-9.22
Alrestatin	2120	-8.92
Hydantoin ARIs		
Minalrestat	190816	-10.88
Ranirestat	153948	-10.41
Fidarestat	160024	-7.50
Sorbinil	337359	-6.92
Suggested potential ARIs		
Oleanolic acid	10494	-10.90
AD5467	197383	-10.84
γ -mangostin	13873657	-9.63
Arctiin	100528	-9.85
Arctigenin	64981	-9.55
10C	76370315	-9.32
Caffeic acid phenethyl ester	5281787	-9.08
Substrates and substrate analogs		
UVI2008	124081750	-10.71
PGA1	5281912	-10.01
Retinol	445354	-9.91
PGH ₂	445049	-9.71

Trans-(–)-kusunokinin was positioned within the active pocket in a manner reminiscent of well-established ARIs such as epalrestat, zenarestat, and minalrestat, exhibiting a similar location and orientation. Notably, Trp20 and Trp111 emerged as recurring residues that interacted with the aromatic rings of ARIs. These residues, either individually or in combination, played a pivotal role in maintaining the conformation of the ARIs through π - π stacking interactions with the aromatic rings. Furthermore, Trp20 and Trp111 demonstrated a dual role, participating not only in π - π stacking interactions but also forming hydrogen bonds, alongside Tyr48 and His110 (Figure 32).

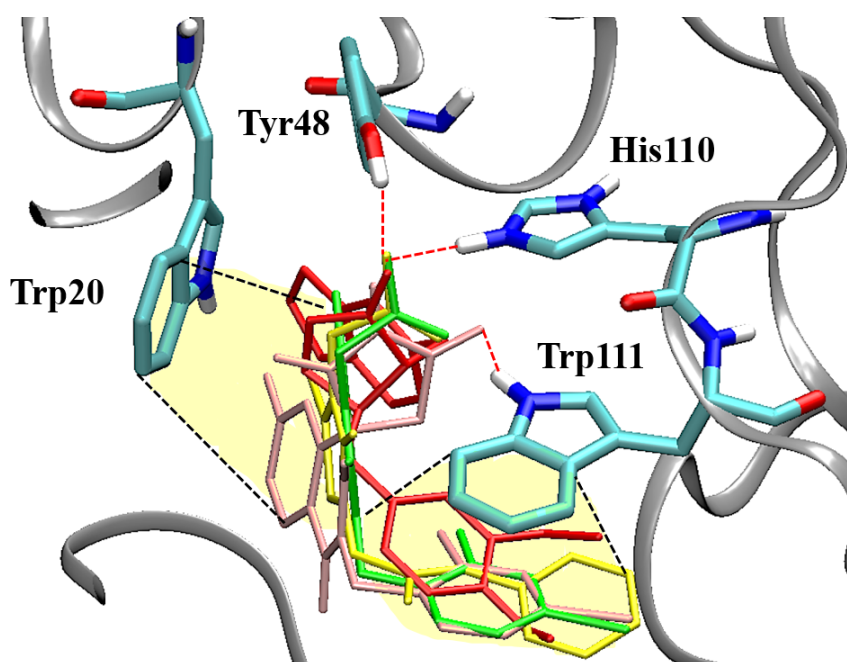


Figure 32. Observed interaction of *trans*-(–)-kusunokinin and ARIs with AKR1B1. Ligands are showed in the binding site including epalrestat (yellow), zenarestat (green), minalrestat (pink) and *trans*-(–)-kusunokinin (red). Red dashed lines indicate hydrogen bonds, whereas black dashed lines surrounded yellow represent the π - π interaction. Conformational sampling of self-redocking were executed from 50 genetic algorithm runs with a population size of 200 and were analyzed using VMD package.

3. Molecular dynamics trajectory analysis

Molecular docking simulations might not accurately capture the dynamic behavior within the actual reaction environment. To address this limitation and to

better represent the realistic dynamic behavior of both ligand-free AKR1B1 and ligand-AKR1B1 complexes, molecular dynamics simulations were conducted. These simulations were carried out in a solution containing 0.10 M NaCl, at a temperature of 310 K, and at a pressure of 1 atm. The analysis of molecular dynamics trajectory was performed for the protein ligand with the statistical parameters: RMSD, RMSF, pattern of distance geometry, molecular mechanics/Generalized-Born surface area (MM/GBSA), and protein-ligand interaction analysis.

RMSD was performed to measure the similarity of atomic coordinates between ligand-free AKR1B1 and ligand-AKR1B1 complexes in dynamics progression (Figure 33). All MD trajectories of ligand-free AKR1B1, *trans*-(-)-kusunokinin-AKR1B1 and inhibitor-AKR1B1 became stable after 90 ns. This proved 90-150 ns simulation was in equilibrium state and be suitable for analysis. In this duration time, backbone RMSD data of ligand-AKR1B1 complexes indicated no significant flexibility and distinction from the ligand-free AKR1B1.

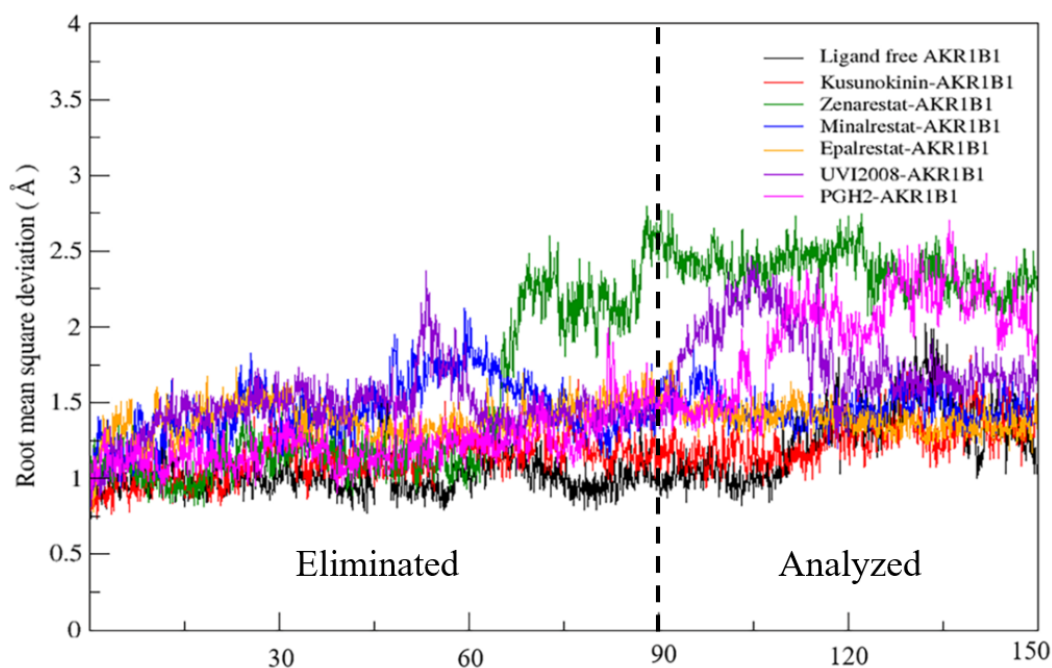


Figure 33. RMSD of the molecular dynamic trajectory from the simulation of AKR1B1. The observed simulations were ligand free-AKR1B1, and AKR1B1 with six docked molecule complexes. RMSD calculation was conducted using VMD package.

Besides, the RMSF was performed to identify the flexibility of side chain amino acid (Figure 34). In each residue, RMSF was computed from C_{α} atom. The RMSF of ligand-

AKR1B1 complexes exhibited the similar flexibility pattern throughout mostly the AKR1B1 structure. However, AKR1B1 residue 210 to 230 and 295 to 305 in UVI2008-AKR1B1 and PGH₂-AKR1B1 were observed the distinctive RMSF with more flexible. In addition, AKR1B1 residue 5 to 10 and 120 to 130 in Minalrestat-AKR1B1 were observed more distinctive RMSF than other ligand-AKR1B1 complexes including ligand-free AKR1B1.

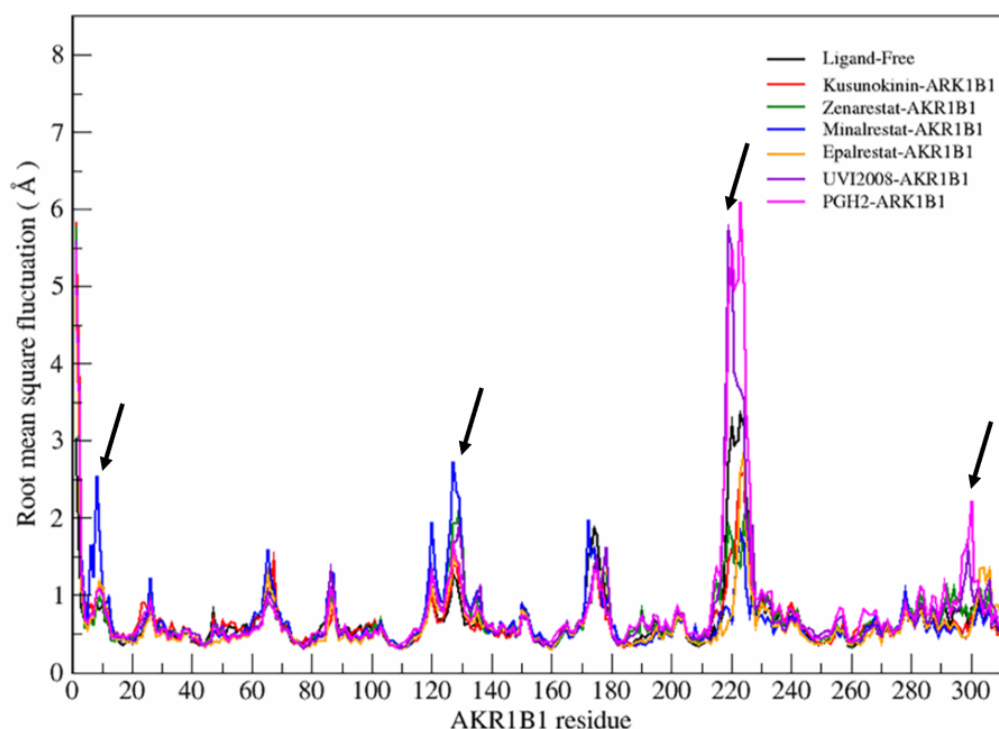


Figure 34. RMSF of molecular dynamic trajectory from the simulation of AKR1B1. The observed simulations were ligand free-AKR1B1, and AKR1B1 with six docked molecule complexes. The distinctive observed RMSF were indicated by black arrow. RMSF was computed using the cpptraj module.

To investigate the alteration effect in AKR1B1 structure or conformation resulting from ligand binding. Distance pattern of ligand-AKR1B1 complexes were performed by plotting the distance between each amino acid and origin point at the center of the structure and compared to ligand-free AKR1B1 as a reference structure. The same distance pattern means this residue shared the same distance from an origin, implying the structure of the amino acid remained the same. On the contrary, if the ligand-bound structure showed different distance pattern from the reference structure, it means that the binding of ligand effects to alteration of the structure and conformation of protein (Figure

35). The results exhibited the similar pattern among seven AKR1B1 simulations. These finding suggested that the binding of *trans*-(-)-kusunokinin, AKR1B1 substrate, and AKR1B1 inhibitors did not alter the AKR1B1 conformation (Figure 36).

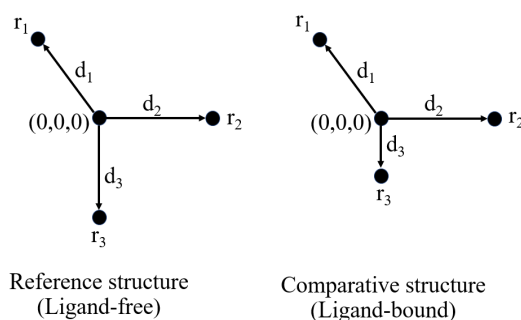


Figure 35. Pattern of distance geometry. Distance pattern of reference structure (ligand-free) that set the origin point (0,0,0) and align with the comparative structure (ligand-bound). Residue 1 (r_1) and residue 2 (r_2) of both structures show the same distance (d_1 and d_2) but residue 3 (r_3) shows the different distance (d_3).

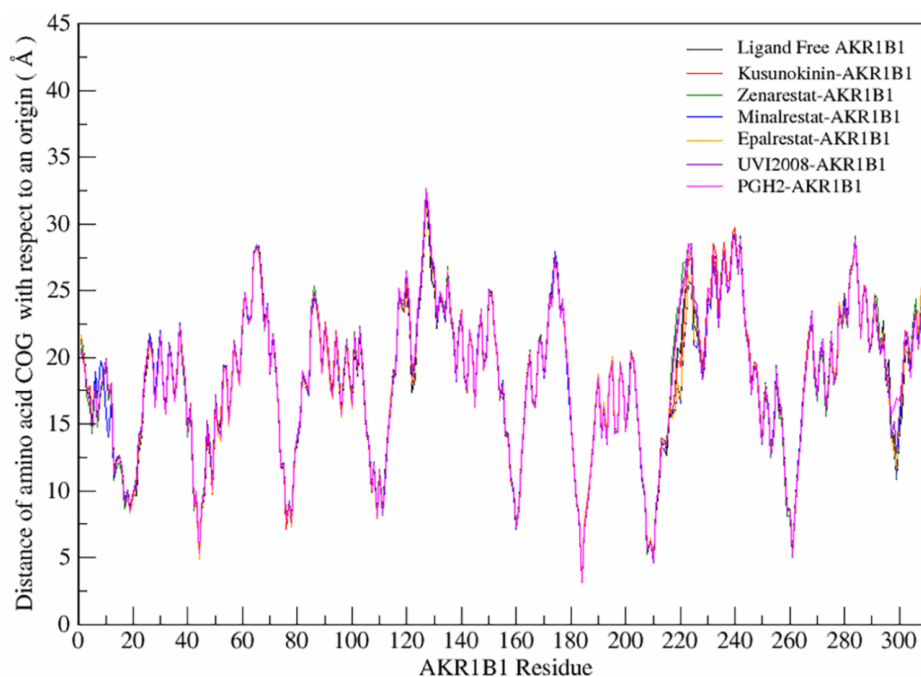


Figure 36. Distance pattern of AKR1B1 complexes with and without ligands in molecular dynamic simulations. The pattern of distance geometry was acquired using the cpptraj module.

Apart from the comparison of the overall dynamic property and conformational change, the average MM/GBSA binding free energy was used to calculate the *trans*-(-)-kusunokinin-AKR1B1 binding affinity in comparison to the other three experimentally identified AKR1B1 inhibitors, namely zenarestat, minalrestat, and epalrestat. According to MM/GBSA calculations, *trans*-(-)-kusunokinin showed the binding free energy of -42.23 kcal/mol. It showed comparable to other selected ARIs, which in the range of -29.63 to -38.96 kcal/mol (Table 15). The result predicted that *trans*-(-)-kusunokinin could have comparable binding affinity to other AKR1B1 inhibitors.

Table 15. *Trans*-(-)-kusunokinin and selective ARIs with the values of MM/GBSA binding energy toward AKR1B1.

Ligands	MM/GBSA binding energy (kcal/mol)
<i>Trans</i> -(-)-kusunokinin	-42.23 ± 0.09
Epalrestat	-38.96 ± 0.08
Minalrestat	-36.55 ± 0.07
Zenarestat	-29.63 ± 0.10

4. Binding mode insight of *trans*-(-)-kusunokinin, ARIs, and AKR1B1 substrate throughout the MD progression

According to the *trans*-(-)-kusunokinin binding mode insight, the aromatic ring on 1,2 dimethoxybenzene consistently interacted with Trp111 by π - π stacking, and the oxygen atoms at the ketone group on the compound's γ -butyrolactone ring interacted with His110, a crucial catalytic site in the AKR1B1 anion binding pocket, by hydrogen bonding (Figure 37a). While carboxylic acid group of zenarestat and epalrestat access into His110 with the stable hydrogen bond (Figure 37b and 37d). However, the minalrestat hydantoin ring can only make momentary hydrogen connections with His110. (Figure 37c).

Furthermore, an aromatic ring of *trans*-(-)-kusunokinin plays an important role in stabilized orientation using π - π stacking with Trp111 which resembles all selected ARIs (Figure 35a, 35b, 35c and 35d). Moreover, Tyr48 and Trp20 residues can temporarily form hydrogen bond and π - π stacking, with some ARIs. Trp111 was too responsible to π - π stacking with an aromatic ring of UVI2008, an AKR1B1 substrate analog (Figure 37e), as

well as PGH₂ binding using π -alkyl interaction from PGH₂ hydrocarbon chain (Figure 37f). These findings are in good agreement with the report that Trp111 is the key residue to stabilize orientation in all ARIs and acts as specific binding mode of AKR1B1.

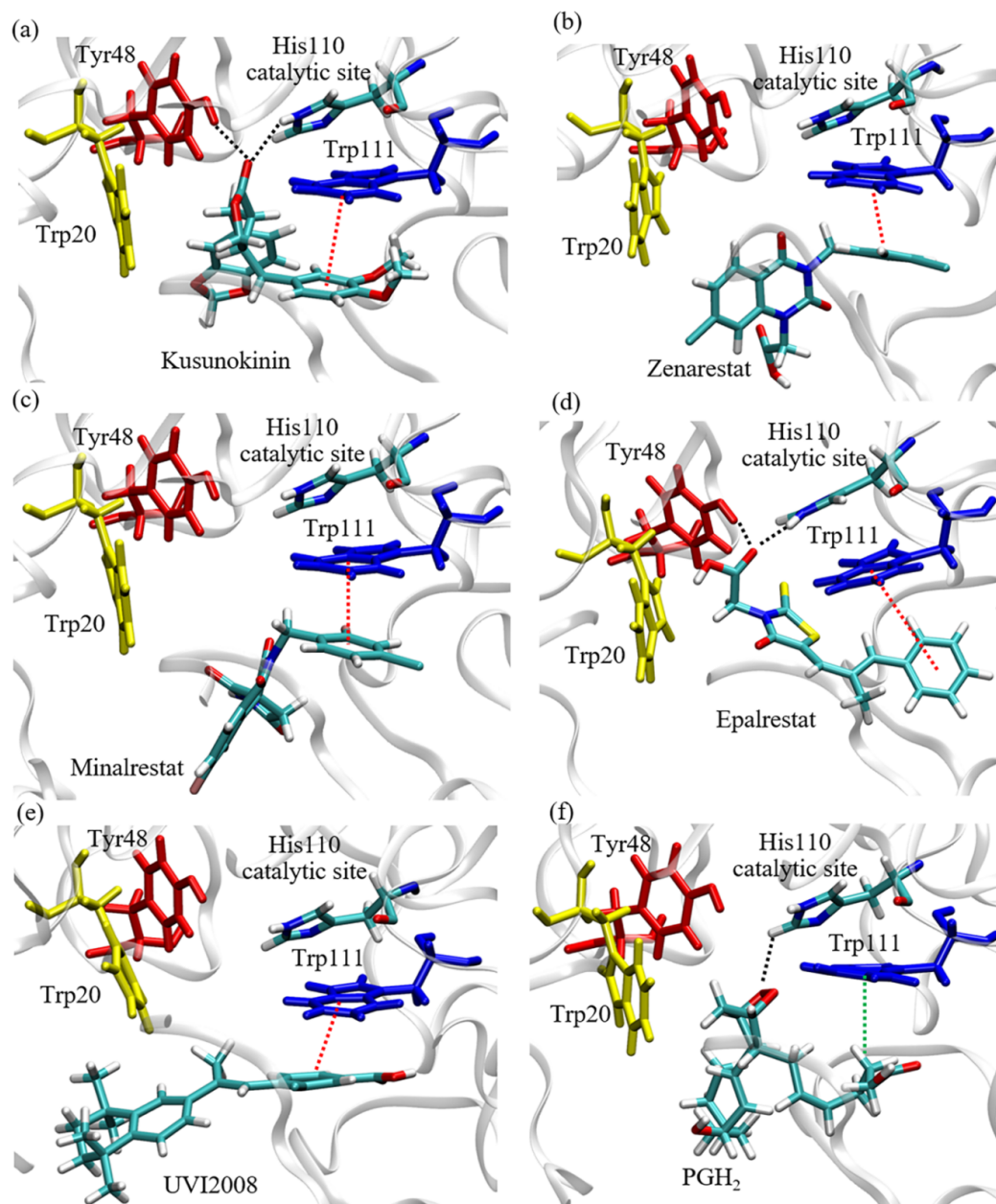


Figure 37. Insight binding mode of *trans*-(-)-kusunokinin, ARIs and AKR1B1 substrate throughout the MD progression. The key binding residues in AKR1B1 are denoted in the figure. The black, red and green dotted lines represented hydrogen bond, π - π interaction, and π -alkyl interaction respectively. The structure visualization was conducted using VMD package.

Part II. Validation of *trans*-(±)-kusunokinin target by *in vitro* studies

1. AKR1B1 expression on breast and ovarian cancer cells

To explore the correlation between AKR1B1 expression levels and distinct subtypes of breast and ovarian cancer, we conducted an investigation employing Western blotting. Our findings revealed that within the breast cancer cell cohort, Triple negative breast cancer (TNBC) cells, specifically BT549 and Hs578T cells, exhibited markedly elevated AKR1B1 protein levels in comparison to the luminal A subtype represented by MCF cells. Notably, among the TNBC cells, Hs578T cells displayed the most pronounced overexpression of AKR1B1. Moreover, within the ovarian cancer cell cohort, the non-serous ovarian cancer cells, NS (A2780 and SKOV3 cells) showcased the highest levels of AKR1B1 expression. This observation contrasts with the AKR1B1 levels in the high-grade serous ovarian cancer cell line (OVCAR3 cells). Collectively, our results suggest an association between heightened AKR1B1 expression and the aggressive migration phenotype present in TNBC and NS cells. Importantly, a survival analysis of breast and ovarian cancer patients, utilizing data from the KM-plotter database, disclosed that patients exhibiting elevated AKR1B1 expression experienced median survival rates of 48 and 19.3 months, respectively. In contrast, patients with lower AKR1B1 expression levels displayed notably prolonged median survival rates of 100 and 21 months for breast and ovarian cancer, respectively. These findings collectively imply that heightened AKR1B1 expression in breast and ovarian cancer patients is linked with unfavorable prognoses in comparison to those displaying lower AKR1B1 expression levels.

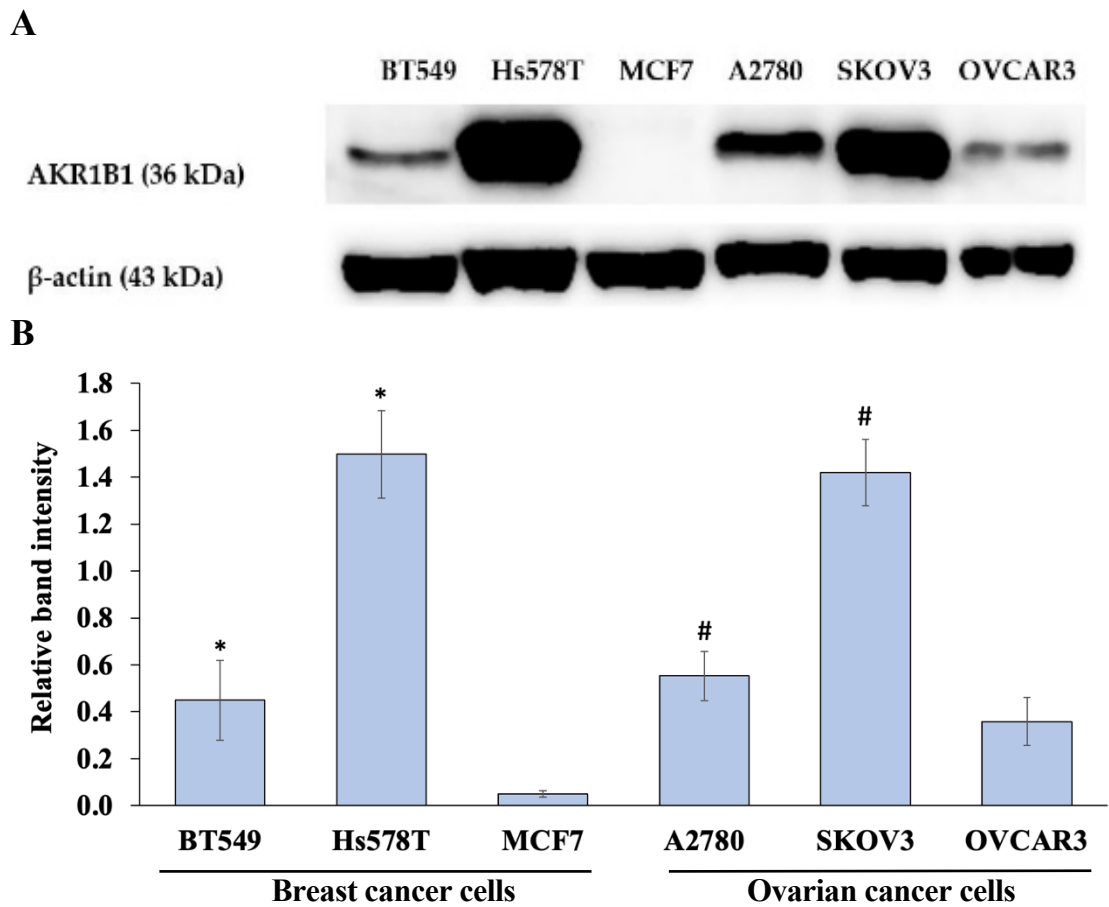


Figure 38. Expression level of AKR1B1 on the breast (BT549, Hs578T, and MCF7) and ovarian (A2780, SKOV3, and OVCAR3) cancer cells. **(A)** Cells were grown in a 10 cm culture dish and were harvested at 80% confluence. Then, cells were extracted the protein and performed Western blotting **(B)** Quantitative protein level of AKR1B1 was normalized with β -actin band intensity. Data are represented as mean \pm SD of three independent experiments. Statistically significant differences were determined by the student's *t*-test (* $p < 0.05$ versus MCF7, # $p < 0.05$ versus OVCAR3).

2. Cell viability of breast and ovarian cancer cells with (\pm)KU treatment

Cell viability of breast and ovarian cancer cell toward 72 h treatment of *trans*-(\pm)-kusunokinin ((\pm)KU) was assessed using the MTT test. The IC₅₀ value of (\pm)KU were compared to *trans*-(-)-artiin ((-)-AR) lignan, well-known aldose reductase inhibitors (ARIs) (zopolrestat (ZP) and epalrestat (EP)), and chemotherapeutic drugs (doxorubicin (DOX) and cisplatin (CIS)). The outcomes demonstrated that, except for SKOV3 and OVCAR3 cells, the IC₅₀ value of (\pm)KU displayed the potential cytotoxic with IC₅₀ values less than 10 μ M in MCF7, Hs578T, BT549, and A2780 cells. In addition, (\pm)KU had the most cytotoxic effects on the ovarian and breast cancer cell lines MCF7 and A2780, respectively. On both cell lines, interestingly, (\pm)KU demonstrated a cytotoxic impact with an IC₅₀ value lower than well-known ARIs (Figure 39). We found that well-known ARIs (ZP and EP) showed cytotoxicity in all cancer cells leading to displayed distinctive curves from (\pm)KU, (-)-AR, doxorubicin, and cisplatin (Figure 30-35). Furthermore, cisplatin also displayed distinctive curves from (\pm)KU, (-)-AR, doxorubicin on breast cancer cells (Figure 41-42) because it is not suitable for breast cancer treatment. However, all drugs had a dose-dependent decrease in cell viability percentage as shown by the dose-response curve. (Figure 40-45).

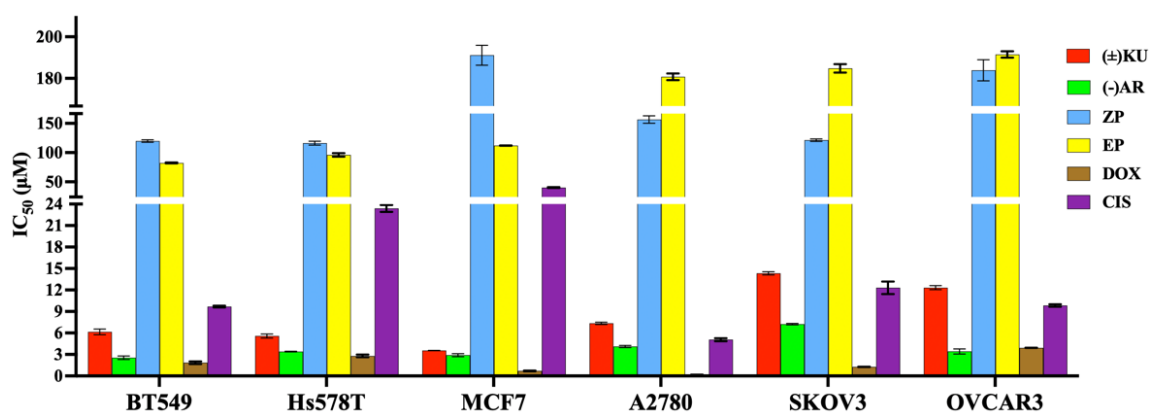


Figure 39. IC₅₀ values of (\pm)KU, ARIs, and chemotherapeutic drugs against breast and ovarian cancer cells. Cells were treated the compounds for 72 h and then were performed MTT assay. Data are represented as mean \pm SD with three independent experiments. (\pm)KU, *trans*-(\pm)-kusunokinin; (-)-AR, *trans*-(-)-artiin; ZP, zopolrestat; EP, epalrestat; DOX, doxorubicin; CIS, cisplatin.

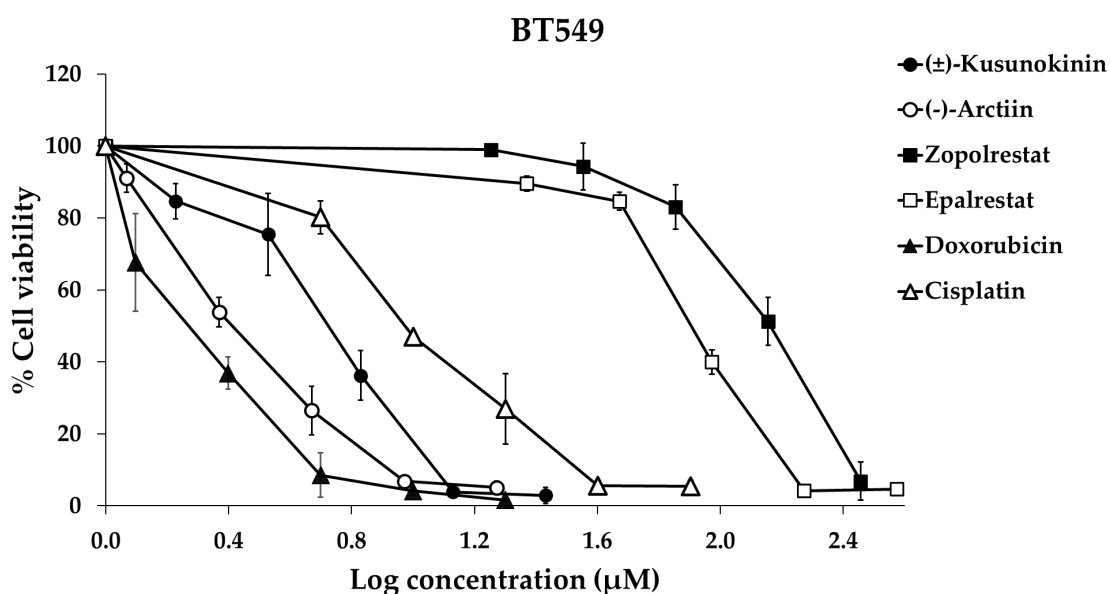


Figure 40. Cell viability of BT549 cells. Cells were treated with the compounds for 72 h and determined cell viability by MTT assay. All data represent as mean \pm SD with three independent experiments.

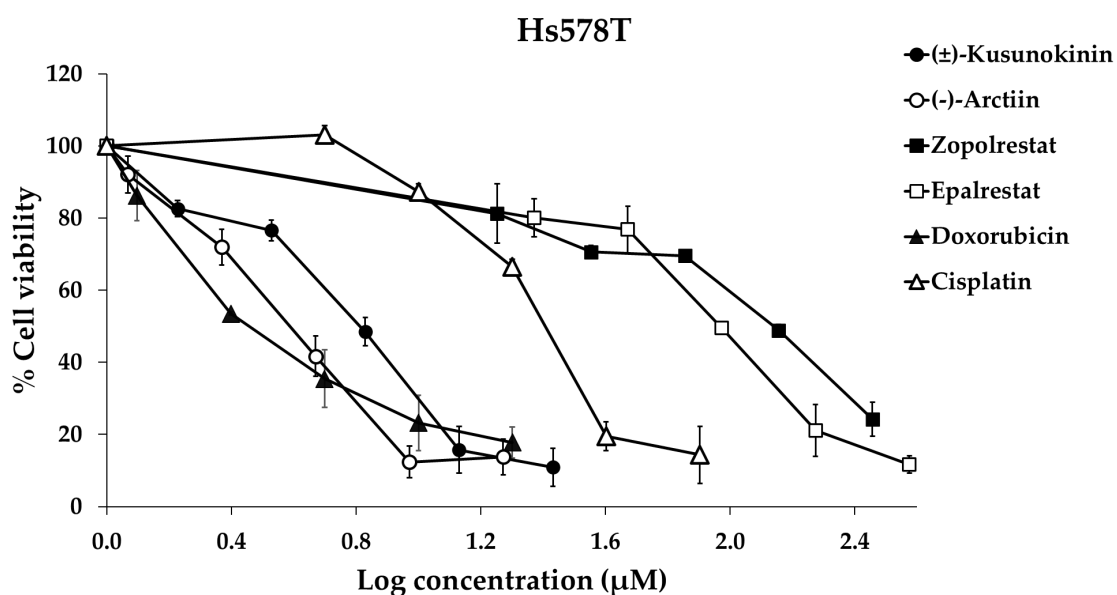


Figure 41. Cell viability of Hs578T cells. Cells were treated with the compounds for 72 h and determined cell viability by MTT assay. All data represent as mean \pm SD with three independent experiments.

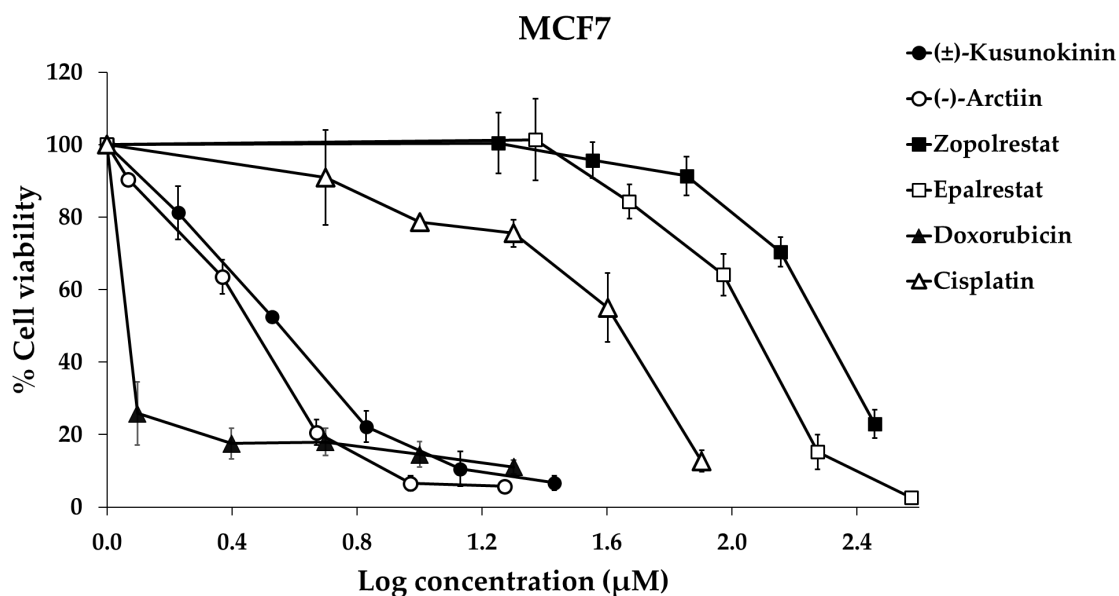


Figure 42. Cell viability of MCF7 cells. Cells were treated with the compounds for 72 h and determined cell viability by MTT assay. All data represent as mean \pm SD with three independent experiments.

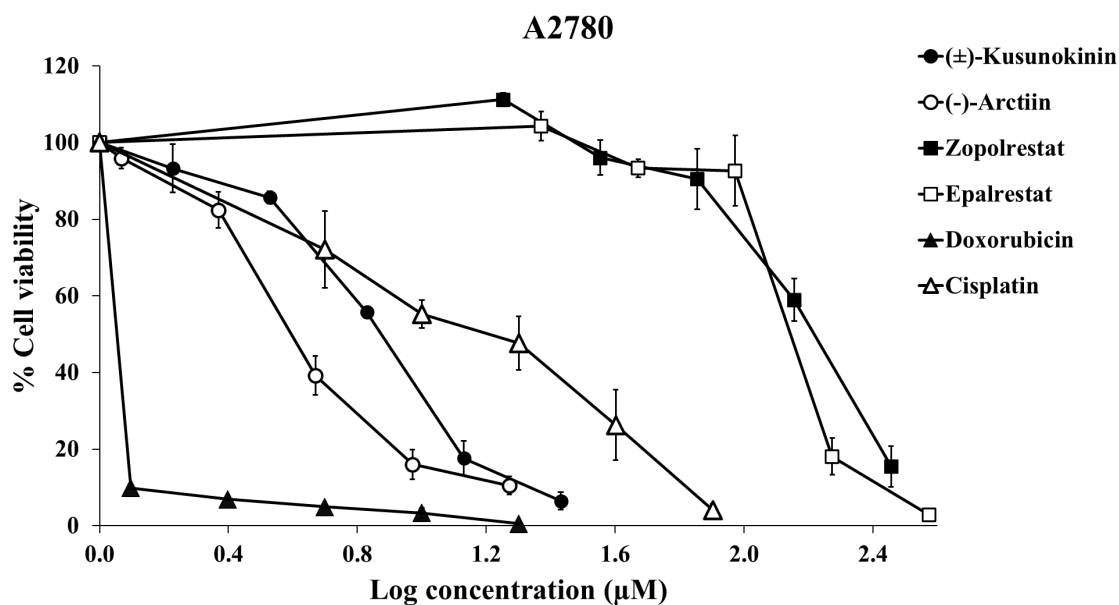


Figure 43. Cell viability of A2780 cells. Cells were treated with the compounds for 72 h and determined cell viability by MTT assay. All data represent as mean \pm SD with three independent experiments.

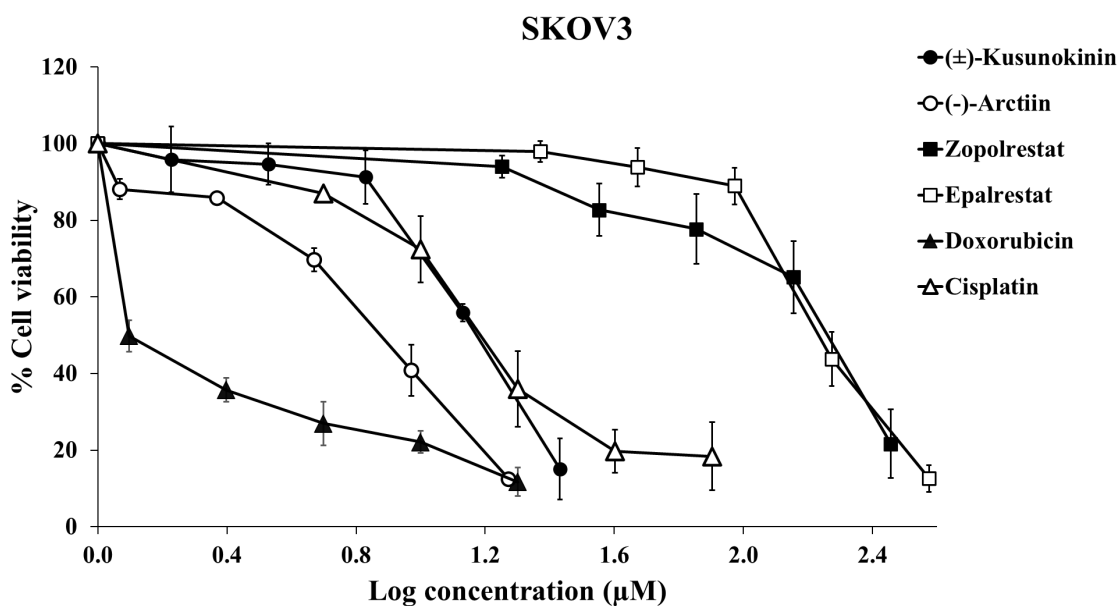


Figure 44. Cell viability of SKOV3 cells. Cells were treated with the compounds for 72 h and determined cell viability by MTT assay. All data represent as mean \pm SD with three independent experiments.

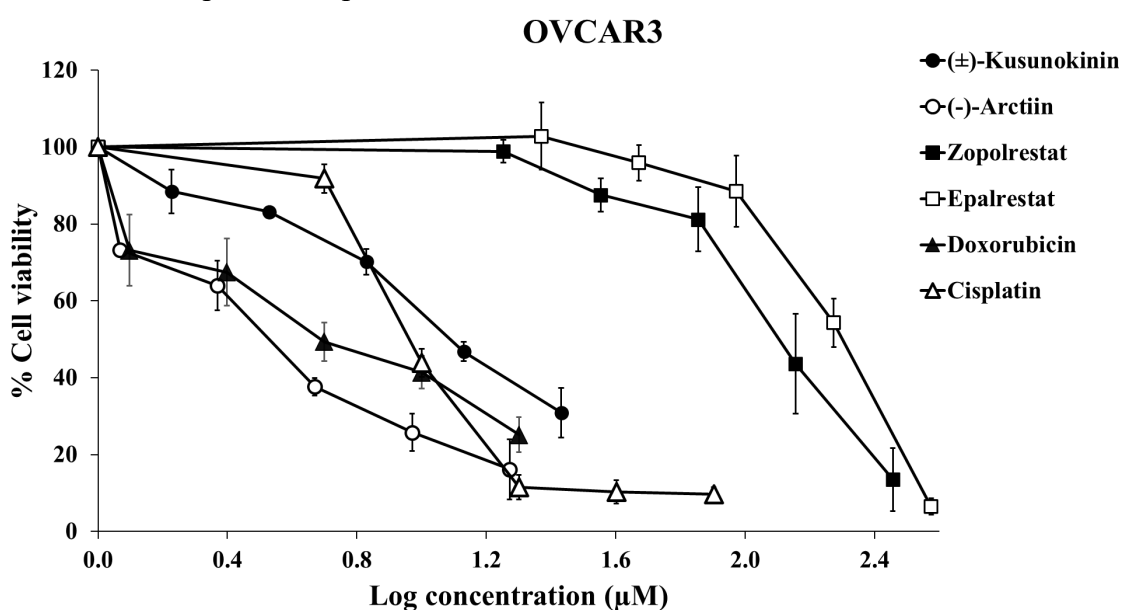


Figure 45. Cell viability of OVCAR3 cells. Cells were treated with the compounds for 72 h and determined cell viability by MTT assay. All data represent as mean \pm SD with three independent experiments.

3. Aldose reductase activity

To ascertain the potential of (\pm)KU as an inhibitor of aldose reductase, an examination was conducted by evaluating the reduction of NADPH, a key cofactor in the enzyme's reaction. This approach allowed for the analysis of (\pm)KU's inhibitory impact on aldose reductase, an enzyme responsible for converting glucose substrate into sorbitol. To ensure that dimethyl sulfoxide (DMSO), the solvent for (\pm)KU, did not interfere with the reaction, the aldose reductase activities of two control conditions were compared: a solvent control (with DMSO) and an enzyme control (without DMSO). Notably, the slopes of the curves representing these control conditions exhibited no significant differences (Figure 46A).

Furthermore, the background control, devoid of the enzyme, was utilized to eliminate its effect from all conditions. Epalrestat, a recognized aldose reductase inhibitor, was employed as a positive control. The aldose reductase activity was then depicted through logarithmic progress curves, illustrating the percentage of activity across varying concentrations of compounds ((\pm)KU, (-)AR, zopolrestat, and epalrestat) in nanomolar (nM). Interestingly, all substances demonstrated a dose-dependent inhibition of aldose reductase activity (Figure 46B).

In particular, (\pm)KU displayed considerable potential in inhibiting aldose reductase activity, yielding an IC_{50} value of $9.72 \pm 0.18 \mu\text{M}$. Notably, this performance surpassed that of the previously reported aldose reductase inhibitor lignan (-)AR, which exhibited an IC_{50} value of $13.65 \pm 49 \mu\text{M}$. In comparison, zopolrestat and epalrestat, both recognized inhibitors of AKR1B1 specifically designed for targeting aldose reductase, exhibited IC_{50} values of $31.03 \pm 0.14 \text{ nM}$ and $0.77 \pm 0.01 \mu\text{M}$, respectively (Figure 46C).

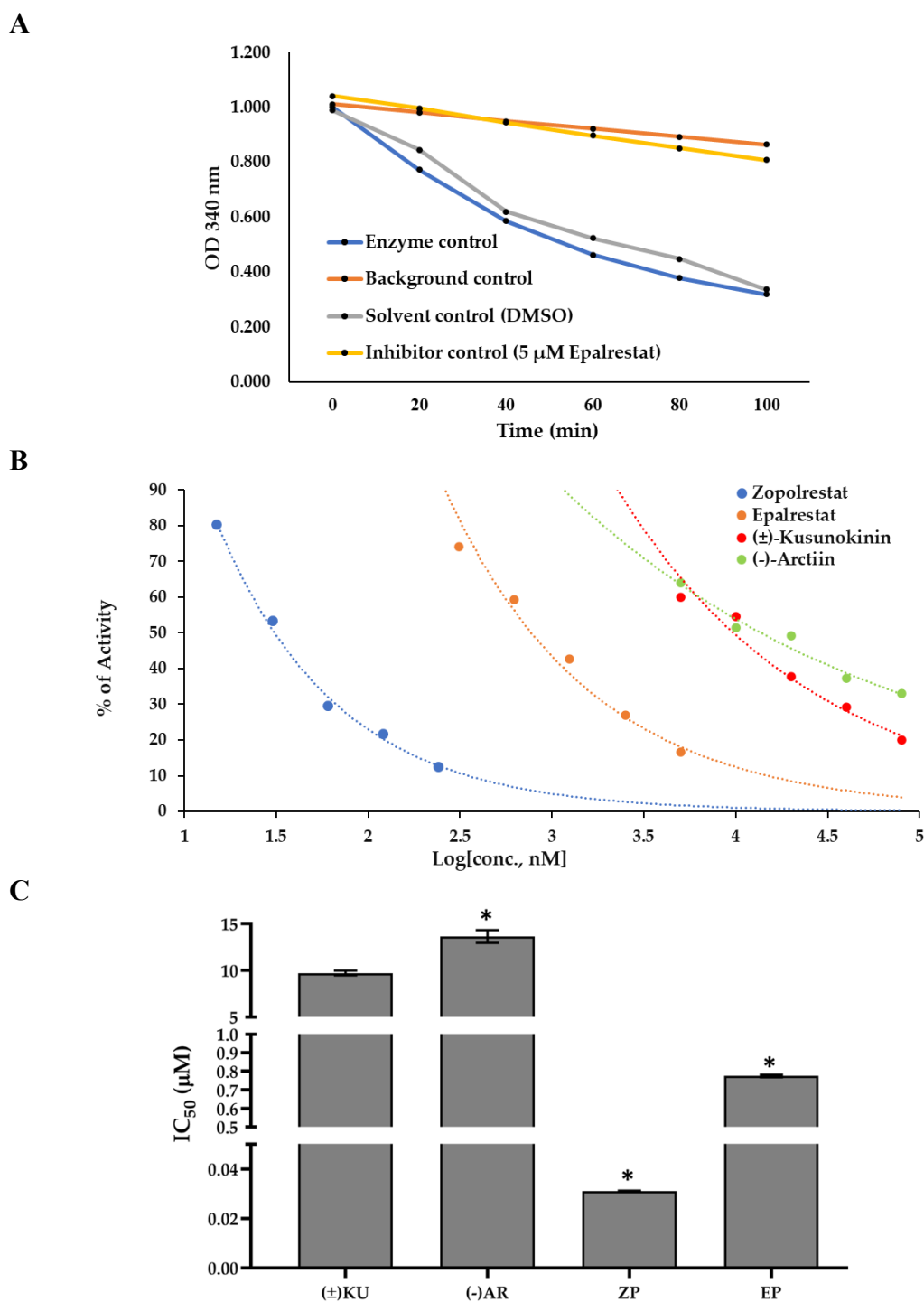


Figure 46. Aldose reductase activity. **(A)** Progress curves of the aldose reductase reaction control. **(B)** Progress curves of aldose reductase enzyme activity of tested compounds at various concentrations. **(C)** IC₅₀ values of tested compounds in the inhibition of aldose reductase activity. Data representation as mean \pm SD with two independent experiments. Statistically significant differences in IC₅₀ values of (±)KU vs. ARIs were determined using a one-way analysis of variance followed by Tukey's multiple comparisons tests (* $p < 0.05$).

4. Cellular thermal shift assay (CETSA)

In silico studies suggested the potential binding of (\pm)KU to AKR1B1. Nevertheless, there is limited evidence supporting AKR1B1 as a specific target of (\pm)KU based on *in vitro* investigations. To ascertain whether (\pm)KU directly interacts with AKR1B1, we employed cellular thermal shift assay (CETSA), a label-free method that confirms compound-protein interactions. CETSA is rooted in the concept that drug binding enhances protein thermal stability.

Upon subjecting Hs578T and SKOV3 cell lysates to temperatures of 75°C and 60°C, respectively, the results revealed a significant decrease in the abundance of the AKR1B1 protein. However, when cell lysates were treated with (\pm)KU, we observed a stabilization of AKR1B1 protein levels after heating, in contrast to untreated lysates. This phenomenon was particularly evident at 75°C and 60°C for Hs578T and SKOV3 cells, respectively (Figure 47).

Further analyses were conducted utilizing these specific temperatures and various concentrations of (\pm)KU. The results indicated that (\pm)KU exhibited a dose-dependent effect in enhancing the stability of the AKR1B1 protein levels across both cell lines. Notably, in the Hs578T cell lines, the AKR1B1 protein was significantly stabilized at (\pm)KU concentrations of 10 and 20 μ M. Similarly, in the SKOV3 cell line, significant stabilization was observed at (\pm)KU concentrations of 5, 10, and 20 μ M (Figure 48).

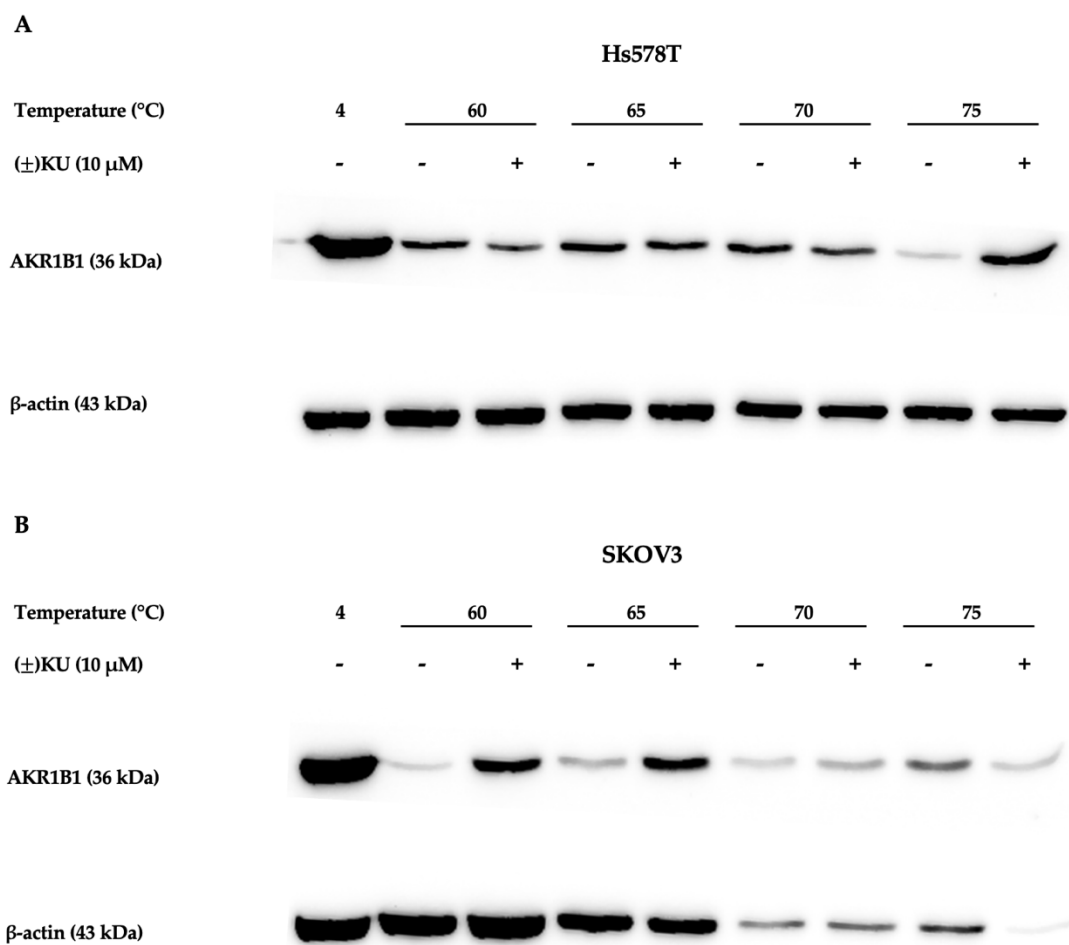


Figure 47. CETSA with various of temperatures. CETSA-based determination of target engagement of (±)KU toward AKR1B1 on (A) Hs578T cells and (B) SKOV3 cells at various of temperatures. Cells were treated with 10 μM (±)KU final concentration for 1 h. Then, cells were heated at designated temperature for 3 min and cooled down at 25°C for 3 min. Cells were snap-frozen with liquid nitrogen and were determined the protein levels using Western blot analysis.

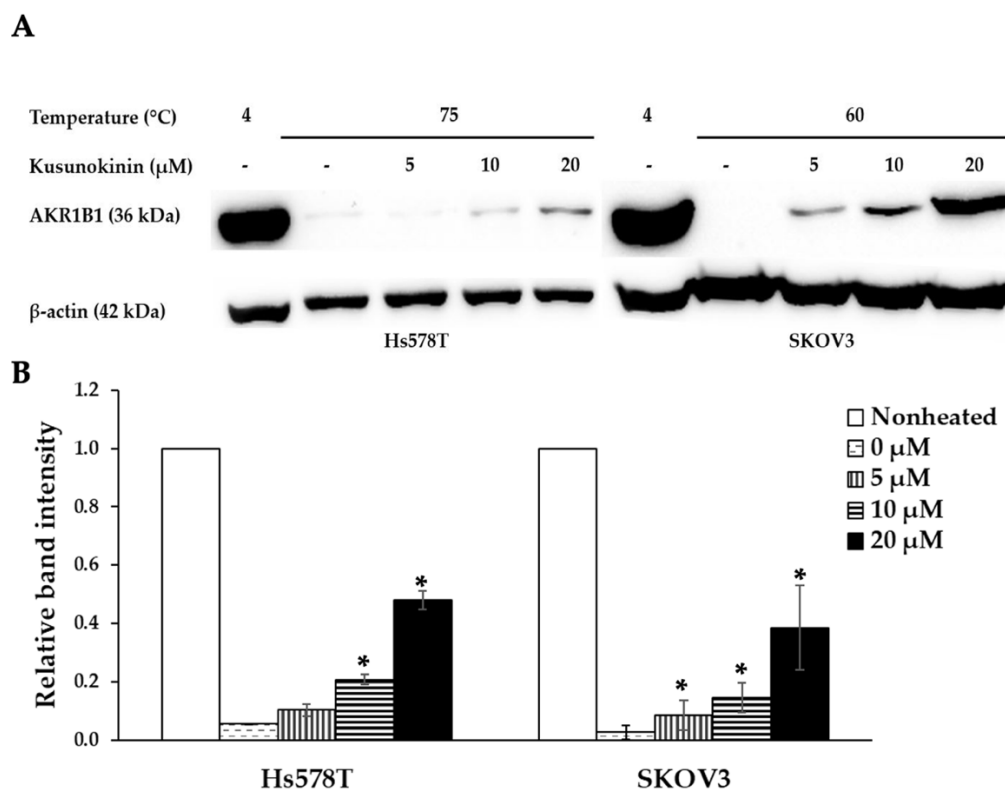


Figure 48. CETSA with various concentration of (\pm)KU. CETSA-based determination of target engagement between (\pm)KU and AKR1B1. **(A)** AKR1B1 levels were determined using Western blot analysis. **(B)** The quantitative protein level of AKR1B1 was normalized with β -actin band intensity. Data are represented as mean \pm SD with three independent experiments. Statistically significant differences between treated cells vs. nontreated cells were determined by the student's *t*-test (* $p < 0.05$).

5. (\pm)KU inhibited lipid peroxidation in high glucose condition

To assess the inhibitory effects of (\pm)KU on high glucose-induced AKR1B1-mediated oxidative stress responses, we employed the TBARS assay to detect lipid peroxidation on Hs578T cell lines. Hs578T cells were selected for this evaluation due to their demonstrated potential for greater cytotoxic effects compared to SKOV3 cells.

In our experimental setup, Hs578T cells were incubated with varying concentrations of (\pm)KU and epalrestat at 0.25X, 0.50X, and 1.00X IC_{50} levels. For (\pm)KU, these concentrations were 1.40, 2.79, and 5.58 μ M, while for epalrestat, they were 24.02, 48.04, and

96.08 μM . After a 24-h incubation period, the cells were subjected to oxidative stress induction using a high glucose concentration of 100 mM for 1 h.

Subsequently, we quantified malondialdehyde (MDA) levels, a product of lipid peroxidation that forms MDA-TBA adducts. Our findings revealed that cells induced with high glucose exhibited a marked increase in MDA levels compared to non-treated cells. Intriguingly, cells pre-treated with (\pm)KU and epalrestat exhibited a dose-dependent reduction in MDA levels (Figure 49A). However, it's noteworthy that at concentrations corresponding to the IC_{50} values of cytotoxicity on Hs578T cells, (\pm)KU resulted in a lower decrease in MDA levels compared to epalrestat.

Furthermore, we expanded our analysis by investigating MDA levels when cells were pre-treated with (\pm)KU and epalrestat at the same concentration (1.5, 3.0, and 6.0 μM). Our observations demonstrated that (\pm)KU exhibited a more pronounced reduction in MDA levels compared to epalrestat (Figure 49B).

6. (\pm)KU suppressed AKR1B1 level

To assess the comparative potential of (\pm)KU and the AKR1B1 inhibitor epalrestat in inhibiting AKR1B1 expression, we conducted experiments using Hs578T cells. The cells were treated with (\pm)KU or epalrestat at concentrations equivalent to 0.25X and 0.50X IC_{50} levels. Specifically, these concentrations were 1.40 and 2.79 μM for (\pm)KU and 24.02 and 48.04 μM for epalrestat. The treatment duration was set at 48 h.

Our analysis encompassed the assessment of AKR1B1 protein levels along with those of its downstream signaling molecules, including PKC δ , NF- κB , AKT, Nrf2, COX2, Twist2, E-cadherin, and N-cadherin. Our findings illustrated that (\pm)KU exerted a substantial suppressive effect on AKR1B1 levels in a dose-dependent manner, mirroring the impact observed with epalrestat. Additionally, at a concentration equivalent to 0.50X IC_{50} , (\pm)KU displayed significant down-regulation of multiple signaling molecules, including PKC δ , NF- κB , AKT, Nrf2, COX2, Twist2, and N-cadherin. Intriguingly, (\pm)KU also exhibited an up-regulatory effect on E-cadherin (Figure 50).

Importantly, the outcomes revealed that (\pm)KU demonstrated a potential to reduce AKR1B1 levels and modulate downstream signaling molecules comparable to the effects of epalrestat, even at a lower concentration. These results suggest that (\pm)KU possesses

the capability to suppress AKR1B1 expression and regulate associated signaling pathways in a manner similar to the actions of epalrestat (Figure 50).

7. Down-regulation of AKR1B1 by (\pm)KU led to alteration of signaling molecules of oxidative stress and EMT markers

To elucidate the underlying mechanism by which (\pm)KU impacts oxidative stress responses and the epithelial-mesenchymal transition (EMT) process through AKR1B1 inhibition, we conducted a comprehensive study using Hs578T cells. These cells were subjected to treatments with 2.79 μ M (\pm)KU, 48.04 μ M epalrestat, 100 nM siRNA-AKR1B1, or a combination of 100 nM siRNA-AKR1B1 with each compound. In this investigation, we included untreated cells, dharmafect-transfection reagent treated cells, and siRNA-luciferase treated cells as negative controls. EP and siRNA-AKR1B1 treatments were utilized as positive controls to assess AKR1B1 levels and the modulation of signaling molecules related to oxidative stress and EMT markers, encompassing PKC δ , NF- κ B, AKT, Nrf2, COX2, Twist2, E-cadherin, and N-cadherin.

Our findings demonstrated that (\pm)KU exhibited a marked down-regulation of AKR1B1 levels, akin to the potential displayed by EP and siRNA-AKR1B1 treatments, when compared to the negative control groups. Intriguingly, a synergistic effect of AKR1B1 suppression emerged when combining siRNA-AKR1B1 with (\pm)KU or EP. Furthermore, our analysis revealed a similar trend in the suppression of signaling molecules, encompassing NF- κ B, Nrf2, and N-cadherin. However, this synergistic effect was not evident for PKC δ , AKT, COX2, and Twist2. Conversely, E-cadherin levels demonstrated an up-regulation in response to (\pm)KU, EP, and siRNA-AKR1B1 treatments, but decreased upon the combination treatment (Figure 51).

These results provide compelling evidence that (\pm)KU effectively suppresses AKR1B1 expression and modulates associated signaling molecules, mirroring the action of EP. Additionally, the observed synergistic effects with siRNA-AKR1B1 combinations indicate a promising avenue for further exploration in understanding the therapeutic potential of (\pm)KU in the context of oxidative stress responses and EMT processes.

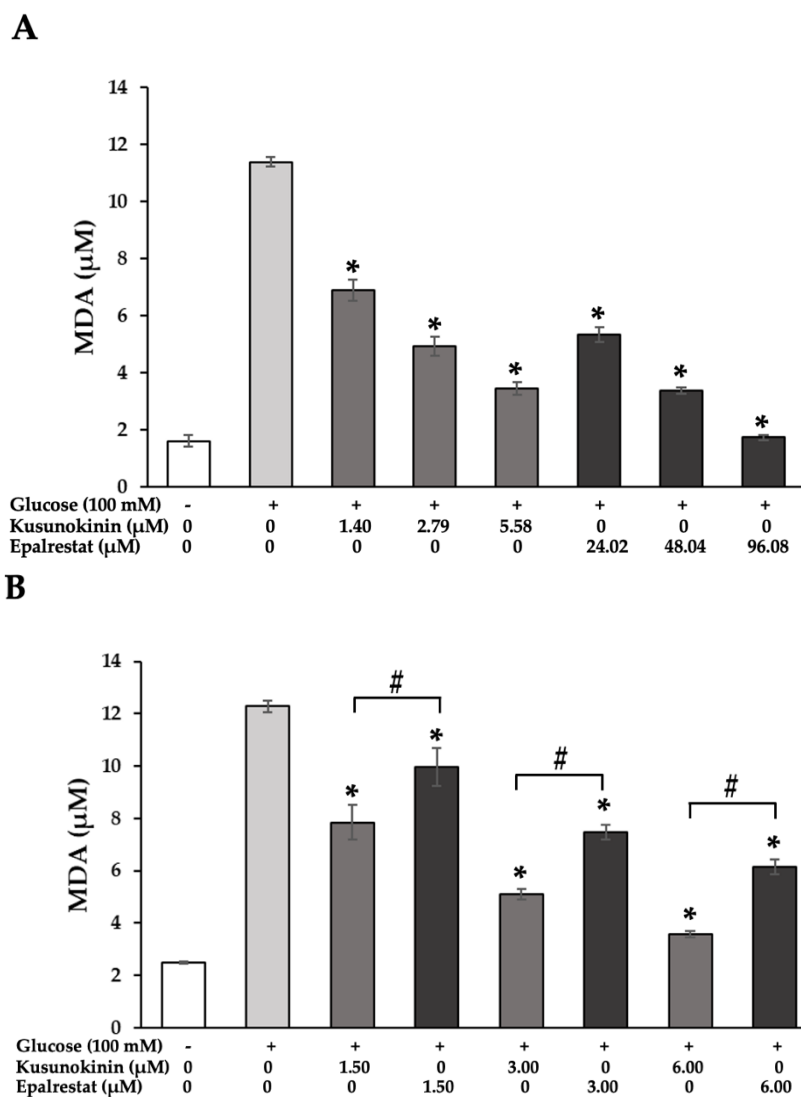


Figure 49. Lipid peroxidation on Hs578T in high glucose conditions. **(A)** Quantitative MDA level on Hs578T-pretreated cell with (\pm)KU and EP at 0.25X, 0.50X and 1.00X IC_{50} values of cytotoxicity and **(B)** at the same concentration (1.5, 3.0, 6.0 μ M). All graphs showed mean \pm SD with four independent experiments. Statistically significant differences were determined using a one-way analysis of variance followed by Tukey's multiple comparisons tests (* $p < 0.05$ versus only glucose treatment, # $p < 0.05$ is considered of (\pm)KU to compare to epalrestat treatment).

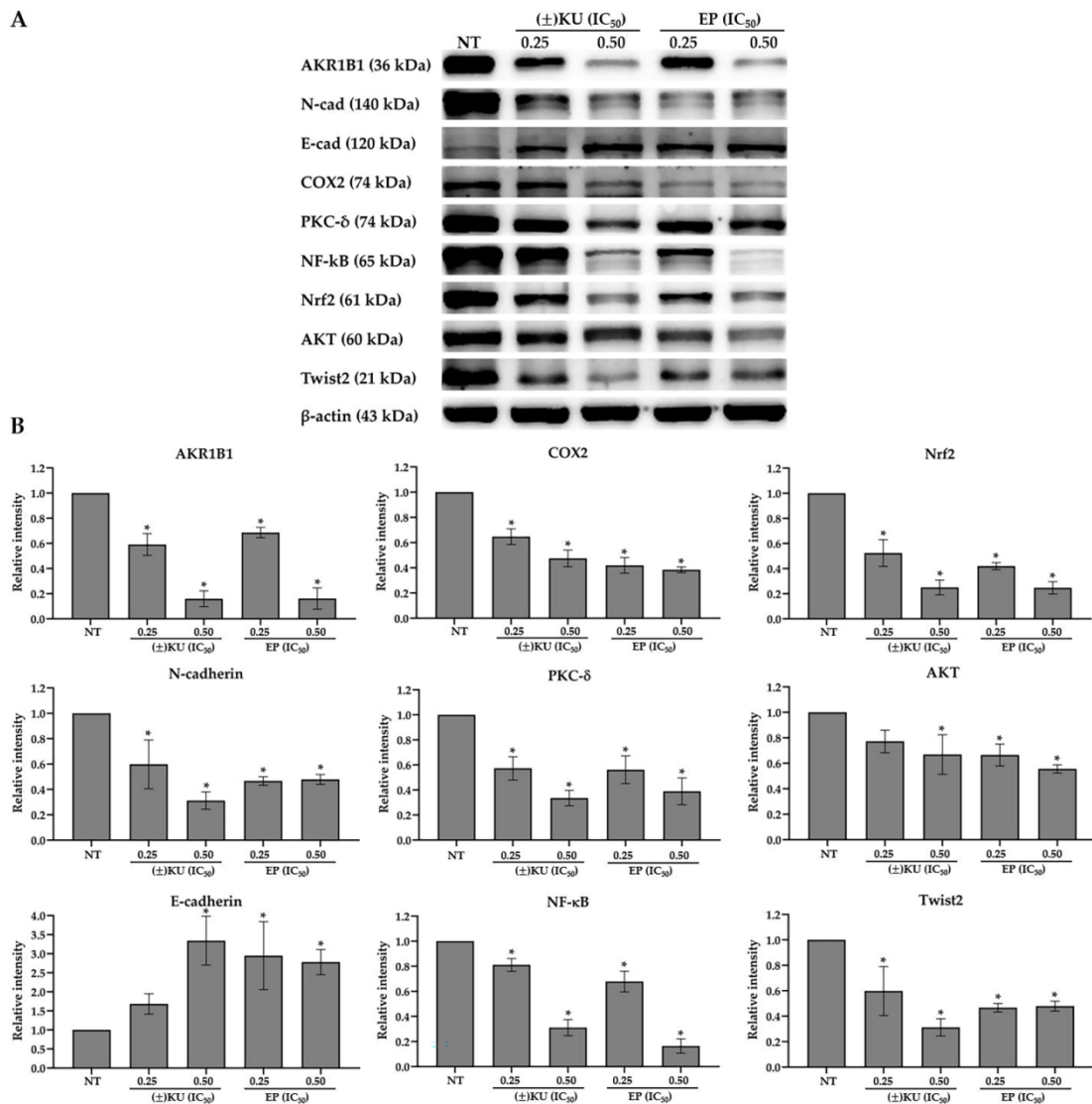


Figure 50. Suppression of AKR1B1 and regulation of signaling molecules by (\pm)KU. Hs578T cells were treated with (\pm)KU and epalrestat at the concentration of 0.25X and 0.50X IC_{50} (1.40, 2.79 μ M for (\pm)KU and 24.02, 48.04 μ M for epalrestat, respectively) for 48 h. **(A)** The expression of AKR1B1 and its downstream molecules (PKC δ , NF- κ B, AKT, Nrf2, COX2, Twist2, E-cadherin and N-cadherin) were determined by Western blot analysis. **(B)** Quantitative protein level of AKR1B1 and its downstream molecules were normalized with β -actin band intensity. Data are represented as mean \pm SD with three independent experiments. Statistically significant differences between treated cells vs. nontreated cells were determined by a one-way analysis of variance followed by Tukey's multiple comparisons tests (* $p < 0.05$). (\pm)KU, *trans*-(\pm)-kusunokinin; EP, epalrestat.

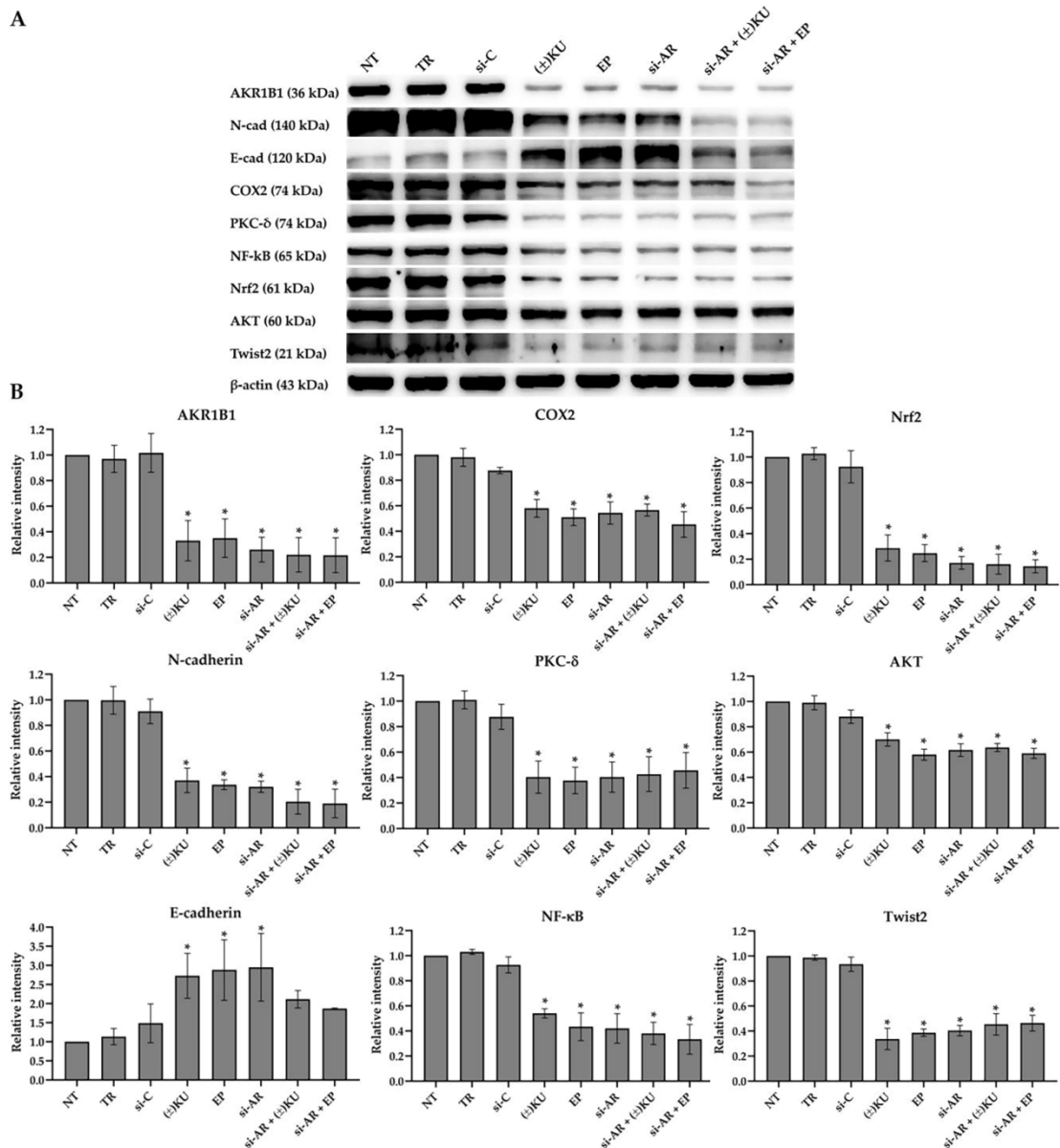


Figure 51. Effect of (\pm)KU on signaling molecules through the downregulation of AKR1B1. Hs578T cells were treated with 2.79 μ M (\pm)KU or 48.04 μ M epalrestat or 100 nM siRNA-AKR1B1 or a combination for 72 h. **(A)** The expression of AKR1B1 and its downstream molecules were determined by Western blot analysis. **(B)** Quantitative protein level of AKR1B1 and its downstream molecules were normalized with β -actin band intensity. Data are represented as mean \pm SD with three independent experiments. Statistically significant differences between treated cells vs. nontreated cells were determined by a one-way analysis of variance followed by Tukey's multiple comparisons tests ($*p < 0.05$). NT, non-treated cells; TR, transfection reagent; si-C, siRNA control; (\pm)KU, *trans*-(\pm)-kusunokinin; EP, epalrestat; si-AR, siRNA-AKR1B1.

CHAPTER 4

DISCUSSION

Part I. Identification of *trans*-(-)-kusunokinin target by *in silico* studies

Previously, *trans*-(-)-kusunokinin inhibited breast cancer proliferation by partially binding and down-regulating CSF1R protein and significantly suppressing AKT levels (Rattanaburee et al., 2020). These suggested that *trans*-(-)-kusunokinin could regulate AKT through binding not only with CSF1R but also with other target proteins (Rattanaburee et al., 2020). Thus, we explored the new *trans*-(-)-kusunokinin target by selecting 114 possible target proteins from 8 mechanisms, including cell proliferation, multidrug resistance, epigenetic regulation, cell migration, cell survival, cell cycle progression, angiogenesis, and DNA repair. The results exhibited that *trans*-(-)-kusunokinin showed the best binding potential with AKR1B1 and provided an outstanding docking score of 11.11 kcal/mol, which is better than the native ligand (IDD594). Moreover, the other cell proliferation-related proteins, including MEK2, TrkC, TrkB, and FGFR3, were possible kusunokinin targets with binding energies of -10.14, -9.67, -9.60, and -9.49 kcal/mol, respectively (Figure 52).

Based on molecular docking, previous studies revealed that *trans*-(-)-kusunokinin targets CSF1R with the best binding energy of -11.53 kcal/mol. CSF1R directly activates the Ras/MEK/ERK pathway to drive cell proliferation. In the condition of CSF1R suppression, a src-dependent mechanism will activate the PI3K/AKT pathway that relays downstream molecules of cell cycle progression such as c-myc, CDK4 and cyclin D1 (Lee et al., 2000). The inhibition of CSF1R by *trans*-(-)-kusunokinin or siRNA-CSF1R revealed that it suppresses AKT levels significantly (Rattanaburee 2020). Interestingly, the inhibition of AKR1B1 can also decrease AKT levels by reducing the phosphorylation of AKT, leading to tumorigenesis prevention (Saxena et al., 2018). Moreover, the inhibition of AKR1B1 hinders growth factor-induced cell cycle progression through the PI3K/AKT/E2F-1 pathway (Ramana et al., 2010).

We suspected that the suppression of AKT by *trans*-(-)-kusunokinin may also come from AKR1B1 inhibition. Hence, the upstream molecules that upregulate AKR1B1 gene expression underwent molecular docking. AKR1B1 is a metabolic enzyme that

upregulates gene expression by signaling from Triiodothyronine (T_3) binding with thyroid hormone receptor alpha (TR_α) or thyroid hormone receptor beta (TR_β) and heterodimerizing with the retinoid X receptor (RXR) located on thyroid hormone response elements (TREs) (Chi et al., 2013). These upstream molecules exhibited potential binding energy but not as well as AKR1B1 (Figure 52).

Moreover, the $PGF_{2\alpha}$ signaling-related proteins, including phospholipases A2 (PLA2), cyclooxygenase 2 (COX2) and NF- κ B also exhibited binding energies higher than AKR1B1 (Figure 52). All these findings can predict that *trans*-(-)-kusunokinin could inhibit AKT levels that hinder cancer cell proliferation by targeting AKR1B1 with the independence of upstream molecules of AKR1B1 or $PGF_{2\alpha}$ signaling-related proteins. Even though MEK2 showed the closeness of binding free energy (-10.14 kcal/mol), AKR1B1 was further investigated due to supporting data that arctigenin and arctiin, the lignan-based compounds with a core structure-like *trans*-(-)-kusunokinin, revealed the AKR1B1 inhibition (Xie et al., 2005).

Trans-(-)-kusunokinin binding site on AKR1B1 is hydrophobically surrounded by several aromatic residues that stabilized *trans*-(-)-kusunokinin orientation by π - π stacking. These results were concordant with molecular docking in previous studies showing that *trans*-(-)-kusunokinin binds CSF1R using π - π interaction at the active pocket (Rattanaburee et al., 2020). *Trans*-(-)-kusunokinin binding site consists of a small hydrophobic pocket, a large hydrophobic specific pocket, and an anion binding pocket. These active pockets were similar to those previously reported of β -aminophenyl propanoic acid derivative binding site, where 2 aromatic rings stabilized orientation by small and large hydrophobic pockets. A carboxylic group of the compound creates a hydrogen bond to the anion-binding pocket (Wang et al., 2013).

Moreover, the position and orientation of *trans*-(-)-kusunokinin buried in the active pocket site of AKR1B1 are similar to well-known ARIs. The results suggested that Trp20 and Trp111 sustained *trans*-(-)-kusunokinin and ARIs orientation by π - π stacking and hydrogen bonding, as well as Tyr48 and His110. These four key residues play an important interaction site in *trans*-(-)-kusunokinin and most ARIs, which is consistent with the earlier report that the anion binding pocket contains Trp20, Tyr48, His110, and Trp111 and Trp20 is the hydrophobic specificity pocket that regulates the accessibility of aromatic ring-containing inhibitors (Zhu, 2013). AKR1B1 requires the

NADPH cofactor to form the holoenzyme, which is able to catalyze the substrate. AKR1B1 catalyzes PGH_2 into $\text{PGF}_{2\alpha}$ and relays the signals in the NF- κ B pathway to regulate the EMT process in various cancers (Wu et al., 2017). The catalytic mechanism of AKR1B1 revealed that 4-pro-R hydrogen from NADPH transfers to the oxygen on the dioxabicycloheptane ring of PGH_2 . The imidazole ring in His110 plays an important role as a proton donor for PGH_2 conversion into $\text{PGF}_{2\alpha}$ (Nagata et al., 2011). The molecular dynamics simulation of PGH_2 toward AKR1B1 exhibited that oxygen on the dioxabicycloheptane ring of PGH_2 contacted the transferable proton of NADPH and stably formed a hydrogen bond with His110, as expected.

The binding mode with His110 exhibited *trans*-(-)-kusunokinin and carboxylic ARIs that can form a hydrogen bond with stable interaction. The obstruction or stable formation of hydrogen bonds with His110 of *trans*-(-)-kusunokinin and ARIs directly plays a crucial role in the prevention of PGH_2 conversion. The mutually observed speculation in both *trans*-(-)-kusunokinin, substrate analog, and all ARI groups was that the interaction of the compound with Trp111 could be a majority contribution to AKR1B1 inhibition because the ligand would reside to interfere with the access of PGH_2 into the catalytic site, even if the compound can create a hydrogen bond with His110 catalytic residue or not.

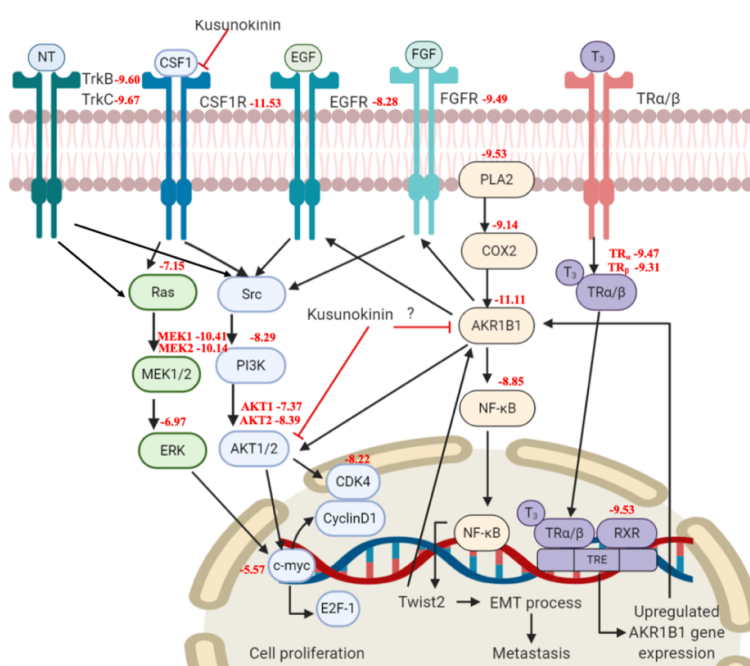


Figure 52. Prediction of targets and propose mechanism of action of *trans*-(-)-kusunokinin.

Part II. Validation of *trans*-(±)-kusunokinin target by *in vitro* studies

Previously, *trans*-(±)-kusunokinin ((±)KU) had been investigated for its potential cytotoxic effects on various cancer cell lines. Notably, these included ovarian cancer lines (A2780, A2780cis, SKOV3, and OVCAR3), colon cancer (HT-29), cholangiocarcinoma (KKU-M213 and KKU-K100), as well as distinct breast cancer subtypes, including luminal A (MCF7), basal-A (MDA-MB-468), and basal-B (MDA-MB-231) (Rattanaburee et al., 2019; Mad-Adam et al., 2022). In this study, we observed that (±)KU exhibited a cytotoxic effect on ovarian cancer cells (A2780, SKOV3, and OVCAR3), with IC₅₀ values comparable to cisplatin, a well-known chemotherapeutic agent for ovarian cancer treatment. This finding was in agreement with a previous report (Mad-Adam et al., 2022). Furthermore, (±)KU demonstrated substantial cytotoxicity across breast cancer cell lines, including both minimally migratory (MCF7) and highly migratory (BT549 and Hs578T) phenotypes. Additionally, the IC₅₀ values of (±)KU against triple-negative breast cancer (TNBC) cell lines (BT549 and Hs578T) aligned with previous findings for other TNBC cells (MDA-MB-468 and MDA-MB-231) (Rattanaburee et al., 2019). Interestingly, we observed that the cytotoxic effect of (±)KU did not exhibit a correlation with the expression of AKR1B1 in breast and ovarian cells. This could potentially be attributed to the multi-targeted action of (±)KU, impacting other factors such as CSF1R, MMP-12, HSP90- α , CyclinB1, and MEK1 (Rattanaburee et al., 2020). Comparatively, AKR1B1 inhibitors (ARIs) displayed relatively weak cytotoxic effects across all ovarian and breast cancer cell lines, particularly on MCF7 and OVCAR3 cells, which lack AKR1B1 expression. Notably, the IC₅₀ values of ARIs against TNBC cell lines (BT549 and Hs578T) were consistent with prior reports. Specifically, the cytotoxicity effect of epalrestat on MDA-MB-231 cells demonstrated an IC₅₀ value of 90.26 μ M. The limited cytotoxicity of epalrestat can be attributed to its slightly hydrophilic properties and short half-life, rendering it less suitable as an anticancer drug (Banala et al., 2019).

(±)KU exerts its inhibitory effects on breast cancer cell proliferation by targeting CSF1R and its downstream signaling molecules, such as AKT, cyclinD1, and CDK1. Computational simulations previously predicted that *trans*-(-)-

kusunokinin binds to the juxtamembrane region of CSF1R, forming π - π stacking interactions at the binding site (Rattanaburee et al., 2020). Moreover, it was found to bind to the ATP binding domain of HER2, although with lower binding affinity and a distinct mode of action from the HER2 inhibitor neratinib (Rattanaburee et al., 2021). Recent studies predicted that *trans*-(-)-kusunokinin could be an inhibitor of AKR1B1, a target implicated in cellular oxidative stress and the EMT process in cancer cells. Notably, its interaction with AKR1B1 was computationally proposed based on stabilizing interactions within the binding pocket, involving π - π stacking and hydrogen bond interactions with key catalytic site residues (Tanawattanasuntorn et al., 2021). However, there was a lack of *in vitro* evidence to confirm this computational prediction. To address this gap, we employed the CETSA, a label-free technique utilized for protein target identification of active compounds within cells (Cui et al., 2022). CETSA has been previously employed to investigate target interactions related to the antiosteoporosis effects of a lignan from *Litsea cubeba* (Peng et al., 2018). In the present study, we conducted CETSA experiments and observed that (\pm)KU could stabilize AKR1B1 protein levels when subjected to high temperatures in cells with AKR1B1 overexpression (Hs578T and SKOV3). Our results indicated significant stabilization of AKR1B1 levels at concentrations of 10 and 20 μ M on both cell lines. These findings support the potential binding of (\pm)KU to AKR1B1, as evidenced by the protective effect of (\pm)KU against AKR1B1 degradation caused by heating. Collectively, these results provide valuable *in vitro* evidence suggesting that (\pm)KU indeed interacts with AKR1B1 and supports its potential as an AKR1B1 inhibitor, in line with earlier computational predictions.

Our investigations further delved into the inhibitory effects of (\pm)KU on AKR1B1 enzyme activity. Notably, we observed that (\pm)KU exhibited the potential to inhibit the conversion of glucose to sorbitol by AKR1B1 enzyme activity in a dose-dependent manner. Interestingly, the inhibitory effect of (\pm)KU was more pronounced compared to that of *trans*-(-)-arctiin, a lignan compound previously reported as an AKR1B1 inhibitor (Xei et al., 2005). Worth mentioning is the structural similarity between (\pm)KU and *trans*-(-)-arctiin, which could underlie their shared inhibitory activity. Interestingly, various lignans derived from different plant sources have demonstrated the potential to inhibit AKR1B1 activity. For instance,

lignans extracted from *Eucommia ulmoides* (Gu et al., 2011), *Fructus arctii* (Xu et al., 2010), and *Viburnum cylindricum* (Zhao et al., 2020) have all exhibited inhibitory effects on AKR1B1 activity. These findings provide additional support for the notion that (\pm)KU, along with lignan compounds sharing structural similarities, could indeed possess potential as AKR1B1 inhibitors.

AKR1B1 plays a crucial role in cellular oxidative stress through its involvement in the polyol pathway, where it catalyzes the conversion of glucose to sorbitol (Khayami et al., 2020). Under normal circumstances, the metabolic activity of glucose through the AKR1B1 pathway is relatively modest. However, in hyperglycemic conditions, the activity of AKR1B1 becomes stimulated, leading to increased generation of reactive oxygen species (ROS) through various mechanisms. In hyperglycemic conditions, several events contribute to the enhanced ROS generation. Firstly, the production of sorbitol from glucose consumes NADPH, a vital coenzyme involved in numerous cellular processes. Additionally, the conversion of oxidized glutathione (GSSG) to its reduced form (GSH) also depletes NADPH. Moreover, the conversion of sorbitol to fructose by sorbitol dehydrogenase (SDH) relies on NAD⁺ as a cofactor. All these processes contribute to a reduction in NADPH and NAD⁺ levels, further exacerbating the imbalance in redox homeostasis (Han et al., 2020). Furthermore, the accumulation of sorbitol itself can lead to oxidative stress, while the conversion of sorbitol to fructose generates advanced glycation end products (AGEs), which can contribute to enhanced ROS production (Figure 53). This heightened ROS generation results in oxidative damage to cellular components, particularly membrane lipids. Notably, the oxidation of membrane lipids leads to the production of stable mediators such as 4-hydroxy-trans-2-nonenal (HNE) and malondialdehyde (MDA), which serve as reliable markers reflecting the extent of oxidative stress (Figure 53) (Sonowal et al., 2019). In summary, AKR1B1's involvement in the polyol pathway during hyperglycemic conditions triggers a series of events that culminate in increased ROS generation, oxidative stress, and subsequent damage to cellular components. This process has implications for various pathological conditions, including those associated with cancer and other chronic diseases.

Previous research has highlighted the protective effects of fisetin against high glucose-induced oxidative damage in HT22 cells, as evidenced by a decrease in MDA

levels (Zhang et al., 2020). Furthermore, in *in vivo* studies involving STZ-induced diabetic rats, it was observed that diabetic rats exhibited elevated MDA levels, indicative of oxidative stress, and subsequent treatment with AKR1B1 inhibitors ameliorated oxidative stress in diabetic complications, leading to a reduction in MDA levels (Zhao et al., 2020; Zhang et al., 2022). Consistent with these prior findings, our research has demonstrated that Hs578T cells exposed to a high glucose environment (100 mM) exhibited a significant increase in MDA levels compared to cells cultured under normal glucose conditions (5.5 mM). Interestingly, exposure to (\pm)KU resulted in a significant reduction in MDA levels, and this effect was more pronounced compared to epalrestat. These results suggest that (\pm)KU may possess a protective effect against high glucose-induced oxidative stress in Hs578T cells, likely through its inhibition of AKR1B1 activity. This finding is noteworthy as it implies that (\pm)KU could potentially serve as a therapeutic agent for conditions associated with oxidative stress, including those linked to high glucose levels, such as diabetes and diabetic complications. Moreover, the comparative effectiveness of (\pm)KU versus epalrestat underscores its potential as a novel and promising candidate for the mitigation of oxidative stress-related pathologies.

AKR1B1 is closely associated with the epithelial-mesenchymal transition (EMT) process, a critical cellular program implicated in cancer progression and metastasis. In cancer studies, AKR1B1 has been shown to strongly correlate with aggressive and invasive cancer phenotypes. Research by Schwab and colleagues demonstrated that knockdown of AKR1B1 in A549 non-small cell lung cancer cells inhibited EMT, proliferation, and the expression of cancer stem cell markers. Furthermore, activation of AKR1B1 induced by high glucose conditions enhanced cell migration and led to alterations in EMT markers, including changes in the expression of E-cadherin, vimentin, and ZEB1, partly through TGF- β stimulation (Schwab et al., 2018). In diabetic studies, AKR1B1-induced EMT processes have also been observed, and these processes are mediated by oxidative stress. For example, in the context of diabetic cataract development, AKR1B1 is implicated in the EMT process. Cataract lenses from hyperglycemic patients with diabetes exhibited significantly higher expression levels of AKR1B1, RAGE (receptor for advanced glycation end products), 3NT (3-nitrotyrosine, a marker of protein nitration), N-cadherin, and MMP9 compared to non-diabetic

cataract lenses (Wu et al., 2020). These findings underscore the role of AKR1B1 in mediating EMT processes and oxidative stress in both cancer and diabetic contexts, further highlighting its significance in disease pathogenesis.

Moreover, AKR1B1 plays a significant role in EMT by participating in the metabolism of aldehydes derived from lipid peroxidation. Specifically, AKR1B1 converts glutathionyl-4-hydroxynonenal (GS-HNE) into glutathionyl-1,4-dihydroxynonene (GS-DHN). This conversion activates phospholipase C (PLC) and protein kinase C (PKC), subsequently facilitating NF- κ B signaling modulation to regulate cell migration and invasion, as illustrated in Figure 53 (Khayami et al., 2019). Previous research has also shown that inhibiting AKR1B1 using sorbinil and zopolrestat impedes EGF/FGF-induced growth, migration, and invasion by disrupting GS-DHN-mediated oxidative stress, leading to NF- κ B activation in HT29 and KM20 colon cancer cells (Tammali et al., 2011).

AKR1B1 also exerts control over the epithelial-mesenchymal transition (EMT) process by influencing prostaglandin biosynthesis. In general, phospholipids are converted to arachidonic acid by phospholipase A2 (PLA2), which can be feasibly activated by GS-DHN. Subsequently, arachidonic acid is transformed into prostaglandin H₂ (PGH₂) by cyclooxygenase 2 (COX2), a crucial downstream molecule of the NF- κ B signaling pathway (Khayami et al., 2019). AKR1B1 is responsible for converting PGH₂ into prostaglandin F_{2 α} (PGF_{2 α}), which activates the PI3K/AKT signaling pathway and potentially triggers the activation of nuclear factor-erythroid 2 related factor 2 (Nrf2), a regulator of AKR1B1 expression (Dodson et al., 2019). PGF_{2 α} directly modulates NF- κ B signaling and indirectly stimulates NF- κ B through the PLC/PKC signaling cascade (Xu et al., 2015). NF- κ B plays a pivotal role in the expression of Twist2, which in turn regulates EMT markers (E-cadherin and N-cadherin) and directly controls AKR1B1 expression, as depicted in Figure 53 (Wu et al., 2017). These previous studies provide support for our current experiments. We evaluated the inhibitory effects of (\pm)KU on Hs578T cells, focusing on AKR1B1 and its downstream molecules (PKC δ , NF- κ B, AKT, Nrf2, COX2, and Twist2), as well as alterations in EMT markers (E-cadherin and N-cadherin). Our findings revealed that (\pm)KU significantly suppressed AKR1B1 and its downstream molecules, and it induced dose-dependent changes in EMT marker levels

(upregulation of E-cadherin and downregulation of N-cadherin). Our results align with previous research; for instance, gedunin, a limonoid compound, demonstrated inhibition of AKR1B1 and its downstream expression (AKT, ERK, and NF- κ B), reduced ROS generation, and inhibited hypoxia-induced cell migration in SCC131 oral cancer cells (Tanagala et al., 2018). Additionally, fidarestat, an AKR1B1 inhibitor, reduced COX2 and NF- κ B expression in HT29 colon cancer cells and inhibited PKC, AKT, and COX2 in azoxymethane-induced colonic premalignant mice (Saxena et al., 2014).

We extended our investigation into the impact of (\pm)KU on Hs578T cells by conducting comparative analyses with an AKR1B1 inhibitor (epalrestat), siRNA-AKR1B1, and combinations of these treatments on Hs578T cells. Our findings indicated that (\pm)KU effectively suppressed AKR1B1 expression and its downstream molecular components, resulting in alterations in EMT marker levels. Remarkably, this effect closely resembled the actions of epalrestat and siRNA-AKR1B1. Furthermore, when we combined siRNA-AKR1B1 with (\pm)KU or epalrestat, we observed a more pronounced reduction in AKR1B1 and N-cadherin expression compared to siRNA-AKR1B1 treatment alone. These results strongly suggest that (\pm)KU inhibits AKR1B1 in a manner similar to epalrestat and exhibits a potential effect akin to siRNA-AKR1B1 treatment. Similarly, previous reports have documented the inhibitory effects of epalrestat on TNBC cells, such as MDA231 and SUM159. Epalrestat treatment and the knockdown of AKR1B1 expression led to changes in the levels of EMT markers, including an increase in E-cadherin and a decrease in vimentin, ultimately reducing cancer cell migration and invasion. Conversely, the overexpression of AKR1B1 via stable vector transfection in luminal breast cancer cells, like T47D and MCF7, exhibited contrasting effects (Wu et al., 2017).

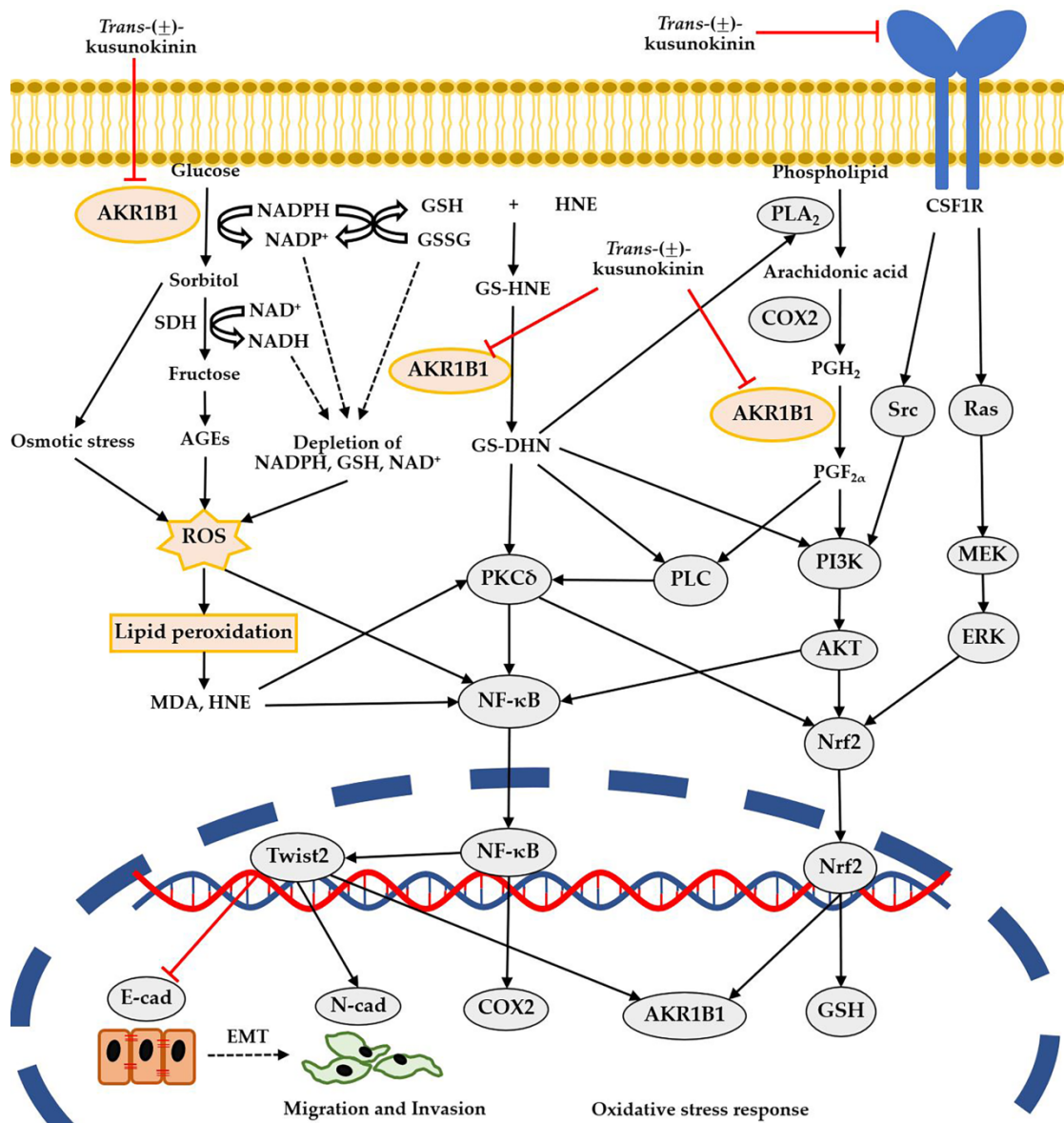


Figure 53. Proposed mechanism of action of *trans*-(±)-kusunokinin in AKR1B1 pathway. *Trans*-(±)-kusunokinin inhibited AKR1B1 leading to reduction of lipid peroxidation and suppression of signaling molecules related to oxidative stress response and migration of breast cancer.

CHAPTER 5

CONCLUSIONS

Part I. Identification of *trans*-(–)-kusunokinin target by *in silico* studies

1. *Trans*-(–)-kusunokinin was predicted as a tentative target of AKR1B1 and MEK2. However, AKR1B1 piqued our interest as a consequence of its higher potential binding energy value and the supporting data that other lignan compounds (arctigenin and arctiin) with similar structures to *trans*-(–)-kusunokinin exhibited as potential AKR1B1 inhibitors.

2. *Trans*-(–)-kusunokinin showed a potential binding affinity better than the AKR1B1 substrate (PGH₂) and was comparable with reported potential well-known AKR1B1 inhibitors.

3. Molecular dynamics behavior revealed that *trans*-(–)-kusunokinin and AKR1B1 inhibitors did not affect the AKR1B1 conformation.

4. The insight binding mode, *trans*-(–)-kusunokinin, was inserted in the active site with a similar position and orientation to AKR1B1 inhibitors and substrates. *Trans*-(–)-kusunokinin structure also shared equivalent properties with the structure of ARIs. An aromatic ring was noticeably a common structure to perform π - π stacking with Trp111 in *trans*-(–)-kusunokinin and both groups of AKR1B1 inhibitors. Interestingly, the γ -butyrolactone ring of *trans*-(–)-kusunokinin was considered as a counterpart of the carboxylic group of AKR1B1 inhibitors to interact with the His110 catalytic site via hydrogen bonds, preventing the substrate PGH₂ from accessing the catalytic site (Figure 54). All combinations implied that *trans*-(–)-kusunokinin could be a promising potential AKR1B1 inhibitor to be used in metastatic cancer treatment in the future.

Part II. Validation of *trans*-(±)-kusunokinin target by *in vitro* studies

1. IC₅₀ values of *trans*-(±)-kusunokinin concordant with the aggressive cancer cell type (MCF7 and A5780, the grade I breast and ovarian cancer cells, respectively, showed the strongest cytotoxicity). While the IC₅₀ values of well-known AKR1B1 inhibitors (zopolrestat and epalrestat) were concordant with the AKR1B1 protein level (MCF7 and OVCAR3), the low expression of AKR1B1 on breast and ovarian cancer cells, respectively, showed the weakest cytotoxicity).

2. *Trans*-(±)-kusunokinin inhibited AKR1B1 enzyme activity with an IC₅₀ value of $9.72 \pm 0.18 \mu\text{M}$ and showed better activity than *trans*-(–)-arctiin, which reported lignan as an AKR1B1 inhibitor (IC₅₀ value of $13.65 \pm 0.49 \mu\text{M}$). Whereas epalrestat and zopolrestat, the well-known AKR1B1 inhibitors, specifically designed for targeting aldose reductase, showed potential IC₅₀ values of $0.77 \pm 0.01 \mu\text{M}$ and $31.03 \pm 0.14 \text{ nM}$, respectively.

3. *Trans*-(±)-kusunokinin protected intracellular AKR1B1 degradation from heating at 60 and 75°C on Hs578T and SKOV3 cells, respectively.

4. *Trans*-(±)-kusunokinin inhibited glucose-induced cellular lipid peroxidation on Hs578T cells with a more decreased MDA level than epalrestat.

5. *Trans*-(±)-kusunokinin suppressed AKR1B1, leading to the suppression of signaling molecules (PKCδ, NF-κB, AKT, Nrf2, COX2, Twist2) and the alteration of the EMT markers (increase E-cadherin level and decrease N-cadherin level) on Hs578T breast cancer cells (Figure 55).

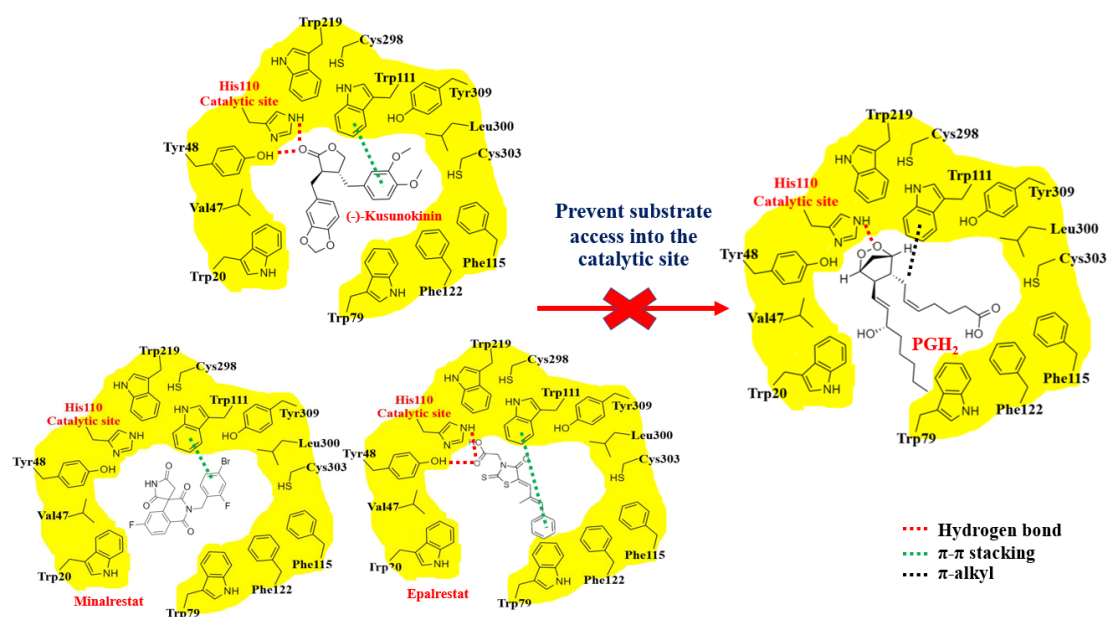


Figure 54. Proposed binding model of *trans*-(±)-kusunokinin and ARIs to prevent the substrate PGH_2 access into the catalytic site of AKR1B1.

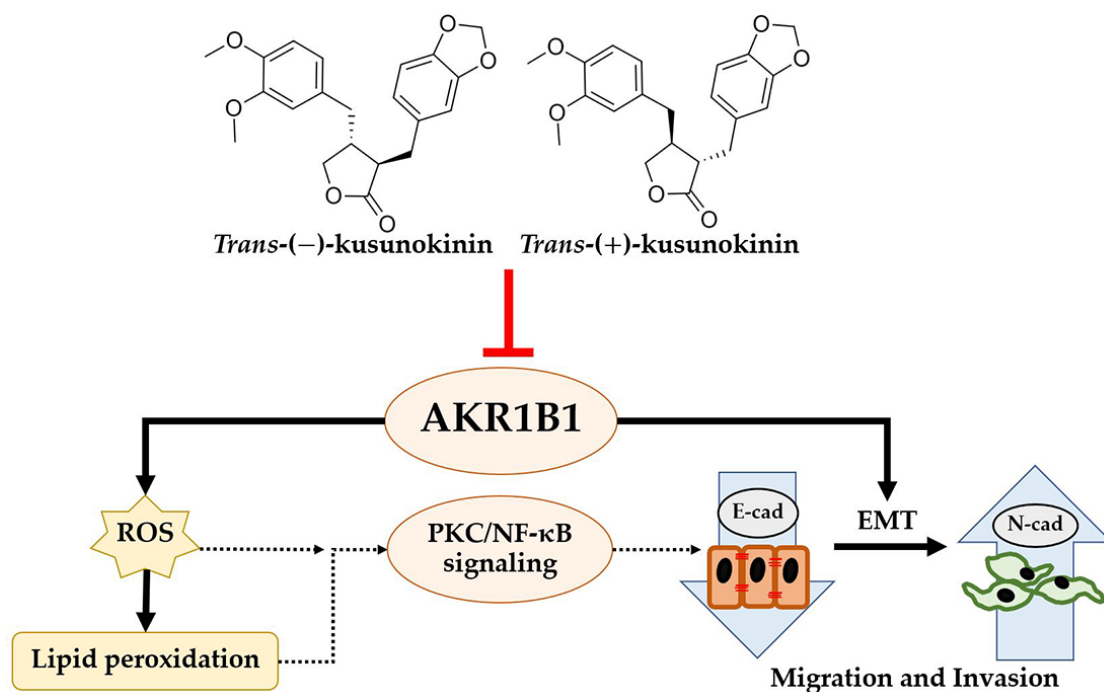


Figure 55. Proposed *trans*-(±)-kusunokinin mechanism of action in breast cancer cells.

REFERENCES

- Albanell J, Codony J, Rovira A, Mellado B, Gascon P. Mechanism of action of anti-HER2 monoclonal antibodies: scientific update on trastuzumab and 2C4. *Adv Exp Med Biol.* 2003;532:253-68.
- Alia MS, Perveza MK, Saleema M, Tareenb RB. Haplophytin-A and B: the alkaloidal constituents of *Haplophyllum acutifolium*. *Phytochem.* 2001;57:1277-80.
- Alimbetov D, Askarova S, Umbayev B, Davis T, Kipling D. Pharmacological targeting of cell cycle, apoptotic and cell adhesion signaling pathways implicated in chemoresistance of cancer cells. *Int J Mol Sci.* 2018;19(6):1690-721.
- American Cancer Society. Treating Breast Cancer [Internet]. [revised January 2023; cited 2023 June 27]. Available <https://www.cancer.org/cancer/types/breast-cancer/treatment.html>.
- Arumugam A, Subramani R, Nandy SB, Terreros D, Dwivedi AK, Saltzstein E et al. Silencing growth hormone receptor inhibits estrogen receptor negative breast cancer through ATP-binding cassette sub-family G member 2. *Exp Mol Med.* 2019;51(1):1-13.
- Awale S, Kato M, Dibwe DF, Li F, Miyoshi C, Esumi H, et al. Antiausterity activity of arctigenin enantiomers: importance of (2R,3R)-absolute configuration. *Nat Prod Commun.* 2014;9(1):79-82.
- Banala VT, Urandur S, Sharma S, Sharma M, Shukla RP, Marwaha D, et al. Targeted co-delivery of the aldose reductase inhibitor epalrestat and chemotherapeutic doxorubicin via a redox-sensitive prodrug approach promotes synergistic tumor suppression. *Biomater Sci.* 2019;7(7):2889-906.
- Bardia A, Mayer IA, Kalinsky K. Sacituzumab Govitecan-hziy in triple-negative breast cancer. Reply. *N Engl J Med.* 2019;380(24):2382.
- Berridge MJ. Module 11: Cell stress, inflammatory responses and cell death. *Cell Signal Biol.* 2014;6:csb0001011.
- Berridge MJ. Module 9: Cell cycle and proliferation. *Cell Signal Biol.* 2014;6:csb0001009.

- Bicalho KU, Terezan AP, Martins DC, Freitas TG, Fernandes JB, Vieira PC et al. Evaluation of the toxicity of *Virola sebifera* crude extracts, fractions and isolated compounds on the nest of leaf-cutting ants. *Psych*. 2012;6:1-7.
- Biovia D. Discovery studio modeling environment, Release 2017, San Diego: DassaultSystèmes, 2016.
- Brown J, Shvartsman HS, Deavers MT, Ramondetta LM, Burke TW, Munsell MF, et al. The activity of taxanes compared with bleomycin, etoposide, and cisplatin in the treatment of sex cord-stromal ovarian tumors. *Gynecol Oncol*. 2005;97(2):489-96.
- Chang ST, Wang DS, Wu CL, Shiah SG, Kuo YH, Chang CJ. Cytotoxicity of extractives from *Taiwania cryptomerioides* heartwood. *Phytochemistry*. 2000;55(3):227-32.
- Chatzopoulou M, Alexiou P, Kotsampasakou E, Demopoulos VJ. Novel aldose reductase inhibitors: a patent survey (2006-present). *Expert Opin Ther Pat*. 2012;22(11):1303-23.
- Chen HJ, Liu PF, Zhang T, Gao Y, Zhang YD, Shen XY, et al. Effects of diphyllin as a novel V-ATPase inhibitor on TE-1 and ECA-109 cells. *Oncol Rep*. 2018;39(3):921-8.
- Chen VW, Ruiz B, Killeen JL, Côté TR, Wu XC, Correa CN, et al. Pathology and classification of ovarian tumors. *Cancer*. 2003;97:2631-42.
- Chen YC, Liao CH, Chen IS. Lignans, an amide and anti-platelet activities from *Piper philippinum*. *Phytochemistry*. 2007;68(15):2101-11.
- Chi HC, Chen CY, Tsai MM, Tsai CY, Lin KH. Molecular functions of thyroid hormones and their clinical significance in liver-related diseases. *Biomed Res Int*. 2013;2013:601361.
- Chuang TC, Hsu SC, Cheng YT, Shao WS, Wu K, Fang GS, et al. Magnolol down-regulates HER2 gene expression, leading to inhibition of HER2-mediated metastatic potential in ovarian cancer cells. *Cancer Lett*. 2011;311(1):11-9.
- Cobrinik D. Pocket proteins and cell cycle control. *Oncogene*. 2005;24:2796-809.
- Cristofanilli M, Gonzalez-Angulo A, Sneige N. Invasive lobular carcinoma classic type: response to primary chemotherapy and survival outcomes. *J Clin Oncol*. 2005;23:41-8.

- Crosas B, Hyndman DJ, Gallego O, Martras S, Pares X, Flynn TG, et al. Human aldose reductase and human small intestine aldose reductase are efficient retinal reductases: consequences for retinoid metabolism. *Biochem J.* 2003;373(3):973-9.
- Cui Z, Li C, Chen P, Yang H. An update of label-free protein target identification methods for natural active products. *Theranostics* 2022;12:1829-54.
- Davidson SJ, Pilkington LI, Dempsey-Hibbert NC, El-Mohtadi M, Tang S, Wainwright T, et al. Modular synthesis and biological investigation of 5-hydroxymethyl dibenzyl butyrolactones and related lignans. *Molecules.* 2018;23:3057-81.
- De Silva SF, Alcorn J. Flaxseed lignans as important dietary polyphenols for cancer prevention and treatment: Chemistry, pharmacokinetics, and molecular targets. *Pharmaceuticals (Basel).* 2019;12(2).
- Dias K, Dvorkin-Gheva A, Hallett RM, Wu Y, Hassell J, Pond GR, Bane AL. Claudin-low breast cancer; clinical & pathological characteristics. 2017;12(1):e0168669.
- Díez-Dacal B, Sánchez-Gómez FJ, Sánchez-Murcia PA, Milackova I, Zimmerman T, Ballekova J, et al. Molecular interactions and implications of aldose reductase inhibition by PGA1 and clinically used prostaglandins. *Mol Pharmacol.* 2016;89(1):42-52.
- Distelhorst CW, Shore GC. Bcl-2 and calcium: controversy beneath the surface. *Oncogene* 2014;23:2875-80.
- Dodson M, Castro-Portuguez R, Zhang DD. NRF2 plays a critical role in mitigating lipid peroxidation and ferroptosis. *Redox Biol.* 2019;23:101107.
- Dohrn L, Salles D, Siehler SY, Kaufmann J, Wiesmüller L. BRCA1-mediated repression of mutagenic end-joining of DNA double-strand breaks requires complex formation with BACH1. *Biochem J.* 2012;441:919-26.
- El-Kabbani O, Darmanin C, Schneider TR, Hazemann I, Ruiz F, Oka M et al. Ultrahigh resolution drug design. II. Atomic resolution structures of human aldose reductase holoenzyme complexed with fidarestat and minalrestat: implications for the binding of cyclic imide inhibitors. *Proteins Struct Funct Bioinf.* 2004;55(4):805-13.

- Evcim U, Gözler B, Freyer AJ, Shamma M. Haplomyrtin and (–)-haplomyrfofin: two lignans from *Haplophyllum myrtifolium*. *Phytochemistry*. 1986;25(8):1949-51.
- Fang X, Hu X. Advances in the synthesis of lignan natural products. *Molecules*. 2018;23:1-22.
- Ganeshpure PA, Stevenson R. Synthesis of aryltetralin and dibenzylbutyrolactone lignans: (±)-lintetralin, (±)-phyltetralin, and (±)-kusunokinin. *J Chem Soc Perkin trans. 1*. 1981(0):1681-4.
- Ge LN, Yan L, Li C, Cheng K. Bavachinin exhibits antitumor activity against nonsmall cell lung cancer by targeting PPARgamma. *Mol Med Rep*. 2019;20(3):2805-11.
- Goldhirsch A, Wood WC, Coates AS, Gelber RD, Thürlimann B, Senn HJ et al. Strategies for subtypes dealing with the diversity of breast cancer: highlights of the St Gallen international expert consensus on the primary therapy of early breast cancer 2011. *Ann Oncol*. 2011;22(8):1736-47.
- Gözler B, Rentsch D, Gözler T, Ünver N, Hesse M. Lignans, alkaloids and coumarins from *Haplophyllum vulcanicum*. *Phytochemistry*. 1996;42(3):695-9.
- Gozler T, Gozler B, Patra A, Leet JE, Freyer AJ, Shamma M. Konyanin: A new lignan from *Haplophyllum vulcanicum*. *Tetrahedron*. 1984;40:1145-50.
- Graidist P, Yazawa M, Tonganant M, Nakatomi A, Lin CCJ, Chang JY, et al. Fortilin binds calcium and blocks Ca²⁺-dependent apoptosis *in vivo*. *Biochem J*. 2007;408:181-91.
- Gu J, Wang JJ, Yan J, Cui CF, Wu WH, Li L, et al. Effects of lignans extracted from *Eucommia ulmoides* and aldose reductase inhibitor epalrestat on hypertensive vascular remodeling. *J Ethnopharmacol*. 2011;133:6–13.
- Hadi LM, Yaghini E, MacRobert AJ, Loizidou M. Synergy between photodynamic therapy and dactinomycin chemotherapy in 2D and 3D ovarian cancer cell cultures. *Int J Mol Sci*. 2020;21(9).
- Hamada Y, Kitoh R, Raskin P. Crucial role of aldose reductase activity and plasma glucose level in sorbitol accumulation in erythrocytes from diabetic patients. *Diabetes*. 1991;40(10):1233-40.
- Hanby AM, Hughes TA. In situ and invasive lobular neoplasia of the breast. *Histopathology*. 2008;52:58-66.

- Hartley RM, Peng J, Fest GA, Dakshanamurthy S, Frantz DE, Brown ML, et al. Polygamain, a new microtubule depolymerizing agent that occupies a unique pharmacophore in the colchicine site. *Mol Pharmacol*. 2012;81(3):431-9.
- Heit JJ, Apelqvist AA, Gu X, Winslow MM, Neilson JR, Crabtree GR, Kim SK. Calcineurin/NFAT signalling regulate pancreatic β -cell growth and function. *Nature* 2006;443:345-9.
- Horner RM. The use of internal controls for relative and competitive quantitative RT-PCR. In: Dieffenbach CW, Dveksler GS, editors. *PCR primer: A laboratory manual*. 2nd ed. New York: CSHL Press. 2003:167-85.
- Hotta N, Kawamori R, Atsumi Y, Baba M, Kishikawa H, Nakamura J, et al. Stratified analyses for selecting appropriate target patients with diabetic peripheral neuropathy for long-term treatment with an aldose reductase inhibitor, epalrestat. *Diabet Med*. 2008;25(7):818-25.
- Hou T, Wang J, Li Y, Wang W. Assessing the performance of the MM/PBSA and MM/GBSA methods. 1. The accuracy of binding free energy calculations based on molecular dynamics simulations. *J Chem Inf Model*. 2011, 51(1), 69–82.
- Huey RM, Morris G, Olson AJ, Goodsell DS. A semiempirical free energy force field with charge-based desolvation. *J Comput Chem*. 2007;28(6):1145-52.
- Humphrey W, Dalke A, Schulten K. VMD: Visual molecular dynamics. *J. Mol Graph*. 1996; 14(1): 33-8.
- Jayaram B, Sprous D, Young MA, Beveridge DL. Free energy analysis of the conformational preferences of A and B forms of DNA in solution. *J Am Chem Soc*. 1998;120(41):10629-33.
- Jordan VC. Fourteenth Gaddum Memorial Lecture. A current view of tamoxifen for the treatment and prevention of breast cancer. *Br J Pharmacol*. 1993;110(2):507-17.
- Karahisar E, Tugay O, Orhan IE, Sezer Senol Deniz F, Vlad Luca S, Skalicka-Wozniak K, et al. Metabolite profiling by hyphenated liquid chromatographic mass spectrometric technique (HPLC-DAD-ESI-Q-TOF-MS/MS) and neurobiological potential of *Haplophyllum sahinii* and *H. vulcanicum* extracts. *Chem Biodiversity*. 2019;16:1-13.

- Kato M, He YM, Dibwe DF, Li F, Awale S, Kadota S, et al. New guaian-type sesquiterpene from *Wikstroemia indica*. *Nat Prod Commun*. 2014;9(1):1-2.
- Kato MJ, Yoshida M, Gottlieb OR. Lignoids and arylalkanones from fruits of *Virola elongata*. *Phytochemistry*. 1990;29(6):1799-810.
- Kaye SB, Lubinski J, Matulonis U, Ang JE, Gourley C, Karlan BY et al. Phase II, open-label, randomized, multicenter study comparing the efficacy and safety of olaparib, a poly (ADP-ribose) polymerase inhibitor, and pegylated liposomal doxorubicin in patients with BRCA1 or BRCA2 mutations and recurrent ovarian cancer. *J Clin Oncol*. 2012;30:372-9.
- Khaled N, Bidet Y. New insights into the implication of epigenetic alterations in the EMT of triple negative breast cancer. *Cancers*. 2019;11(4).
- Kharraishvili G, Simkova D, Bouchalova K, Gachechiladze M, Narsia N, Bouchal J. The role of cancer-associated fibroblasts, solid stress and other microenvironmental factors in tumor progression and therapy resistance. *Cancer Cell Int* 2014;14:41.
- Khayami R, Hashemi SR, Kerachian MA. Role of aldo-keto reductase family 1 member B1 (AKR1B1) in the cancer process and its therapeutic potential. *J Cell Mol Med* 2020;24:8890–902.
- Kim SE. Enzymes involved in folate metabolism and its implication for cancer treatment. *Nutr Res Pract*. 2020;14(2):95-101.
- Kobayashi H, Ohno S, Sasaki Y, Matsuura M. Hereditary breast and ovarian cancer susceptibility genes (Review). *Oncol Rep*. 2013;30(3):1019-29.
- Kollman PA, Massova I, Reyes C, Kuhn B, Huo S, Chong L, Lee M, Lee T, Duan Y, Wang W, Donini O, Cieplak P, Srinivasan J, Case DA, Cheatham TE. Calculating structures and free energies of complex molecules: Combining molecular mechanics and continuum models. *Acc Chem Res*. 2000;33(12):889-97.
- Kollman PA. Free energy calculations: applications to chemical and biochemical phenomena. *Chem. Rev*. 1993;93(7):2395-417.
- Lakhani SR, Ellis IO, Schnitt SJ, Tan PH, Van de Vijver MJ, eds. WHO Classification of Tumours of the Breast. Fourth ed. IARC, Lyon; 2012.

- Ledermann J, Harter P, Gourley C, Friedlander M, Vergote I, Rustin G et al. Olaparib maintenance therapy in platinum-sensitive relapsed ovarian cancer. *N Engl J Med* 2012; 366:1382-92.
- Lee AW. Both src-dependent and-independent mechanisms mediate phosphatidylinositol 3-kinase regulation of colony-stimulating factor 1-activated mitogen-activated protein kinases in myeloid progenitors. *Mol Cell Biol*. 2000;20:6779-98.
- Lemmon MA, Schlessinger J. Cell signaling by receptor tyrosine kinases. *Cell*. 2010;141(7):1117-34.
- Lichota A, Gwozdziński K. Anticancer activity of natural compounds from plant and marine environment. *Int J Mol Sci*. 2018;19(11):3533-71.
- Lipinski CA, Aldinger CE, Beyer TA, Bordner J, Burdi DF, Bussolotti DL, et al. Hydantoin bioisosteres. *In vivo* active spiro hydroxy acetic acid aldose reductase inhibitors. *J Med Chem*. 1992;35(12):2169-77.
- Lopes LMX, Yoshida M, Gottlieb OR. Dibenzylbutyrolactone lignans from *Virola sebifera*. *Phytochemistry* 1983;22:1516-8.
- Maccari R, Ottana R. Targeting aldose reductase for the treatment of diabetes complications and inflammatory diseases: new insights and future directions. *J Med Chem*. 2015;58(5):2047-67.
- Makki J, Myint O, Wynn AA, Samsudin AT, John DV. Expression distribution of cancer stem cells, epithelial to mesenchymal transition, and telomerase activity in breast cancer and their association with clinicopathologic characteristics. *Clin Med Insights Pathol*. 2015;8:1-16.
- Marcotullio MC, Curini M, Becerra JX. An ethnopharmacological, phytochemical and pharmacological review on lignans from Mexican *Bursera* spp. *Molecules*. 2018;23(8).
- Mayer B, Oberbauer R. Mitochondrial regulation of apoptosis. *News Physiol Sci*. 2003;18:89-94.
- McFedries A, Schwaib A, Saghatelian A. Methods for the elucidation of protein-small molecule interactions. *Chemistry & Biology*. 2013;20(5):667-73.
- Merck KGaA. Western Blotting Protocol (Immunoblotting Protocol). 2020 [April 4, 2020]. Available from: <https://www.sigmaaldrich.com/technical-documents/protocols/biology/western-blotting.html>.

- Messiano GB, Vieira L, Machado MB, Lopes LM, de Bortoli SA, Zukerman-Schpector J. Evaluation of insecticidal activity of diterpenes and lignans from *Aristolochia malmeana* against *Anticarsia gemmatalis*. *J Agric Food Chem*. 2008;56(8):2655-9.
- Middel O, Woerdenbag HJ, van Uden W, van Oeveren A, Jansen JF, Feringa BL, et al. Synthesis and cytotoxicity of novel lignans. *J Med Chem*. 1995;38(12):2112-8.
- Mohamed SB, Adlan TA, Khalafalla NA, Abdalla NI, Ali ZS, Munir Ka A, et al. Proteomics and docking study targeting penicillin-binding protein and penicillin-binding protein2a of methicillin-resistant *Staphylococcus aureus* strain SO-1977 isolated from sudan. *evolutionary bioinformatics*. 2019;15:1-13.
- Mora S, Castro VM, Poveda L, Chavarría M, Murillo R. Chemical constituents from *Zanthoxylum setulosum* (Rutaceae). *Bol Latinoam Caribe Plantas Med Aromat*. 2011;10(2):155-8.
- Moraisa TR, Costa-Silva TA, Ferreirac DD, Novaisa BJ, Torrecilha ACT, Tempone AG et al. Antitrypanosomal activity and effect in plasma membrane permeability of (-)-bornyl p-coumarate isolated from *Piper cernuum* (Piperaceae). 2019;89:103001.
- Morgan RJ, Armstrong DK, Alvarez RD, Bakkum-Gamez JN, Behbakht K, Chen LM, et al. Ovarian cancer NCCN clinical practice guidelines in oncology. *J Natl Compr Canc Netw*. 2016;14(9):1134-63.
- Morris G, Huey R, Linkstrom W, Sanner M, Belew R, Goodsell D, Olson AJ. AutoDock4 and AutoDockTools4: Automated docking with selective receptor flexibility. *J Comput Chem*. 2009;30(16):2785-91.
- Nabholtz JM. Long-term safety of aromatase inhibitors in the treatment of breast cancer. *Ther Clin Risk Manag*. 2008:189-204.
- Nagata N, Kusakari Y, Fukunishi Y, Inoue T, Urade Y. Catalytic mechanism of the primary human prostaglandin F2 α synthase, aldo-keto reductase 1B1-prostaglandin D2 synthase activity in the absence of NADP(H). *FEBS J*. 2011;278(8):1288-98.
- Ogungbe IV, Erwin WR, Setzer WN. Antileishmanial phytochemical phenolics: Molecular docking to potential protein targets. *J Mol Gr Modell*. 2014;48:105-17.
- Okunishi T, Umezawa T, Shimada M. Enantiomeric compositions and biosynthesis of *Wikstroemia sikokiana* lignans. *J Wood Sci*. 2000;46(3):234-42.

- Okunishi T, Umezawa T, Shimada M. Stereochemistry of lignan biosynthesis in *Wikstroemia sikokiana*. *Wood Res.* 1997;84:25-27.
- Orrenius S, Zhivotovsky B, Nicotera P. Regulation of cell death: the calcium–apoptosis link. *Nat Rev Mol Cell Biol.* 2013;4:552-65.
- Pai MY, Lomenick B, Hwang H, Schiestl R, McBride W, Loo JA, et al. Drug affinity responsive target stability (DARTS) for small-molecule target identification. *Methods Mol Biol.* 2015;1263:287-98.
- Pan L, Chai HB, Kinghorn AD. Discovery of new anticancer agents from higher plants. *Front Biosci.* 2013;4:142-56.
- Pei XH, Xiong Y. Biochemical and cellular mechanisms of mammalian CDK inhibitors: a few unresolved issues. *Oncogene.* 2005;24:2787-95.
- Peng W, Shen H, Lin B, Han P, Li C, Zhang Q, et al. Docking study and antiosteoporosis effects of a dibenzylbutane lignan isolated from *Litsea cubeba* targeting Cathepsin K and MEK1. *Med Chem Res.* 2018;27:2062–70.
- Peter B, Bernard L. World cancer report. International agency for research on cancer; WHO Press, Lyon, France; 2008.
- Peuhu E, Paul P, Remes M, Holmbom T, Eklund P, Sjöholm R, et al. The antitumor lignan Nortrachelogenin sensitizes prostate cancer cells to TRAIL-induced cell death by inhibition of the Akt pathway and growth factor signaling. *Biochem Pharmacol.* 2013;86(5):571-83.
- Peuhu E, Rivero-Muller A, Stykki H, Torvaldson E, Holmbom T, Eklund P, et al. Inhibition of Akt signaling by the lignan matairesinol sensitizes prostate cancer cells to TRAIL-induced apoptosis. *Oncogene.* 2010;29(6):898-908.
- Pongnikorn D, Suwanrungruang K, Buasom R. *Cancer in Thailand: Vol. IX, 2013–2015.*
- Prasad V, De Jesús K, Mailankody S. The high price of anticancer drugs: origins, implications, barriers, solutions. *Nat Rev Clin Oncol.* 2017;14:381-90.
- Rajalekshmi DS, Kabeer FA, Madhusoodhanan AR, Bahulayan AK, Prathapan R, Prakasan N, et al. Anticancer activity studies of cubebin isolated from *Piper cubeba* and its synthetic derivatives. *Bioorg Med Chem Lett.* 2016;26(7):1767-71.
- Ramana KV, Tammali R, Srivastava SK. Inhibition of aldose reductase prevents growth factor-induced G1-S phase transition through the AKT/phosphoinositide

- 3-kinase/E2F-1 pathway in human colon cancer cells. *Mol Cancer Ther.* 2010;9(4):813-24.
- Ramirez MA, Borja NL. Epalrestat: an aldose reductase inhibitor for the treatment of diabetic neuropathy. *Pharmacotherapy.* 2008;28(5):646-55.
- Rattanaburee T, Thongpanchang T, Wongma K, Tedasen A, Sukpondma Y, Graidist P. Anticancer activity of synthetic (\pm)-kusunokinin and its derivative (\pm)-bursehernin on human cancer cell lines. *Biomed Pharmacother.* 2019;117:109-15.
- Rattanaburee T, Tipmanee V, Tedasen A, Thongpanchang T, Graidist P. Inhibition of CSF1R and AKT by (\pm)-kusunokinin hinders breast cancer cell proliferation. *Biomed Pharmacother.* 2020;129:110361.
- Rosai J. Rosai and Ackerman's Surgical Pathology. Tenth ed. Elsevier, Lyon, France; 2011.
- Roy P, Yu LJ, Crespi CL, Waxman DJ. Development of a substrate-activity based approach to identify the major human liver P-450 catalysts of cyclophosphamide and ifosfamide activation based on cDNA-expressed activities and liver microsomal P-450 profiles. *Drug Metab Dispos.* 1999;27(6):655-66.
- Ryde U. Molecular dynamic simulations of alcohol dehydrogenase with varying coordination number of the catalytic zinc ion. *Proteins Struct Funct Genet.* 1995;21:40-50.
- Sambrook J. Preparation and analysis of eukaryotic genomic DNA. *Molecular cloning.* 2001;1:6-4.
- Sangkhathat S, Thongsuksai P, Sriplung H, Saetang J. Cancer registry and basic cancer epidemiology. *Cancer science.* 2017;1:131-216.
- Saraswat M, Mrudula T, Kumar PU, Suneetha A, Rao Rao TS, Srinivasulu M, et al. Overexpression of aldose reductase in human cancer tissues. *Med Sci Monit.* 2006;12(12):CR525-9.
- Sarges R, Schnur RC, Belletire JL, Peterson MJ. Spiro hydantoin aldose reductase inhibitors. *J Med Chem.* 1988;31(1):230-43.
- Sartorelli P, Carvalho CS, Reimao JQ, Lorenzi H, Tempone AG. Antitrypanosomal activity of a diterpene and lignans isolated from *Aristolochia cymbifera*. *Planta Med.* 2010;76(13):1454-6.

- Saxena A, Shoeb M, Tammali R, Ramana KV, Srivastava SK. Aldose reductase inhibition suppresses azoxymethane-induced colonic premalignant lesions in C57BL/KsJ-db/db mice. *Cancer Lett.* 2014;355:141–7.
- Schnitt SJ, Morrow M. Lobular carcinoma in situ. current concepts and controversies. *Semin Diagn Pathol.* 1999;16:209-3.
- Sharma SV, Bell DW, Settleman J, Haber DA, Epidermal growth factor receptor mutations in lung cancer. *Nat Rev Cancer.* 2007;7:169-81.
- Shawarby MA, Al-Tamimi DM, Ahmed A. Molecular classification of breast cancer: an overview with emphasis on ethnic variations and future perspectives. *Saudi J Med Med Sci.* 2013;1:14-9.
- Shekhar KC, Basnet P, Thapa S, Shrestha B, Giri R. Ni-catalyzed regioselective dicarbofunctionalization of unactivated olefins by tandem cyclization/cross-coupling and application to the concise synthesis of lignan natural products. *J Org Chem.* 2018;83(5):2920-36.
- Sheriha GM, Abouamer K, Elshtaiwi BZ, Ashour AS, Abed FA, Alhallaq HH. Quinoline alkaloids and cytotoxic lignans from *Haplophyllum tuberculatum*. *Phytochemistry.* 1987;26(12):3339-41.
- Shoeb M, Ramana KV, Srivastava SK. Aldose reductase inhibition enhances TRAIL-induced human colon cancer cell apoptosis through AKT/FOXO3a-dependent upregulation of death receptors. *Free Radic Biol Med.* 2013;63:280-90.
- Simpson D, Amos S. Other Plant Metabolites. *Pharmacognosy.* 2017:267-80.
- Sonowal H, Ramana KV. 4-Hydroxy-*trans*-2-nonenal in the regulation of anti-oxidative and pro-inflammatory signaling pathways. *Oxidative Med Cell Longev.* 2019;2019:5937326.
- Sriwiriyan S, Ninpesh T, Sukpondma Y, Nasomyon T, Graidist P. Cytotoxicity screening of plants of genus *Piper* in breast cancer cell lines. *Trop J Pharm Res.* 2014;13(6):921-8.
- Sriwiriyan S, Sukpondma Y, Srisawat T, Madla S, Graidist P. (–)-Kusunokinin and piperloguminine from *Piper nigrum*: An alternative option to treat breast cancer. *Biomed Pharmacother.* 2017;92:732-43.

- Sung H, Ferlay J, Siegel RL, Laversanne M, Soerjomataram I, Jemal A, et al. Global cancer statistics 2020: GLOBOCAN Estimates of incidence and mortality worldwide for 36 cancers in 185 countries. *CA Cancer J Clin.* 2021;71(3):209-49.
- Takaoka D, Imooka M, Hiroi M. Studies of lignoids in Lauraceae. III. A new lignan from the heart wood of *Cinnamomum camphora* Sieb. *Bull Chem Soc Jpn.* 1977;50:2821-2.
- Tammali R, Reddy AB, Saxena A, Rychahou PG, Evers BM, Qiu S, et al. Inhibition of aldose reductase prevents colon cancer metastasis. *Carcinogenesis.* 2011;32:1259-67.
- Tanawattanasuntorn T, Thongpanchang T, Rungrotmongkol T, Hanpaibool C, Graidist P, Tipmanee V. (–)-Kusunokinin as a potential aldose reductase inhibitor: Equivalency observed via AKR1B1 dynamics simulation. *ACS Omega.* 2021;6(1):606-14.
- Tedasen A, Choomwattana S, Graidist P, Tipmanee V. Structure-guided cancer blockade between bioactive bursehernin and proteins: Molecular docking and molecular dynamics study. *J Mol Graph Model.* 2017;74:215-24.
- Tedasen A, Dokduang S, Sukpondma Y, Lailerd N, Madla S, Sriwiriyan S, et al. (–)-Kusunokinin inhibits breast cancer in N-nitrosomethylurea-induced mammary tumor rats. *Eur J Pharmacol.* 2020;882:173311.
- Theile D. Under-reported aspects of platinum drug pharmacology. *Molecules.* 2017;22(3):382-401.
- Thermo Fisher Scientific. TRIzol Reagent [Internet]. 2012 [cited 2020 Apr 4]. Available from: <https://www.thermofisher.com/order/catalog/product/15596026>.
- Tinker AV, Gelmon K. The role of PARP inhibitors in the treatment of ovarian carcinomas. *Curr Pharm Des* 2012;18: 3770-74.
- Ulubelen A, Gil RR, Cordell GA, Mericli AH, Mericli F. Cytotoxicity lignans from *Haplophyllum* species. *Pure Appl Chem.* 1994;66:2379-82.
- Vaezi A, Feldman CH, Niedernhofer LJ. ERCC1 and XRCC1 as biomarkers for lung and head and neck cancer. *Pharmacogenomics Pers Med.* 2011;4:47-63.
- Wang L, Gu Q, Zheng X, Ye J, Liu Z, Li J, Hu X, Hagler A, Xu J. Discovery of new selective human aldose reductase inhibitors through virtual screening multiple binding pocket conformations. *J Chem Inf Model.* 2013;53:2409-22.

- Woo KW, Choi SU, Park JC, Lee KR. A new lignan glycoside from *Juniperus rigida*. *Arch Pharm Res*. 2011;34(12):2043-9.
- Wu TT, Chen YY, Chang HY, Kung YH, Tseng CJ, Cheng PW. AKR1B1-induced epithelial–mesenchymal transition mediated by RAGE-oxidative stress in diabetic cataract lens. *Antioxidants*. 2020;9:273.
- Wu X, Li X, Fu Q, Cao Q, Chen X, Wang M, et al. AKR1B1 promotes basal-like breast cancer progression by a positive feedback loop that activates the EMT program. *J Exp Med*. 2017;214(4):1065-79.
- Xie H, Wang T, Matsuda H, Morikawa T, Yoshikawa M, Tani T. Bioactive constituents from Chinese natural medicines. XV. Inhibitory effect on aldose reductase and structures of Saussureosides A and B from *Saussurea medusa*. *Chem Pharm Bull*. 2005;53:1416-22.
- Xu Z, Yang H, Zhou M, Feng Y, Jia W. Inhibitory effect of total lignan from *Fructus Arctii* on aldose reductase. *Phytother Res*. 2010;24(3):472-3.
- Yashar CM. Basic principles in gynecologic radiotherapy. *Clin Gynecol Oncol*. 2012:659-680.
- You Y. Podophyllotoxin derivatives: current synthetic approaches for new anticancer agents. *Curr Pharm Des*. 2005;11(13):1695-717.
- Yousefzadi M, Sharifi M, Behmanesh M, Moyano E, Bonfill M, Cusido RM, et al. Podophyllotoxin: Current approaches to its biotechnological production and future challenges. *Eng Life Sci*. 2010;10(4):281-92.
- Zhang X, Xu L, Chen H, Zhang X, Lei Y, Liu W, et al. Novel hydroxychalcone-based dual inhibitors of aldose reductase and alpha-glucosidase as potential therapeutic agents against diabetes mellitus and its complications. *J Med Chem*. 2022;65:9174–92.
- Zhao CC, Zhang XH, Chen J, Shao JH, Zhao ZY, Tang YY. Lignans with α -glucosidase, protein tyrosine phosphatase 1B, and aldose reductase inhibitory activities from the fruits of *Viburnum cylindricum*. *Ind Crop Prod*. 2022;178:114601.
- Zhu, C. Aldose reductase inhibitors as potential therapeutic drugs of diabetic complications; *Intech*, 2013;23:19-43.

VITAE

Name Tanotnon Tanawattanasuntorn

Student ID 6110330018

Educational Attainment

Degree	Name of Institution	Year of Graduation
Bachelor of Sciences (Medical Technology)	Prince of Songkla University	2014

List of publication and proceedings

Publications

1. **Tanawattanasuntorn T**, Thongpanchang T, Rungrotmongkol T, Hanpaibool C, Graidist P, Tipmanee V. (–)-Kusunokinin as a potential aldose reductase inhibitor: Equivalency observed via AKR1B1 dynamics simulation. *ACS omega*, 2020;6(1):606-614.
2. **Tanawattanasuntorn T**, Rattanaburee T, Thongpanchang T, Graidist P. *Trans-(±)*-kusunokinin binding to AKR1B1 inhibits oxidative stress and proteins involved in migration in aggressive breast cancer. *Antioxidants*. 2022;11(12):2347.

Poster presentation

1. **Tanawattanasuntorn T**, Thongpanchang T, Graidist P, Tipmanee V. Interaction-guided study of kusunokinin as a possible AKR1B1 inhibitor. The 15th International Symposium of the Protein Society of Thailand. Convention Center, Chulabhorn Research Institute, November 4-6, 2020. Bangkok, Thailand.
2. **Tanawattanasuntorn T**, Rattanaburee T, Thongpanchang T, Graidist P. *Trans-(±)*-kusunokinin suppresses AKR1B1: inhibition of oxidative stress and alteration of epithelial-mesenchymal transition markers on aggressive cancer. 34th EORTC-NCI-AACR Symposium on molecular target and cancer therapeutics, Centre de Convencions Internacional de Barcelona, October 26-28, 2022. Barcelona, Spain.